ESCOLA
SUPERIOR
DE SAÚDE
POLITÉCNICO
DO PORTO

P.PORTO

M

**MESTRADO**
Mestrado em Bioestatística e Bioinformática Aplicada à Saúde

# Profiling Cell Response to a novel biomaterial for Periodontal Tissue Regeneration: a proteomic approach

Cláudia Alexandra Ribeiro Machado

09/**2019**

P.PORTO

ESCOLA SUPERIOR DE SAÚDE

# Profiling Cell Response to a novel biomaterial for Periodontal Tissue Regeneration: a proteomic approach


**Autor**

Cláudia Alexandra Ribeiro Machado

**Orientadores**

Cristina Ribeiro, PhD; INEB/i3S; ISEP

Joana Caldeira, PhD; INEB/i3S

Luísa Castro, PhD; ESS; CINTESIS


Dissertação apresentada para cumprimento dos requisitos necessários à obtenção do grau de Mestre em **Bioestatística e Bioinformática Aplicada à Saúde** pela Escola Superior de Saúde do Instituto Politécnico do Porto.

**Ao meu pai,**

Trago um pouco de ti em tudo o que faço.

This work was financed by Norte Portugal Regional Operational Programme (NORTE 2020) in the framework of the project "Bioengineered Therapies for Infectious Diseases and Tissue Regeneration" (NORTE-01-0145- FEDER-000012).


**Agradecimentos**

Em primeiro lugar: à minha orientadora Cristina, cujo carinho me tem acompanhado ao longo dos últimos anos. Tive um acaso de sorte e há quatro anos fui parar às suas mãos, ainda muito pequenina e sem saber muito sobre muita coisa. Muito, muito obrigada por todas as oportunidades, por toda a confiança depositada e, acima de tudo, por toda a humanidade que demonstra com todos. Sei bem o esforço necessário para "apagar todos os fogos" e não posso deixar de lhe agradecer, não só pelo tempo gasto a ensinar-me, mas também por me deixar voar por terrenos desconhecidos (e eu que só percebia de histologia!).

Às minhas co-orientadoras: à Joana, que aceitou este desafio comigo e que respondeu às minhas dúvidas constantes, sem nunca perder a paciência. Muito obrigada pela voz calma quando eu só dizia "Estou tão perdida!"; e à Professora Luísa pela constante disponibilidade e por ter tornado a estatística um pouco menos assustadora.

Ao grupo MicroEnvironments for NewTherapies e em especial ao Professor Mário Barbosa, por fazer com que este trabalho tenha sido possível.

Ao INEB, a minha segunda casa, não só pelo tempo que aí passo (e às vezes quase supera a primeira) mas porque somos todos uma grande família. Um especial obrigado aos técnicos Dalila, Eliana, Maria, Manuela e Ricardo que fazem o dia-a-dia parecer mais fácil.

Aos meninos do laboratório que foram incansáveis neste período. Ana Luísa, Joana, Mafalda e Morena, um especialíssimo obrigada por sempre se disponibilizarem a ajudar-me quando as coisas andavam mais caóticas. Sem vocês, tinha sido tudo muito mais difícil. Devo-vos um mega almoço!!

À Xô, cujos cafés matinais me levantaram o ânimo e me deram força, vezes sem conta. À Sara, minha companheira nesta aventura que me fez sentir sempre acompanhada. We did it! E à Lily, cuja presença nunca me falha. Há quatro anos escrevi que eram a prova de que os amigos da faculdade eram para sempre, e são mesmo.

Às minhas meninas de sempre: Filipa, Mariana e Sandra – vocês são o meu porto de abrigo e a minha constante desde há muitos anos. Por mais que os nossos caminhos teimem em se distanciar, arranjaremos sempre forma de os cruzarmos. E agora vamos marcar o jantar que ando a adiar há meses!

Ao Nuno, por todo o amor. Por nunca me cobrar e por segurar as pontas quando eu não consigo sozinha.

À minha família. À minha mãe e irmã que me amparam todas as quedas e que compreendem todas as vezes em que nem sempre estou presente. São o meu tesouro mais precioso e tenho-vos sempre comigo.

**Data from this master thesis resulted in the following publication:**

Ribeiro-Machado C, Val d'Oleiros Silva R, Castro L, Cadeira J, Barbosa MA, Ribeiro CC. Profiling Cell Response to a novel biomaterial for Periodontal Tissue Regeneration: a proteomic approach. World Biomaterials Congress 2020. Glasgow, Scotland [abstract submitted]

Additionally, the bilayer formulation referred in this thesis is currently undergoing patent application process.

**Resumo**

Um dos maiores desafios encontrados na cirurgia maxilofacial envolve o preenchimento de grandes defeitos, sendo necessário um biomaterial moldável, alternativo ao autoenxerto ósseo, que promova não só a formação óssea como também integração de tecidos moles.

O nosso grupo desenvolveu um sistema injetável para regeneração óssea composto por microesferas de HAp ricas em Sr e um veículo de alginato reticulado com Sr. Os resultados obtidos inspiraram-nos para desenhar um material injectável de bicamada, composto por uma camada inferior, promotora de regeneração óssea e uma camada superior, promotora da integração com tecidos moles. Foram também incorporados no material plasma rico em plaquetas (PRP) e membranas fetais (FMs), dado serem ricos em factores bioactivos.

A interface entre camadas manteve-se estável mesmo quando o material foi sujeito a forças de compressão. Verificou-se um aumento do número de células e da atividade metabólica, nas hMSCs e fibroblastos, quando em contacto com FMs, assim como um aumento da capacidade de mineralização das hMSCs. A análise proteómica mostrou que a incorporação de fatores bioativos resultou no enriquecimento de proteínas envolvidas na matrix celular, nos dois tipos celulares. Adicionalmente, foi observado um aumento na diferenciação osteoblástica nas formulações contendo FMs, sendo mais evidente quando associado PRP. Concluindo, este biomaterial apresenta-se promissor para reconstrução maxilofacial.

**Palavras-chave:** Biomaterial para libertação de fatores de crescimento, Proteómica, Regeneração de tecido periodontal, Bicamada.

**Abstract**

A current big challenge in maxillofacial field involves large defects filling, where a moldable biomaterial, alternative to bone autografts, is required, ideally promoting both bone formation and soft-tissue integration.

Our group has previously developed an injectable system for bone regeneration composed of Sr-rich HAp microspheres, delivered in an alginate vehicle crosslinked *in situ* with Sr. The excellent results obtained inspired us to design a bilayer injectable biomaterial, composed of a bone-like layer (BL), to induce bone regeneration, and a gingival-like layer (GL) for periodontal tissue integration. The incorporation of platelet-rich plasma (PRP) and fetal membranes (FMs), as natural biocompounds reservoirs, was also implemented.

The bilayer biomaterial presented a stable interface between layers, even when subjected to compressive forces. Both cell types (hMSCs and fibroblasts) exhibit an increase in number and metabolic activity, in response to FMs. Furthermore, hMSCs increased its mineralization capacity in both formulations containing FMs. Proteomic analysis revealed that incorporation of bioactive factors resulted in an ECM-related protein enrichment in both hGFs and hMSCs and in the promotion of hMSCs osteogenic differentiation. This is particularly evident when associating FMs and PRP. The results obtained indicate that the innovative developed bilayer material provides a very promising multifunctional approach for oral and maxillofacial reconstruction.

**Keywords:** Biomaterials for growth factors delivery, Proteomics, Periodontal tissue regeneration, Bilayer

## Index


**1.** Introduction ..... 1

**1.1.** Periodontal tissue ..... 1

**1.1.1.** Gingival tissue ..... 1

**1.1.2.** Alveolar and jaw bone ..... 2

**1.2.** Periodontal tissue regeneration ..... 6

**1.3.** Candidate therapeutics for periodontal tissue regeneration ..... 7

**1.3.1.** Bone grafts ..... 8

**1.3.2.** Guided tissue regeneration ..... 8

**1.3.3.** Synthetic bone substitutes ..... 9

**1.3.4.** Natural and synthetic hydrogels ..... 11

**1.3.5.** Use of bioinorganic ions on bone regeneration ..... 12

**1.3.6.** Bioactive factors ..... 13

**1.4.** Aims of the thesis ..... 16

**2.** Methodology ..... 17

**2.1.** Bilayer biomaterial formulation ..... 17

**2.1.1.** Sr-HAp microspheres preparation ..... 17

**2.1.2.** RGD-coupled alginate synthesis ..... 17

**2.1.3.** Platelet-Rich Plasma ..... 17

**2.1.4.** Fetal Membranes ..... 18

**2.1.5.** Gingival-like layer (GL) ..... 20

**2.1.6.** Bone-like layer (BL) ..... 21

**2.1.7.** Dynamic Mechanical Analysis ..... 21

**2.1.8.** Micro-Computed Tomography (Micro-CT) ..... 21

**2.2.** *In vitro* biological assessment ..... 21

**2.2.1.** Human Mesenchymal Stem Cells (hMSCs) culture ..... 21

**2.2.2.** Human Dermal Fibroblasts (hDF) culture ..... 22

**2.2.3.** Human Gingival Fibroblasts (hGFs) culture ..... 22

**2.2.4.** Metabolic activity and viability ..... 22

**2.2.5.** Proliferation and morphology assessment ..... 22

**2.2.6.** Osteogenic differentiation capacity ..... 23

**2.3.** Proteomic Analysis ..... 23

**2.3.1.** Protein extraction, quantification and digestion ..... 23

**2.3.2.** Liquid chromatography–tandem mass spectrometry (LC–MS/MS) analysis ..... 23
**2.3.3.** Bioinformatic analysis ..... 24
**2.4.** Statistical Analysis ..... 24
**3.** Results ..... 25
**3.1.** System structure and characterization ..... 25
**3.2.** Fetal Membranes ..... 28
**3.2.1.** FMs structure and decellularization efficacy ..... 28
**3.2.2.** FMs effect on hDFs metabolic activity ..... 30
**3.3.** PRP effect on hDF viability and metabolic activity ..... 31
**3.4.** Effect of GL in hGFs viability, proliferation and morphology ..... 32
**3.5.** Effect of BL in hMSCs viability, morphology, proliferation and differentiation ..... 34
**3.6.** Proteomic profile of hGFs response ..... 36
**3.7.** Proteomic profile of hMSCs response ..... 42
**4.** Discussion ..... 47
**5.** Conclusion and Future Remarks ..... 57
References ..... 58

**Figure Index**

Figure 1 – Schematic representation of the periodontal tissue morphology....1
Figure 2 – Anatomical components of the periodontal tissue....3
Figure 3 –MSCs expression markers during differentiation into osteogenic lineage....4
Figure 4 – Schematic representation of bone remodeling process in bone homeostasis....6
Figure 5 – Schematic representation of Sr dual mechanism of action....13
Figure 6 – Schematic representation of GL and BL formulations to be tested....21
Figure 7 – Strontium distribution within the HAp microspheres, by STEM-EDS analysis....25
Figure 8 – Fetal Membranes particles size quantification....26
Figure 9 – Mechanical comparison between different GL and BL formulations, by DMA....27
Figure 10 – Characterization of the bilayer biomaterial, by Micro-CT (A) and DMA (B)....28
Figure 11 – Evaluation of fetal membranes (FMs) extracellular matrix after decellularization, using histology (A) and transmission electron microscopy (B)....29
Figure 12 – Evaluation of fetal membranes (FMs) extracellular matrix after decellularization, using both scanning electronic microscopy (A) and atomic force microscopy (B). ....30
Figure 13 – FMs concentration effect on fibroblast metabolic activity....31
Figure 14 – PRP concentration effect on fibroblast viability and metabolic activity....32
Figure 15 – GL formulations effect on hGFs survival and morphology....33
Figure 16 – GL formulations effect on hGFs proliferation and metabolic activity....34
Figure 17 – BL formulations effect on hMSCs survival and morphology....35
Figure 18 – BL formulations effect on hMSCs proliferation, metabolic activity and differentiation....36
Figure 19 – LC-MS/MS data analysis....38
Figure 20 – Enriched Gene Ontology clusters, following DAVID analysis, for hGFs response to the tested formulations. ....39
Figure 21 – Reactome analysis organized by pathway categories....40
Figure 22 – Unique pathways affected by each tested formulation, from reactome analysis ....41
Figure 23 – LC-MS/MS data analysis....43
Figure 24 – Enriched Gene Ontology clusters, following DAVID analysis, for hMSCs response to tested formulations. ....44
Figure 25 – Reactome analysis organized by pathways categories....45
Figure 26 – Unique pathways affected by each tested formulation, from reactome analysis....46

## Abbreviations, Acronyms and Sigla

| | |
|---|---|
| AFM | Atomin Force Microscopy |
| ALP | Alkaline phosphatase |
| AM | Amniotic membrane |
| ATP | Adenosine triphosphate |
| BL | Bone-like layer |
| BMPs | Bone morphogenic proteins |
| BSA | Bovine Serum Albumin |
| BSP | Bone sialoprotein |
| CA | Calcium |
| CaSR | Ca sensing receptor |
| CM | Chorionic Membrane |
| COL | Collagen |
| CSLM | Confocal scanning laser microscope |
| DMA | Dynamic Mechanical Analysis |
| DMEM | Dulbecco's Modified Eagle's Medium |
| DMSO | Dimethyl sulfoxide |
| ECM | Extracellular Matrix |
| EDC | N-(3-Dimethylaminopropyl)-N′-ethylcarbodiimide hydrochloride |
| EDTA | Ethylenediamine tetraacetic acid |
| EG-VEGF | Endocrine gland-derived vascular endothelial growth factor |
| FBS | Fetal Bovine Serum |
| FGF | Fibroblast growth factors |
| FMs | Fetal membranes |
| FTF | Freeze-thaw-freeze |
| FTF | Freeze-thaw-freeze |
| GAL-7 | galectin 7 |
| GDL | Glucone delta-lactone |
| GL | Gingival-like layer |
| GO | Gene onthology |
| GTR | Guided tissue regeneration |
| HAp | Hydroxyapatite |
| hDFs | Human Dermal Fibroblasts |
| HE | Hematoxylin and Eosin |
| hGFs | Human Gingival Fibroblasts |
| hMSCs | Human Mesenchymal Stem Cells |
| ICAM1 | Intracellular adhesion molecule |
| IFN-$\alpha$ | Interferon alpha |
| IFN-$\gamma$ | Interferon gamma |
| IGF | Insulin-like growth factor |
| IL-1F5 | Interleukin 1 |
| LC-MS/MS | Liquid chromatography-tandem mass spectrometry |
| M-CSF | Macrophage colony-stimulating factor |
| Micro-CT | Micro-Computed Tomography |
| MMP | Metalloproteinases |
| MSCs | Mesenchymal stem cells |
| NaCl | Sodium chloride |
| $NH_2OH$ | Hydroxyl |
| OBs | Osteoblasts |
| OCN | Osteocalcin |
| OCs | Osteoclasts |
| OPG | Osteoprotegerin |
| OPN | Osteopontin |
| Osx | Osterix |
| P | Phosphate |
| P/S | Penicillin/streptomycin |
| PBS | Phosphate buffer solution |
| PDGF | Platelet-derived growth factor |
| PDL | periodontal ligament |
| PEG | poly (ethylene glycol) |
| PGA | poly (glucolic acid) |
| PI | Propidium Iodide |
| PLA | poly (L-lactic acid) |
| PMNs | Polymorphonuclear leukocytes |
| PRP | Platelet-Rich Plasma |
| PSR/AB | Picro-Sirius Red with Alcian Blue |
| RANK | Receptor activator of nuclear factor |
| RANKL | RANK ligand |
| RBC | Red Blood Cell |
| RGD | (Glycine)-4-arginine-glycine-aspartic acid-serine-proline |
| RIPA | Radio-Immunoprecipitation Assay |
| SEM | Scanning Electronic Microscopy |
| Sr | Strontium |
| SrCO3 | Strontium carbonate |
| SrRan | Sr ranelate |
| sulfo-NHS | Sulfo-N-hydroxysulfosuccinimide |
| TBS | Tris-buffered saline |
| TCP | Tricalcium phosphates |
| TEM | Transmission Electronic Microscopy |

| | |
|---|---|
| TGF-β | transforming growth factor-beta |
| TIMP-2 | Tissue inhibitor of metalloproteinases 2 |
| TSP | Thrombospondin |
| VEGF | Vascular endothelial growth factors |
| Wnt | Wingles |
| α-MEM | Alpha-Minimum Essential Medium |

# 1. Introduction

## 1.1. Periodontal tissue

The periodontal tissue is composed of both soft tissues – the gingival epithelium, the gingival connective tissue and the periodontal ligament (PDL) – and hard tissues - the alveolar bone tissue and the cementum/dentin (Figure 1) (1, 2). Each of these structures differs from its location, tissue architecture and biochemical composition, but they are all highly interconnected and function together. It is described that the extracellular matrix (ECM) of one compartment has an influence in the cellular activities of the adjacent structures (3). Therefore, in order to develop a successful strategy for periodontal tissue regeneration, the relationship between these structures must be considered.

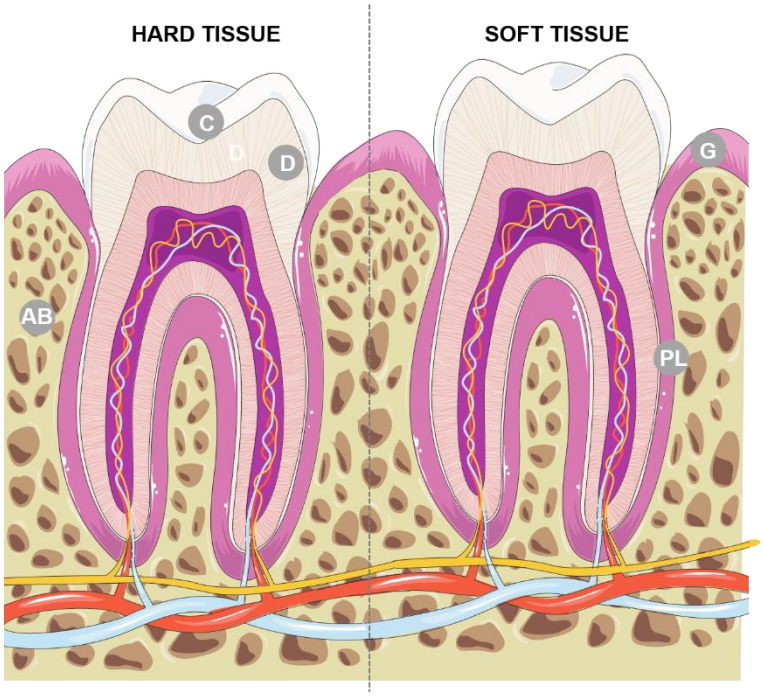


**Figure 1 – Schematic representation of the periodontal tissue morphology.** Constituents of the hard tissue structures: AB – Alveolar Bone; C – Cementum; D – Dentin; and the soft tissue structures: G – gingival tissue and PL – periodontal ligament.

### 1.1.1. Gingival tissue

The gingival mucosa is the main responsible for the defense against pathogens and mechanical stress. It is composed of a dense and vascular fibrous tissue with a keratinized stratified squamous epithelium – the connective tissue and the gingival epithelium, respectively (4).

The gingival epithelium can be divided into three functional compartments: the oral epithelium, which faces the oral cavity; the sulcular epithelium, which lines the sulcus and, finally, the junctional epithelium, which plays a crucial role in sealing the periodontal tissue from the oral environment, at the end of the sulcus (Figure 2) (5, 6).

Although the epithelial structure was thought to only provide a physical barrier to infection, it is now known that epithelial cells also play an active role in the innate host defense to bacteria. Both the keratinized

epithelium of the oral and sulcular compartments provide protection for the underlying periodontal tissue and act as barriers against bacteria and their products. On the other hand, the junctional epithelium presents a unique structure: it is not keratinized, it has significant intracellular spaces and exhibits a high cell turnover. These properties result in a permeable epithelium and thus render it crucial in regulating tissue health. Not only does it form the epithelial attachment to the tooth surface, but it also provides a vehicle for the movement of substances between the gingival connective tissue and the oral cavity. This compartment is naturally infiltrated by high number of polymorphonuclear leukocytes (PMNs) and lymphocytes (particularly T lymphocytes) and plays both an instructive and communicative role in host defense against bacterial infection (6–8).

The connective tissue has three major components: collagen fibers (60%); fibroblasts (5%), blood vessels and nerves and matrix (35%). Naturally, this structure is densely collagenous, being composed of a prominent system of predominantly type I collagen fibers, called the gingival fibers. Its main function is to protect the root surface and alveolar bone from the external oral environment, to support the gingiva against the tooth, to provide the rigidity necessary to withstand the forces of mastication and to provide support and fixation of teeth to the alveolar bone (6, 8).

The development, maintenance and repair of the connective tissue is mostly controlled by fibroblasts, which have a mesenchymal origin. Although in the past they have been considered a passive contributor to the tissue due to their differentiated state, more recently, studies have shown they can undergo a phenotype change, in response to cytokines and growth factors, ultimately leading to a different role in the tissue (6, 8). Their main function is to synthesize and maintain the components of the ECM, being involved in a number of regulatory processes of tissue homeostasis. Namely, fibroblasts are involved in matrix remodeling or turnover either by phagocytosis of collagen or by synthesis of matrix metalloproteinases, thus being capable of degrading collagens, proteoglycans and other matrix components (9). Fibroblasts are particularly sensitive to their microenvironment, that is the surrounding matrix, growth factors or cytokines (8).

### 1.1.2. Alveolar and jaw bone

Alveolar bone is one of the tissues responsible for the support of the tooth and 70% of its composition is apatite crystals, deposited on collagen type I (2, 10). It is composed of two components: the alveolar process and the alveolar bone proper (Figure 2). The alveolar process is part of the two jaw bones (maxilla and mandible), which is responsible for housing the developing tooth buds and, once erupted, the roots; it provides, therefore, the structural support for the dentition. The second component is the alveolar bone proper, which is the portion that lines the tooth socket and provides the attachment for the periodontal ligament and its associated tooth (11).

The alveolar process consists of two outer cortical plates of compact bone and an inner region of trabecular bone. Lining the tooth sockets a thin plate of bone can be found, termed the lamina dura (12).

Both cortical and trabecular bone consist of lamellar bone that provides bone maintenance and remodeling. Intertrabecular spaces are filled with bone marrow, containing mainly adipose cells as well as osteogenic cells and hematopoietic tissue (5).

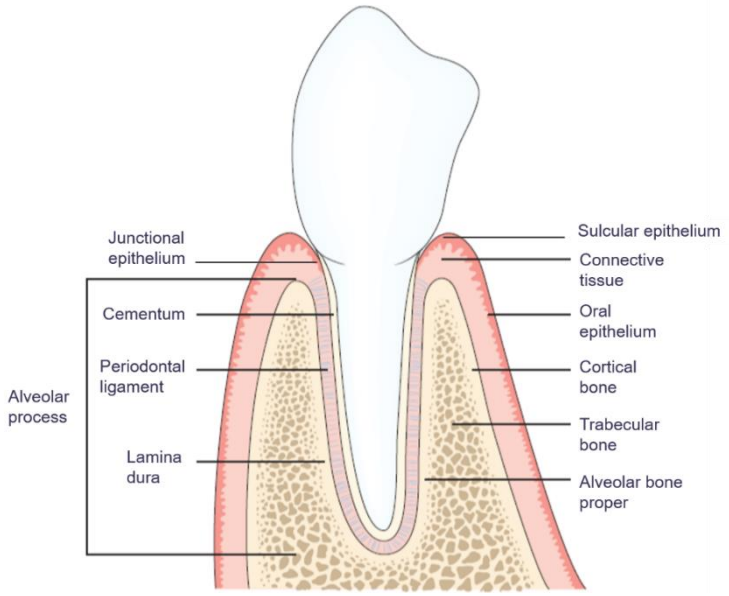


**Figure 2 – Anatomical components of the periodontal tissue.** The figure depicts the structures that compose the gingival tissue (oral, sulcular and junctional epithelium) and the structures composing the alveolar bone (alveolar bone proper and alveolar process, presenting both cortical and trabecular bone). Adapted from (13)

#### 1.1.2.1 Osteogenesis

The alveolar bone is originated through intramembranous bone formation, during the formation of the mandible and maxilla, meaning that bone is formed directly by osteoblasts differentiation from mesenchymal stem cells (MSCs), without needing the pre-existing cartilage as in the long bones development (endochondral ossification) (10). Two major types of cells are involved in this process – osteoblasts and osteoclasts.

Osteoblasts (OBs) are responsible for the production and mineralization of bone matrix. They present a cuboidal shape and are traditionally located along the bone surface (14). After OBs have completed their function, they can either become bone lining cells (or inactive OBs), become osteocytes, cells which are encased in the mineralized bone, or undergo programmed cell death (10).

The MSCs differentiation towards the osteoprogenitor lineage requires the expression of specific genes, such as bone morphogenetic proteins (BMPs) and member of the Wingles (Wnt) pathways (14). Once there is the establishment of osteoblast progenitors expressing RunX2 and Osterix (Osx), the three-stage differentiation process can occur (Figure 3). The first stage is the cell proliferation, when OB progenitors exhibit fibronectin, collagen type I (COL I), transforming growth factor-beta (TGF-β), and osteopontin (OPN). In the second stage, the matrix maturation, they cease the cell proliferation and start differentiating, while maturating the ECM, expressing markers such as alkaline phosphatase (ALP) and collagen I. In the

third and last phase, matrix mineralization starts with the increase of osteocalcin, which promotes the deposition of mineral substance. In the end, morphological changes take place and osteoblasts gain their characteristic cuboidal shape (15).

The synthesis of bone matrix by OBs occurs in two separate steps: deposition of organic matrix and its mineralization. In the first step, the OBs secrete collagen proteins, mainly type I collagen, noncollagen proteins (OCN, osteonectin, bone sialoprotein (BSP) II and osteopontin), and proteoglycans, which form the organic matrix. Afterwards, mineralization of bone matrix takes place into two phases: the vesicular and fibrillar phase. The vesicular phase occurs when the so-called matrix vesicles are released from the apical membrane of the OBs into the newly formed bone matrix, in which they bind to proteoglycans and other organic components. Since they hold a negative charge, the sulphated proteoglycans immobilize calcium ions that are stored within the matrix vesicles. Then, OBs secrete enzymes that degrade proteoglycans, the calcium ions are released from them and cross the calcium channels (formed by annexins) presented in the matrix vesicles membrane. Meanwhile, phosphate-containing compounds are degraded by the ALP secreted by OBs, releasing phosphate ions inside the matrix vesicles. In the end, both phosphate and calcium ions inside the vesicles nucleate, forming the HAp crystals. The fibrillar phase occurs when the saturation of calcium and phosphate inside the matrix vesicles leads to the rupture of these and to the HAp crystals to spread into the matrix (14, 16).

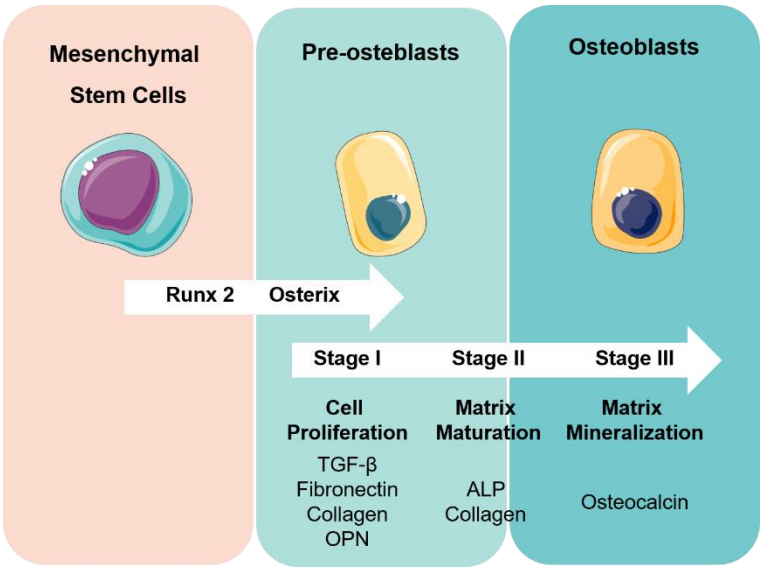


**Figure 3 –MSCs expression markers during differentiation into osteogenic lineage.** When a MSC population expressing RunX2 and Osterix is established, the three-stage differentiation to OBs begins : cell proliferation, matrix maturation and matrix mineralization, each presenting characteristics markers. Abbreviations: TGF-β – transforming growth factor-beta; OPN – osteopontin; ALP – alkaline phosphatase.

### 1.1.2.2 Osteoclastogenesis

Osteoclasts (OCs) are multinuclear cells that originate from hematopoietic stem cells. They present some specific characteristics such as the multinuclearity, the formation of an actin ring structure and the

formation of a ruffled border that allows the attachment to the bone ECM, required for their function – bone resorption (17).

OCs are regulated by several factors such as the macrophage colony-stimulating factor (M-CSF), RANK ligand (RANKL), both secreted by OBs. Together these factors promote the activation of transcription factors and gene expression in OCs. While M-CSF is responsible for stimulating OCs proliferation and inhibiting their apoptosis, RANKL is crucial for osteoclastogenesis, by binding to its receptor RANK and inducing OC formation (18, 19). Additionally, osteoprotegerin (OPG), which is produced by OBs, stromal cells and gingival/periodontal fibroblasts, can also bind to RANK (20). Since it prevents the RANK/RANKL interaction, it ultimately leads to the inhibition of osteoclastogenesis (21).

#### 1.1.2.3 Bone remodeling

Bone is a very dynamic tissue and is constantly being formed and resorbed, through a process named bone remodeling. While both bone formation and regulatory events are similar between alveolar and other skeletal bones, alveolar bone varies, since it has a very rapid turnover and is lost in the absence of the tooth. During bone remodeling, both OBs and OCs will deposit and resorb bone, respectively, and allow teeth to move through the bone, being it due to growth or to orthodontic treatment. OCs will resorb the bone located at the socket at the side towards which the tooth is moving, while new bone is formed in the opposite side by OBs (12). Therefore, the bone of the socket wall is constantly being remodeled and its structural organization can vary along the wall (5). In a healthy environment the surface of the inorganic parts of the bone are lined by OBs. Those which become incorporated within the mineral tissue are named osteocytes and maintain contact with each other via canaliculi, while OCs can be found in the Howship's lacunae (22). Nevertheless, there are situations in which the bone homeostasis is disrupted and bone remodeling is unbalanced, either due to an increase/decrease of new bone formation or due to an increase/decrease of bone resorption (Figure 4).

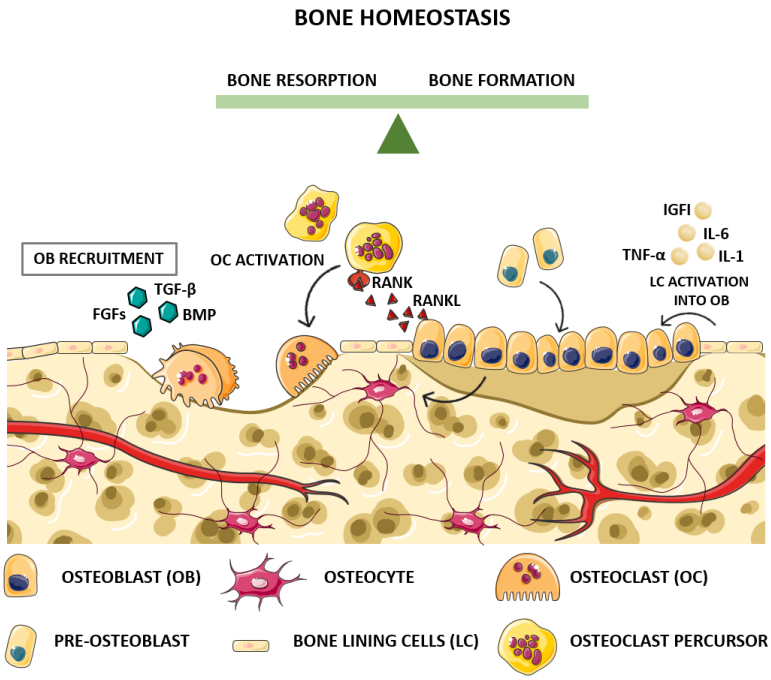


**Figure 4 – Schematic representation of bone remodeling process in bone homeostasis.** The intracellular communication between OBs and OCs is critical for bone homeostasis. OBs can influence OCs through several pathways, such as the OPG/RANKL/RANK. Likewise, OCs can influence OBs activation and recruitment through the release of cytokines from the resorbed bone matrix. Abbreviations: FGF – fibroblast growth factor; TGF-β – transforming growth factor – beta; BMP – bone morphogenetic protein; RANK – Receptor activator of nuclear factor; RANKL – Receptor activator of nuclear factor ligand; IL-6 – interleukin 6; IL-1 – interleukin 1; TNF-α – tumor necrosis factor alpha; IGF1 – insulin growth factor 1.

## 1.2. Periodontal tissue regeneration

Due to the heterogeneity of the craniofacial region, defects become extremely challenging to reconstruct while maintaining the original functionality, esthetic, as well as both physiological and anatomical properties. Maxillofacial defects can represent major challenges in tissue reconstruction by needing multiple, extensive, and complicated surgical interventions, with significant bone damage associated (23). Different classifications of maxillofacial defects have been described in the literature along time. Although its usefulness in the clinical practice is of high value, since it aids in the description and provides guidance to the surgeon, there is no nomenclature accepted as universal. Nevertheless it is established they can be classified as congenital or acquired. Congenital defects can be either genetic or pathologic and are born with the individual, as in the case of cleft palate. This defect can drastically affect the anatomy and, therefore, the normal life of the newborn by inhibiting the successful suction needed for breast-feeding. The main reason for it is the occurrence of risk habits during pregnancy (eg smoking, drug abuse, alcoholism) (24). On the other hand, acquired defects can either be due to a trauma or to a disease developed throughout life (eg periodontitis or tumor resections) (25).

Wound healing of the periodontal tissue, similarly to other body sites, is composed of a sequence of controlled events, beginning with the chemoattraction of the cells and ending with the formation and maturation of a new ECM. This ECM is the main responsible for connecting the margins of the wound, supplying cells, neovascularization and wound restoration (26, 27).

Although periodontal regeneration is the ideal outcome, since in this scenario a complete structural and functional reconstitution of the lost/injured part is achieved, in most cases only periodontal repair is possible. In these situations, the wound is filled with a tissue that does not fully restore the architecture or function of the original tissue. This is mainly due to the highly complex organization of both soft and hard tissues and the need to achieve regeneration of not only gingival connective tissue (which is normally destroyed by inflammation) but also the formation of cementum, restoration of lost bone and re-establishment of connective tissue fibers. At the cellular level, this process requires a high coordination between different cell types in terms of proliferation and differentiation (26–28).

The success of the periodontal regeneration is influenced by several factors that can be organized into four main groups: bacterial contamination, innate wound healing potential, site characteristics and surgical procedure. Poor control of bacterial plaque by the patient, which is commonly associated with lack of visits maintenance, are well documented to have an effect on the treatment outcome and can lead to a reduction in the new bone formation and in its attachment to the soft tissues (29). An impairment of the individual healing capacity can also have a major role in regeneration, being it due to age, genetics, systemic disease (such as diabetes) or to life habits (such as smoking) as it can affect the healing process. Among the site characteristics, the defect morphology is the most investigated in the literature.

One of the most important variables is the defect depth, since not only does the stability of the wound decreases as the size of the defect increases, but also do wider defects have higher possibility to develop secondary infections by clot displacement. Lastly, the surgical procedure can also impact the periodontal regeneration process. Some of the factors that might affect it are: the surgical approach, the operator skill and the devices available (27).

### 1.3. Candidate therapeutics for periodontal tissue regeneration

For the last decades, the main strategy for periodontal regeneration has been focused upon disease prevention, slowing/stopping disease progression, regenerating local tissue and maintaining the achieved outcome. For this, non-surgical therapies, such as scaling and root surface debridement, have been the first choice of approach and, when failing, a surgical approach is indicated. Although there is extensive literature highlighting advantages and disadvantages of each bone substitutes, no consensus can be found about the optimal approach (Table 1). All current strategies generally result in the repair of the defect site, lacking epithelial attachment and, thus, leading to the loss of the original tissue architecture (2, 30).

Therefore, there is an urgent need to develop a strategy that entitles complete periodontal regeneration. Ideally, a bone substitute should be biocompatible, easily molded into the defect area, should promote bone integration and present suitable mechanical properties, while displaying a degradation rate compatible with new bone formation (31). Additionally, the material should entail one or all of the following three biological performances: osteogenesis, where the formation of new bone is made by undifferentiated cells, which are stimulated to develop into their bone-forming cell lineage – OBs; osteoinduction, where the material possess the ability to recruit and induce immature cells to develop into OBs, from the surrounding tissue, leading to bone growth; and, finally, osteoconduction, where the material presents the ability to support bone growth on its surface (2).

### 1.3.1. Bone grafts

Bone grafts aim to restore the alveolar bone and have been thoroughly investigated during the last decades (31-34). In general, bone grafts can be classified as autografts, allografts and xenografts. Autografts are autogenous bone implants, from an extra- or intraoral source obtained from the same patient. The most common local to get autogenous bone grafts is the iliac crest, which has been demonstrated to possess osteogenic, osteoinductive and osteoconductive capacities. Although this is currently the "gold standard", the need for a second surgical area and the limited material availability lead to the search of new materials. Allografts, which are obtained from different individuals but within the same species, are mainly constituted of lyophilized bone or demineralized lyophilized bone. Studies have reported that the demineralization of lyophilized bone can potentiate the exposure of morphogenetic bone proteins, that will induce osteogenic differentiation. Thus, this type of graft is considered to be osteoinductive (35). Xenografts are obtained from other animal species, most commonly bovine. This material is chemically treated in order to eliminate the tissue organic component, while preserving the trabecular architecture that is described to be osteoconductive (27, 33).

Bone grafts have been reported to be more successful than the debridement technique (considered the conservative therapy, where the tissue is scraped and a strict hygiene must be followed) in 60-65% of the cases (36). Nevertheless, histological findings describe that although regeneration of bone and cementum was found, the ligament fibers were not functionally oriented (27).

### 1.3.2. Guided tissue regeneration

Guided tissue regeneration (GTR) aims to reestablish the periodontal attachment, using a membrane (with variable porosity) implanted between the root surface and the epithelium. Traditionally, during improper periodontal regeneration, defects are first filled with cells (epithelial and fibroblasts), which then create a fibro-epithelial tissue that prevents the sequential correct regeneration of the defect. By employing the membrane, the epithelial/fibroblast migration to the root surface is avoided, facilitating the maintenance of the defect for target periodontal tissue regeneration (eg bone grafts). Thus, the aim of this membrane is

to avoid the formation of a junctional epithelium near the root surface and adjacent alveolar bone, allowing undifferentiated stem cells within the PDL to migrate to the side and differentiate to the specific cell type. Although this technique has been reported as supporting substantial attachment level and higher defect filling, it also has a high degree of variability, mainly due to the unpredictable differentiation potential of the individual progenitor cells (2).

### 1.3.3. Synthetic bone substitutes

The shortage of natural bone grafts lead to the development of synthetic bone substitutes, or alloplasts. Nowadays there are already several commercially available types of materials, among them calcium sulfate, calcium phosphate ceramics, bioactive glass or even combinations among them.

**Calcium sulfate** is a biodegradable and osteoconductive ceramic and can be found commercially under the form of hard pellets or as an injectable fluid that hardens *in vivo*. It presents rapid resorption rate and low mechanical strength, which limits its application to small bone defects. In fact this makes up to its biggest disadvantage, since several authors report a lack of bone filling due to the rate of degradation being faster than the actual bone deposition (37–39). Additionally, its degradation products have been described to cause an acidic microenvironment and, as consequence, an inflammatory response (40).

**Calcium phosphate** ceramics is a family of ceramics mainly constituted by calcium and phosphate. The calcium-to-phosphate (Ca/P) ratio can largely influence both their absorption rate and mechanical properties. Among these:

- **Hydroxyapatite** is the natural mineral form of calcium apatite and presents both osteoconductive and osteointegrative properties. Due to its macroporosity structure, syntethic HAp scaffolds allows the adhesion, proliferation and differentiation of osteoprogenitor cells, as well as, neovascularization and, subsequently, new bone ingrowth. The calcium-to-phosphate (Ca/P) ratio of stoichiometric hydroxyapatite is 1.67. Nanocrystalline HAp have crystallites more close in size to the ones present in bone and a faster degradation rate.
- **Tricalcium phosphates** (TCP) presents a Ca/P ratio of 1.5, lower than HAp, having a faster degradation rate and, likewise, weaker mechanical properties (34). In a study by Eggli *et al* it was shown that after 6 months of implantation, TCP had a 85.4% of its volume degraded, against the 5.4% of HAp, after the same period (41).

Although osteoconductive, ceramics usually do not present osteoinductive or osteogenic characteristics on their own. However, they can be combined with ions or growth factors in order to potentiate their properties, an issue that will be addressed in the next sections.

Table 1 – Bone grafts and substitutes, advantages and disadvantages.

| | | Material | Examples | Osteo-genic | Osteo-inductive | Osteo-conductive | Mechanical support | Advantages | Disadvantages |
|---|---|---|---|---|---|---|---|---|---|
| Bone grafts | Vital | **Autografts** | Intraoral origin (eg maxillary tuberosity) | +++ | +++ | +++ | – (+ when cortical bone) | Non-immunogenic | Donor-site morbidity<br>Complications<br>Limited availability |
| | | | Extraoral origin (eg iliac crest) | | | | | | |
| | | **Allografts** | Fresh frozen bone | – | +++ | +++ | | No donor site within the patient<br>Available in large quantities | Possibility of disease transfer and antigenicity |
| | Non-vital | **Allografts** | Lyophilized bone | – | +++ | +++ | | Available in large quantities<br>High expression of bone growth stimulating factors | High donor variability<br>Must undergo processing techniques, leading to a decrease in their biological performance |
| | | | Demineralized lyophilized bone | | | | | | |
| | | **Xenografts** | Anorganic bovine bone | – | + | + | | Commercially available | Unpredictable results<br>Graft dislodgment |
| Bone substitutes | | **Alloplastic** | Calcium sulphate | – | – | + | + | Commercially available<br>Compressive strength higher than cancellous bone | Requires a dry environment to set (when in contact to moisture decreases the compressive strength) |
| | | | Calcium phosphates | | | + | ++ | Compressive strength similar to bone<br>Biocompatible | High or slow rate of resorption (HAp and Tricalcium phosphates, respectively) |
| | | | Polymethyl and hydroxyethyl-methacrylate polymers | | | – | +++ | Easy handling<br>High mechanical property | Exotermic reaction that can cause damage to adjacent tissues<br>Mechanical mismatch<br>Non-degradable |
| | | | Bioactive crystals | | | + | + | Promotes osteogenesis, allowing rapid bone formation | Degradation products can lead to higher pH value |

### 1.3.4. Natural and synthetic hydrogels

Hydrogels are hydrated polymeric biomaterials, of natural or synthetic origin, and can be used as scaffolds in periodontal tissue engineering (42). Hydrogels are highly attractive since they are easy to prepare, present low toxicity and are biodegradable. In particular, injectable hydrogels can be easily molded to different shapes, being capable of filling irregular lesions through an injection of a prepared solution that will crosslink *in situ*, thus resulting in a minimally invasive procedure (43). Additionally, hydrogels can be tailored, either to confer mechanical or structural properties and have been widely investigated as vehicles for drug-controlled release materials (44).

Synthetic polymers have been extensively used due to their biocompatibility, their tailored degradation rates and the ability to control the structural properties in a reproducible manner. They can be produced by a variety of fabrication techniques, being able to meet clinical requirements in terms of size and shape. Nowadays, there are several polymers already approved for *in vivo* applications, such as poly (glucolic acid) (PGA), poly (L-lactic acid) (PLA) and poly (ethylene glycol) (PEG), the last being increasingly applied in periodontal regeneration field, since it can be used either as a membrane or a hydrogel (45, 46). Nevertheless, some disadvantages continue to restrain its use, namely the limitation in polymer architecture control, structural dynamics and biostabilization (47).

Natural polymers are derivatives of natural materials, such as chitosan, and are highly attractive due to their biocompatibility, biodegradability, their affinity for biomolecules and wound healing activity. Their chemical and physical properties can be very easily modified, allowing the incorporation of biological agents. However, their main drawbacks concern reproducibility, since their composition may vary from batch to batch (48).

Alginate is a natural polymer, extracted from brown algae and has been extensively studied in the literature (49). Its structure is composed of linear copolymers of β-(1–4) linked d-mannuronic acid (M units) and β-(1–4)-linked l-guluronic acid (G units). It forms hydrogels in the presence of divalent cations, which will bind to the alginate chains, creating ionic bridges, thus leading to the gelation of the alginate solution (50). Alginate represents an interesting option for tissue engineering, since it offers the possibility to modify its properties. Although being a non cell-interactive polymer, alginate can be modified with peptides containing the amino acid sequence arginine-glycine-aspartic acid (Arg-Gly-Asp, RGD) in order to promote cell adhesion (51).

Since hydrogels, per se, do not present mechanical properties suitable for bone tissue regeneration, they have been increasingly combined with bone substitutes, such as ceramics, not only to improve their mechanical properties but also their porosity, injectability or degradation rate (52-55).

### 1.3.5. Use of bioinorganic ions on bone regeneration

In light of the effects that nutritional inbalance of ions has in the human body, several studies have been done trying to incorporate metallic ions, in the hope of a safe local delivery. Not only those ions (such as magnesium, strontium, silicon, zinc or copper) are regarded as cofactor of enzymes, coenzymes or prosthetic groups, but they are also involved in ion channels and in the process of secondary signaling. The use of bioinorganic ions in tissue engineering is highly attractive since they present low cost and long shelf life (34).

Strontium, a divalent cation, is a bone-seeking element and represents 0.035% of all the mineral content found in the skeletal system. Since Sr has similarities with Ca, it shares some of the osteoblast-mediated processes that are dominated by Ca in bone metabolism (Figure 5). It is described that Sr activates the Ca sensing receptor (CaSR) in OBs, in order to stimulate the OPG production and, consequently, suppressing the expression of RANKL, inhibiting osteoclastogenesis. Ultimately, Sr has the capacity to promote OBs proliferation, differentiation and survival, while inducing OCs apoptosis, resulting in a decrease in bone resorption (56).

Given the dual roles of Sr on bone formation, one Sr salt, Sr ranelate (SrRan), has been developed and used clinically in the treatment of osteoporosis in postmenopausal women. Clinical studies confirmed an increase in bone mineral density and a reduction in the risk of fracture (34).

However, several concerns have been raised about the adverse effect of Sr ranelate, since although in small number, cardiovascular events and venous thrombosis have been reported. Thus, the prescription of Sr ranelate is only restricted to patients with severe osteoporosis for whom other treatments are not possible. In addition, the use of SrRan is severely unrecommended for patients with uncontrolled hypertension and those with history of ischaemic heart disease, peripheral arterial disease and cerebrovascular disease (57).

In an effort to overcome Sr systemic effects, several studies have attempted to incorporate Sr into synthetic mineral ceramics, by an exchange of ions on apatite surface or by heteroionic substitution. Meininger *et al* have shown that the Sr substitution in magnesium phosphate cements was able to increase OBs activity and cell number, as well as suppressing OCs proliferation *in vitro* (58). In another study, Ehret *et al* showed that Sr incorporation into a 3D polyshaccharide matrix supplemented with HAp, not only supported MSCs osteogenic differentiation *in vitro* but also enhanced the tissue mineralization as well as osteoid and new blood vessel formation in an *in vivo* subcutaneous mice model (59).

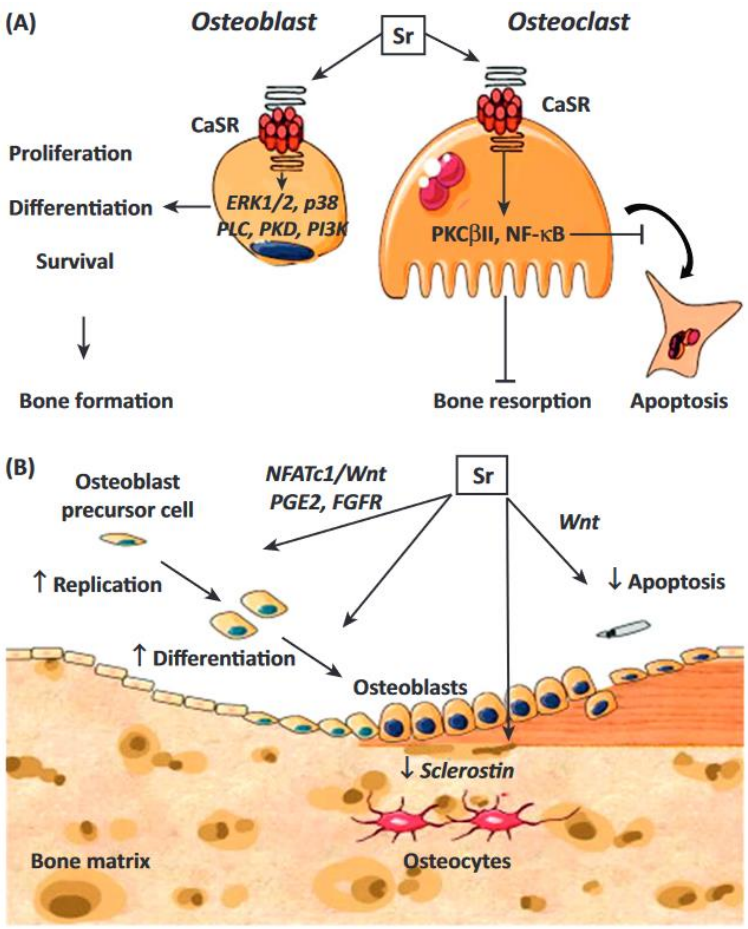


**Figure 5 – Schematic representation of Sr dual mechanism of action.** Sr has the ability to promote osteogenesis, by stimulating OBs activity, while inhibiting osteoclastogenesis through its effect on OCs. Adapted from (60). Abbreviations: ERK½ - extracellular-signal-regulated kinase½; PI3K – phosphatidylinositide 3-kinases; P38 – a mitogen-activated protein kinases; PLC – phospholipase C; PKD – protein kinase D; PKCβII – protein kinase C βII; NF-kB – nuclear factor kappa beta; NFATc – nuclear factors of activated T cells; PGE2 – prostaglandin E2; FGFR - fibroblast growth factor receptor.

### 1.3.6. Bioactive factors

As it was mentioned before, most bone substitutes, such as synthetic ceramics, do to not possess osteoinductive properties. While their osteoconductive capacity is able to facilitates anchorage and migration of progenitor cells, which would then, ideally, secrete growth factors to promote bone regeneration, in some situations growth factors secretion may be missing (eg disruption of the wound healing microenvironment). Therefore, the local delivery of growth factors that would potentiate the tissue's natural healing process has been extensively investigated. Currently, some growth factors have already undergone preclinical and clinical trials, such as the case of bone morphogenetic proteins (BMPs), fibroblast growth factors (FGF), vascular endothelial growth factors (VEFG) and platelet-rich plasma (PRP), where an increase in bone mass, as well as accelerated wound healing, was described (34). Nonetheless, the main drawback about the use of growth factors appears to be its *in vivo* half-life. As so,

the development of controlled-release delivery systems that will deliver these factors in both a space and time dependent manner is needed in order to potentiate their effectiveness (2).

#### 1.3.6.1 Platelet-Rich Plasma (PRP)

PRP is produced through the isolation and concentration of platelets from autogenous peripheral blood, and numerous commercial devices are already available for its isolation. PRP contains several growth factors, amongst which the platelet-derived growth factor (PDGF), FGF, insulin-like growth factor (IGF), TGF-β and VEGF, which appear to be critical for periodontal regeneration, by promoting proliferation of epithelial cells, fibroblasts and MSCs, as well as, neovascularization (61, 62).

It has been shown that the use of PRP leads to a greater and denser bone volume, when comparing to autologous grafts alone, which is believed to be due to the presence of growth factors (63). A study from Verma *et al* reported that PRP not only leads to an improvement of the soft tissue healing and faster bone regeneration, but it also influences the levels of PDGF released (64). More recently, some authors reported an antimicrobial activity of PRP against several pathogens, amongst them the *Porphyromonas gingivalis,* the most common in periodontal tissues (65-67). However, PRP application still has serious limitations since the results remain highly unreproducible (donor variability).

#### 1.3.6.2 Fetal Membranes

Fetal membranes (FMs) have been used in the treatment of both acute and chronic wounds for a long period of time (eg venous leg ulcers). FMs are highly attractive for tissue engineering since they are inexpensive, easily obtained and are currently seen as medical waste (68).

FMs are composed of two layers: the amniotic membrane (AM) and the chorionic membrane (CM). While the AM functions mainly as structural barrier, the CM acts as an immunological buffer, protecting the fetus from the maternal immune system. Roughly, the AM is composed of a cubical epithelium, a basal membrane and a stroma containing collagen type I, III, V and VI. On the other hand, the CM is composed of a cellular layer, a reticular layer and trophoblast layer. The latter is highly rich in collagen type I, III, IV, V and VI. The spongy layer separates the AM from the CM, it is mainly composed of proteoglycans and is responsible for the sliding movement between both layers (69).

Reports have shown that FMs not only have an effect on pain reduction, but also present anti-inflammatory and antimicrobial properties, being associated to a scarring reduction, by promoting epithelial healing (68, 70-72). Their beneficial properties are attributed to their capacity to function as a protective physical barrier and to their content full of a variety of growth factors and cytokines (73).

Although little is known about the growth factor content of fetal membranes, a study from McQuiling *et al* where the proteomic profile of AM and CM is compared, through ELISA microarrays, and describes that both membranes exhibit a similar content. Nevertheless, the CM had significantly higher levels of endocrine gland-derived vascular endothelial growth factor (EG-VEGF), PDGF - both related to

angiogenesis - and tissue inhibitor of metalloproteinases 2 (TIMP-2) – related to immune regulation – while the AM presented higher levels of galectin 7 (GAL-7) and TGF-β1 – both related to regeneration – as well as interleukin 1 (IL-1F5) – related to immune regulation (74).

Nevertheless, and since FMs can not be used in their native form due to the potential initiation of host immune response (leading to the development of a fibrous capsule), decellularization must be performed in order to allow its use as allogenous material (75). Decellularization aims to isolate the tissue ECM, while removing all inhabiting cells but, currently, no consensus is found on the literature on the optimal decellularization protocol that applies to both membranes.

## 1.4. Aims of the thesis

Current challenges in the maxillofacial field involve large defects that require a moldable biomaterial, which allows reconstruction in an aesthetically pleasing way. Nowadays, bone grafts are the solution for these cases. However, the search continues for a biomaterial that not only promotes bone regeneration, but also enables soft-tissue integration and presents antimicrobial properties.

Our group has developed a system, composed of Sr-doped HAp microspheres, delivered in an alginate vehicle crosslinked with Sr (76). This material has the capacity of promoting bone regeneration, both *in vitro* and *in vivo* (77, 78). It also displays an immunomodulatory effect, by promoting M2 macrophages, an anti-inflammatory associated phenotype (79). Furthermore, the presence of Sr in the system was able to decrease antimicrobial activity (80). As so, it constitutes a highly interesting biomaterial for oral cavity lesions.

Herein, we propose to develop a bilayer injectable biomaterial, composed of a bottom layer capable of inducing bone regeneration, and a top layer capable of promoting the periodontal tissue integration. Different formulations were tested in order to improve the Sr-hybrid system, so that a bone regeneration inductive hybrid material is obtained, with a gingival pro-supportive profile. Moreover, the incorporation of growth factors natural reservoirs, such as PRP and FMs were also be implemented, aiming to promote tissue regeneration.

With this work, we intended to:

- Develop and characterize a bilayer hybrid system, composed of a bone-like layer and a gingival-like layer;
- Evaluate the effect of the decellularization in the FMs;
- Determine the optimal formulation and concentration of decellularized FMs particles, to be incorporated into the system;
- Determine the optimal concentration of PRP that should be incorporated into the system;
- Evaluate the biological response of both human gingival fibroblast (hGFs) and human mesenchymal stem cells (hMSCs) to the biomaterial, in terms of viability, proliferation and differentiation;
- Investigate the molecular mechanisms responsible for the biomaterials effect in both gingival fibroblasts and mesenchymal stem cells, by proteomic profiling of both cell populations.

# 2. Methodology

## 2.1. Bilayer biomaterial formulation

### 2.1.1. Sr-HAp microspheres preparation

Strontium (Sr)-Hydroxyapatite (HAp) microspheres were prepared as described elsewhere (81). Briefly, HAp powder was dissolved in a 3% w/v alginate (Protanal 10/60, FMC BioPolymer) solution, until a homogeneous paste was obtained. The paste was then extruded by a dropwise method, crosslinked in a Sr chloride ($SrCl_2$, 0.1 M, Sigma) solution and allowed to stabilize for at least 30 minutes. The extrusion flow rate was regulated, in order to control the size of the microspheres, by using a syringe pump (Cole-Parmer) and a coaxial air stream (Encapsulation Unit Var J1-Nisco). Afterwards, microspheres were washed in deionized water (to remove non cross-linked ions) and dried overnight at 60 ºC. Later, microspheres were sintered at 1200 ºC to burn-off the polymer and allow for the aggregation of the ceramic granules. Once more, microspheres were washed with deionized water, dried and, finally, sieved in order to select particles with the size range of 500-560 μm of diameter. Microspheres were sterilized through an autoclave cycle at 120 ºC. Strontium distribution within microspheres was analysed by STEM-EDS, following procedure further described in 2.1.4.2.2.

### 2.1.2. RGD-coupled alginate synthesis

Ultra-pure sodium alginate with high content of guluronic acid unites (>60%, NovaMatrix, FMC Biopolymers) was used for hydrogel preparation. The cell-adhesion peptide sequence (glycine)-4-arginine-glycine-aspartic acid-serine-proline (G4RGDSP, GenScript), hereafter abbreviated as RGD, was coupled to alginate using carbodiimide chemistry (82). Briefly, a 1% w/v alginate solution in 0.1 M MES buffer (Sigma) was prepared and stirred overnight. Afterwards, sulfo-N-hydroxysulfosuccinimide (Sulfo-NHS, Thermo Scientific), N-(3-Dimethylaminopropyl)-N′-ethylcarbodiimide hydrochloride (EDC, Sigma) - at a 1 M:2 M per gram of alginate - and RGD – 20 mg/g alginate - were added. After 24 hours, the reaction was quenched with hydroxyl ($NH_2OH$, Sigma) – 18 mg/g alginate. Dialysis was then performed with MWCO 3500 membranes (Spectrum Lab), using solutions of decreased sodium chloride (NaCl, Merck) concentration finishing with deionized water. The final alginate solution was then lyophilized, sterilized by filtration and stored at -20 ºC until further use. In order to determine the peptide concentration in the alginate, the BCA Protein Assay (Pierce) was used, as previously described (83).

### 2.1.3. Platelet-Rich Plasma

PRP was isolated from blood kindly donated from Hospital São João, according to a previously described protocol (84). Briefly, 10 ml of whole blood with anticoagulant (Ethylenediamine tetraacetic acid - EDTA) was centrifuged at 900g for 5 minutes, at room temperature. The lower layer (red blood cell - RBC) was discarded. The upper layer with buffy coat was transfered to a new, sterile centrifuge tube. A second spin

was performed at 2000 g for 15 min at room temperature. The upper 2/3 of the supernatant were discarded. The obtained pellet was ressuspended, labeled as PRP and freezed at -80ºC (85).

#### 2.1.3.1 Platelet-Rich Plasma powder preparation

PRP was subjected to a freeze-thaw-freeze (FTF) cycle, for cell lysis and platelets activation (84). Briefly PRP was freezed at -80 °C, thawed at 37 °C for 1 hour and, finally, freezed again at -80 °C for 24 h. Frozen PRP was lyophilized at -80 °C for 72 h, in order to obtain a dry powder. Finally, the crushed PRP powder was sterilized (through ultraviolet sterilization, 10 min, twice) and incorporated into the alginate solution, in the desirable concentration. Different concentrations were tested based on literature findings - 5%, 10% and 100% (86-88) .

### 2.1.4. Fetal Membranes

FMs were isolated from placental tissue resulting from caesarean section, donated from Hospital Infante D.Pedro, Aveiro, after proper informed consent. Samples were kept at 4 °C in normal 0.9% saline solution, until further processing (maximum 24 h). All procedures were performed under sterile conditions. Amniotic and chorionic membranes were separated and washed with Phosphate Buffer Solution (PBS), supplemented with antibiotics (Penicillin and Streptomycin) and fungicide. Finally, both membranes were preserved at -80 °C in a Dulbecco's Modified Eagle's Medium (DMEM): Glycerol (1:1 ratio), until further analysis.

#### 2.1.4.1 Fetal Membranes decellularization

Decellularization protocol followed previous preliminary work, in which a successful FMs decellularization was optimized (89). Briefly, FMs were incubated in an EDTA hypotonic buffer (pH 7.8) for 18 h and then washed with PBS. Chemical decellularization was performed with 1% Triton X-100 and 1 M Dimethyl sulfoxide (DMSO), for 24 h. FMs were washed with a hypotonic buffer and digested with DNAse (Applichem) at 100 U/ml, for 3 h at 37 °C. To promote cell debris mechanical remotion, cell scrapers were used, before a final wash with PBS.

#### 2.1.4.2 Fetal Membranes characterization

Both amniotic and chorionic membranes were characterized in order to better understand the structure of the samples as well as to verify the decellularization efficacy, namely, the complete remotion of nuclei and maintenance of the extracellular matrix (ECM).

##### 2.1.4.2.1 Histology

FMs were fixed using 10% Neutral Buffered Formalin, overnight, processed and paraffin embedded. Afterwards, 3 μm sections were obtained and stained for Hematoxylin and Eosin (HE), Picro-Sirius Red with Alcian Blue (PSR/AB) and DAPI. Briefly, HE sections were deparaffinized and rehydrated, stained 3

min in Gill's Hematoxilin, 6 min in running water, dehydrated, stained 1 min in Eosin Y, cleared and mounted in Entellan. For PSR/AB staining, sections were deparaffinized and rehydrated, stained 3 min in Gill's Hematoxylin and, after a tap water washed, stained in Alcian Blue pH 2.5 for 30 min. Then, sections were washed with tap water, stained in Picro-Sirius Red solution for 1 hour and differentiated with acidified water for 30 seconds. After a quick dehydration in 96% and 100% ethanol, sections were mounted in Entellan. For DAPI staining, sections were deparaffinized and mounted with Fluroshield with DAPI (Sigma). Sections were imaged using Inverted Fluorescence Microscopy (Axiovert 200M, Zeiss) and cell nuclei were quantified using an ImageJ macro.

#### 2.1.4.2.2 Transmission Eletronic Microscopy (TEM)

FMs were fixed overnight with 2.5% Gluteraldehyde and 4% Paraformaldehyde (1:1). After being rinsed with PBS, samples were fixed with 2% osmium tetraoxide, dehydrated in a graded ethanol series and embedded in Epon resin. Ultrathin sections were cut using a diamond knife, contrasted with uranyl acetate and lead citrate and examined in a Jeol JEM 1400 transmission electron microscope at 80 kV.

#### 2.1.4.2.3 Scanning Eletronic Microscopy (SEM)

Critical point drying was performed in order to preserve the three-dimensional structure of the FMs. Briefly, FMs were fixed using 2.5% Glutaraldehyde in 0.1 M PBS, overnight. Afterwards, FMs were washed three times with PBS and dehydrated with an ethanol series (30%, 50%, 70%, 80%, 90%, 95% and 100%) for 10 minutes, two times. FMs were adhered to coverslips and critical point dried was performed using Leica EM CDP300 Automated Critical Point Dryer. The SEM examination was performed using a High resolution (Schottky) Environmental Scanning Electron Microscope with X-Ray Microanalysis and Electron Backscattered Diffraction analysis: Quanta 400 FEG ESEM / EDAX Genesis X4M. Samples were coated with an Au/Pd thin film by sputtering, using the SPI Module Sputter Coater equipment.

#### 2.1.4.2.4 Atomic Force Microscopy (AFM)

Atomic Force Microscopy (AFM) images were obtained with a PicoPlus scanning probe microscope interfaced with a Picoscan 5500 controller (Keysight Technologies, USA) using the PicoView 1.20 software (Keysight Technologies, USA), coupled to an Inverted Optical Microscope (Observer Z1, Zeiss, Germany). Each sample was imaged in air, with a 50×50 $\mu m^2$ piezoelectric scanner. All measurements were performed in Tapping mode® at RT using a bar-shaped silicon cantilever tip (AppNano, USA) with a spring constant of 25 –75 N/m.

### 2.1.4.3 FMs incorporation into the alginate

According to the literature, solubilized AM and AM extracts are the most common used formulations. Nevertheless, our hypothesis included the incorporation of FMs particles into the alginate. Therefore, both FMs particles, solubilized FMs and FMs extracts effect were tested on fibroblasts, at different

concentrations (0.5, 1, 10 and 20 mg/ml) based on literature findings. FMs underwent ultraviolet sterilization (exposed 10 min, twice) and stored until further use.

#### 2.1.4.3.1 FMs particles

For the particles fabrication, FMs were lyophilized at -80 °C for 72 h. Afterwards, lyophilized FMs were either thoroughly cut into particles using scissors or using a mill. FMs particles were imaged using a stereomicroscope (SZX10, Olympus) with a digital camera (Moticam, Motic) and particles size was measured using ImageJ v1.52 software (USA).

#### 2.1.4.3.1 FMs extract

FMs extracts were performed according to a protocol described by Baradaran-Rafii *et al* (90). Briefly, membranes were cut into small pieces and grinded into powder using a pestle and a mortar (in liquid nitrogen). The powder was then dissolved in either DMEM or distilled water at 0.5, 1, 10 and 20 mg/ml concentration. Solution was sonicated at maximum power, three times, for 10 min, on ice and afterwards, centrifuged at 4000 g for 10 min. The collected supernatant was then centrifuged for 5 min at 15000 g, filtered through a 0.2 μm filter and stored at -80 °C.

#### 2.1.4.3.2 FMs solubilization

For FMs solubilization, a protocol adapted from Murphy *et al*, 2017 was used (91). Briefly, membranes were cut into small pieces and thoroughly washed with PBS. Afterwards, membranes were dragged through falcons in order to take out the excess of water. After freezing them for 24 h at -80 °C, FMs were lyophilized for 72 h and cut into small pieces. Digestion was carried using Pepsin at 1:10 (Sigma) and after ultraviolet sterilization (exposed 10min, twice), 10 ml of 0.01 N Hydrochloric acid was added and left for 48 h at 37 °C. Finally, a 10 min centrifugation of 4500 rpm was performed and the supernatant was collected. The solution was neutralize to pH=7 with Sodium hydroxide and stored at -80 °C.

### 2.1.5. Gingival-like layer (GL)

For the upper layer, RGD-alginate was crosslinked by internal gelation with Sr carbonate without the presence of the Sr-HAp microspheres. Briefly, RGD-alginate was thoroughly mixed with an aqueous suspension of Sr carbonate ($SrCO_3$, Sigma) at a $SrCO_3$/COOH molar ratio of 1.6. A fresh solution of glucone delta-lactone (GDL, Sigma) was added to trigger gel formation. The $SrCO_3$/GDL molar ratio was set to 0.125 with a total polymer concentration of 3.5% w/v in deionized water and a final RGD concentration of 527 μM in the hydrogel. Moreover, as an alternative, either PRP or FMs (both particles, extracts and solubilized FMs) were incorporated into the alginate with the desirable concentration (Figure 6). Formulations were imaged using a stereomicroscope (SZX10, Olympus) with a digital camera (Moticam, Motic).

### 2.1.6. Bone-like layer (BL)

For the bottom layer, RGD-alginate was combined with Sr-HAp microspheres and crosslinked by internal gelation with Sr carbonate. Similar to the GL, RGD-alginate was mixed with both $SrCO_3$ and GDL, leading to a gel formation. Afterwards, Sr-HAp microspheres were homogeneously mixed with the alginate solution at 35% w/v. Likewise, both PRP and FMs were incorporated into the alginate with the desirable concentration (Figure 6). Formulations were imaged using a stereomicroscope (SZX10, Olympus) with a digital camera (Moticam, Motic).

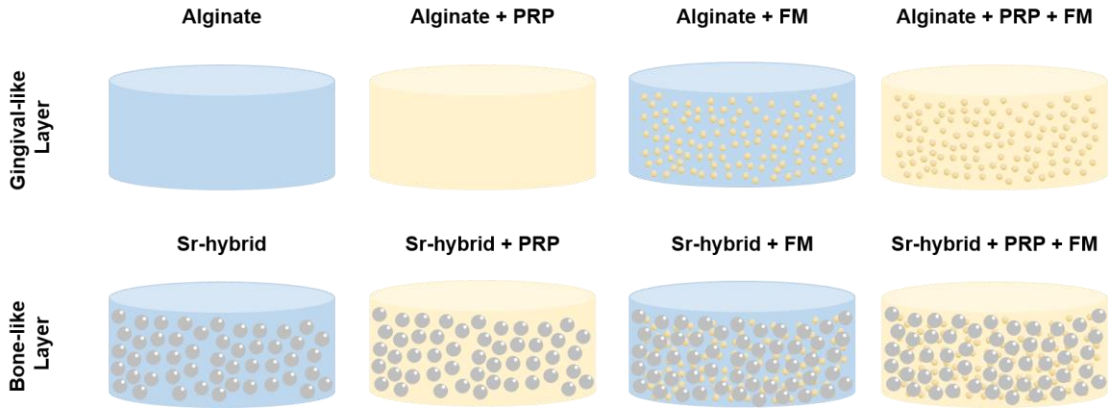


**Figure 6 – Schematic representation of GL and BL formulations to be tested.** Both Alginate 3.5% and Sr-hybrid will function as controls, respectively, for the following experiments.

### 2.1.7. Dynamic Mechanical Analysis

The DMA compression mode (DMA 8000, PerkinElmer) was used to study the viscoelastic properties of the different formulations. Cylinders with 5 mm diameter and height were prepared in adequate polymeric mold and tested. This analysis consists of a parallel-plate measuring system that compresses the samples between the plates. A frequency of oscillation of 1 Hz and displacement amplitude of 1% of the thickness, were used throughout the experiments. All samples were left to reticulate overnight in a humidified environment, to prevent samples dehydration.

### 2.1.8. Micro-Computed Tomography (Micro-CT)

Samples were analyzed by micro-CT (SkyScan1276, Bruker). Each sample was analyzed in high resolution mode, using a pixel size of 17.37 µm, and an exposure time of 2150 ms. The X-ray source was set at 70 kV of energy and a current of 57 µA. Reconstruction of the total 2394 slices was performed using NRecon software (v 1.7.4.2), with a post alignment of 91.50 and ring artifact correction set at 6.

## 2.2. *In vitro* biological assessment

### 2.2.1. Human Mesenchymal Stem Cells (hMSCs) culture

Human MSCs were purchased from Lonza (PT-2501, Lot no. 0F3825, 22Y, female) and routinely cultured in media composed of low-glucose DMEM supplemented with 10% v/v fetal bovine serum (FBS, MSC-

qualified, HyClone, GE Healthcare Life Sciences) and 1% v/v penicillin/streptomycin (P/S, Gibco). Cultures were maintained at 37 °C under a humidified atmosphere of 5% v/v $CO_2$, with culture medium being changed twice a week. Cells were trypsinized when reaching ca. 70% confluence. hMSCs were used in passage 6 and cultured with DMEM 10% FBS with 1% P/S. For culture in direct contact, 60000 cells were seeded on top of the bone-like layer formulation. For the proteomic assay, 30000 cells were seeded on 6-well plates, while the biomaterial was place on the top compartment of transwell. Media was replaced every 3 days.

### 2.2.2. Human Dermal Fibroblasts (hDF) culture

Human DF were cultured at 37 °C under a humidified atmosphere of 5% v/v $CO_2$, with high-glucose medium being changed twice a week. Cells were subcultured at 70% confluency by 0.25% trypsin/EDTA solution (Gibco). A total of 60000 cells were cultured in direct contact with the gingival-like layer formulation. Media was replaced every 3 days.

### 2.2.3. Human Gingival Fibroblasts (hGFs) culture

Human GFs were cultured at 37 °C under a humidified atmosphere of 5% v/v $CO_2$ in air, with Alpha-Minimum Essential Medium ($\alpha$-MEM) media supplemented with 10% FBS (Biowest) and 1% P/S. Media was changed twice a week. Cells were subcultured at 70% confluency by 0.25% trypsin/EDTA solution (Gibco). For culture in direct contact, 60000 cells were seeded on top of the gingival-like layer formulation. For the proteomic assay, 30000 cells were seeded on 6-well culture plates, while the biomaterial was placed on the top compartment of the transwell. Media was replaced every 3 days.

### 2.2.4. Metabolic activity and viability

Metabolic activity was evaluated by performing the Rezasurin assay. For this, cells were incubated with a 10% Resazurin solution in media for 4 hours at 37 °C, protected from light. After this, two replicates (100 µl each) were collected and transferred to a 96-well black culture plate and fluorescence was measured, using a microplate reader (Synergy MX, Biotek) with the Gen5 software (Biotek).

Live/Dead assay was used to assess viability of cells cultured on hybrid systems. Briefly, the biomaterial was washed with TBS and then incubated with Calcein and Hoestch solution for 20 min at 37 °C, protected from light. Afterwards, samples were incubated with Propidium Iodide (PI) for 1 min. Calcein stained live cells green and PI stained dead cells in red. Samples were imaged with confocal scanning laser microscope (CSLM, Leica SP5). Further image treatment was performed using ImageJ.

### 2.2.5. Proliferation and morphology assessment

Proliferation was evaluated through Ki67 staining on the hybrid systems, by CSLM. First, culture medium was removed from the wells, cells washed with Tris-buffered saline (TBS) and fixed for 20 min with 4% Paraformaldehyde. After washing in TBS, cells were permeabilized using 0.1% Triton X-100 in TBS for 5

min and further washed. Blocking was performed for 30 min with 5% w/v bovine serum albumin (BSA, Merck) and later incubated with Ki67 (1:150, ThermoFisher Scientific) for 2 h. Afterwards, samples were washed with 1% w/v BSA and incubated with the secondary anti-rabbit conjugated with Alexa Fluor 647. Finally, samples were incubated for 1h with Alexa Fluor 488 Phalloidin (Molecular Probes, Invitrogen) for cell morphology assessment. After a final washing step, cells were kept at 4 °C until being imaged by CSLM.

### 2.2.6. Osteogenic differentiation capacity

Alkaline phosphatase (ALP) staining was performed on hMSCs, seeded on the hybrid systems. Samples were washed, fixed (as previously described in 2.2.5) and incubated for 45 min in Naphthol AS-MX phosphate/Fast Violet B salt (Sigma), protected from light. Alizarin staining was also performed on hMSCs, seeded on the hybrid systems. Samples were fixed and, after a washing step with TBS, stained with Alizarin Red 1% w/v solution for 10 min. Afterwards, samples were washed three times with TBS to remove staining excess. Images were obtained using a stereoscope (SZX10, Olympus).

## 2.3. Proteomic Analysis

### 2.3.1. Protein extraction, quantification and digestion

After 14 and 21 days (for hGFs and hMSCs, respectively), cells from the transwell experience were thoroughly washed with PBS for eight times, in order to remove the FBS contaminant. After that, cells were trypsinized and centrifuged for 10 min at 400 g. The resulting cell pellet was lysated with Radio-Immunoprecipitation Assay (RIPA) buffer supplemented with protease and phosphatase inhibitors (NaF, $Na_3VO_4$, PMSF, Aprotinin, Leupeptin and $Na_3VO_4$), for 30 min on ice. Afterwards, a centrifugation of 14000 rpm for 10 min was performed and supernatants were collected. In order to determine the protein content of each condition, the DC™ Protein Assay kit (BioRad) was used, according to manufacturer instructions, and the absorvance was read at 750 nm using the microplate reader (Synergy MX, Biotek) with the Gen5 software (Biotek).

The volume corresponding to 100 µg of protein from each sample was used. The reduction and alkylation of cysteines residues was performed, using a buffer containing tris (2-carboxyethyl) phosphine (TCEP) and methyl methanethiosulfonate (MMTS). Sp3 beads were used in order to wash the purified protein lysate from contaminants, as described in the literature (92). Trypsin was used for protein digestion overnight at 37 °C. After digestion, formic acid (FA) 100% was added to each sample. Next, samples were dried, resolubilized in 70% isopropanol and 30% TEAB 1 M, and sonicated.

### 2.3.2. Liquid chromatography-tandem mass spectrometry (LC-MS/MS) analysis

Protein identification and quantitation were performed by nano LC-MS/MS, using the Ultimate 3000 liquid chromatography system coupled to a Q-Exactive Hybrid Quadrupole-Orbitrap mass spectrometer

(Thermo Scientific, Bremen, Germany). Samples were loaded onto a trapping cartridge for 3 min and separated on an nano-C18 column at 300 nL/min. Data acquisition was controlled by Xcalibur and Tune software (Thermo Scientific, Bremen, Germany). The mass spectrometer was operated in data-dependent positive acquisition mode alternating between a full scan (m/z 380-1580) and subsequent HCD MS/MS of the 10 most intense peaks from full scan.

### 2.3.3. Bioinformatic analysis

The detected mass spectra was processed and visualized using Proteome Discoverer software (v 2.1, Thermo Scientific) and searched against the UniProt database (*Homo sapiens*), in order to identify the matching proteins. An independent False Discovery Rate analysis using the target-decoy approach provided with the software was set at 1% and used to assess the quality of the identifications. Morpheus (v1.66) was used for hierarchical clustering, using Spearman correlation. Lastly, in order to explore the functions and pathways affected, a Gene Ontology (GO) analysis was performed using both the Database for Annotation, Visualization and Integrated Discovery Bioinformatics Resources (DAVID, v6.8) software, and pathways analysis was performed using Reactome software (v3.6) (93).

## 2.4. Statistical Analysis

When otherwise not specified, statistical analysis was performed using Prism5. The quantitative variables evaluated throughout this thesis were: FMs particles size (μm); biomaterials storage and loss modulus (MPa); FMs surface roughness (μm); metabolic activity; ki67 positive cells (%) and total number of cells. Since obtained data corresponded to quantitative variables, the following procedure was applied. Shapiro-Wilks normality test was performed in order to evaluate data distribution. When normally distributed, One Way ANOVA was used, followed by the Bonferroni's Multiple Comparison Test in order to compare biomaterial formulations. For non-parametric data, the Kruskal-Wallis test was used, followed by Dunns test. Asterisks indicate statistical significance: * $p< 0.05$; ** $p<0.01$; *** $p<0.001$.

# 3. Results

## 3.1. System structure and characterization

Hydroxyapatite microspheres with a 500–560 μm diameter were produced and analyzed by STEM-EDS, to assess the Sr incorporation (Figure 7B–E). The ultrastructure of the microspheres, shown in Figure 7A', presented a porous network with the HAp crystals being within the range of 0.43 μm to 1.5 μm. Four sequential areas from periphery to center were considered. Although minimal, a continuous decrease in the Sr weight (%) was observed, from periphery to center (4.03% to 3.28%, respectively – Figure 7F).

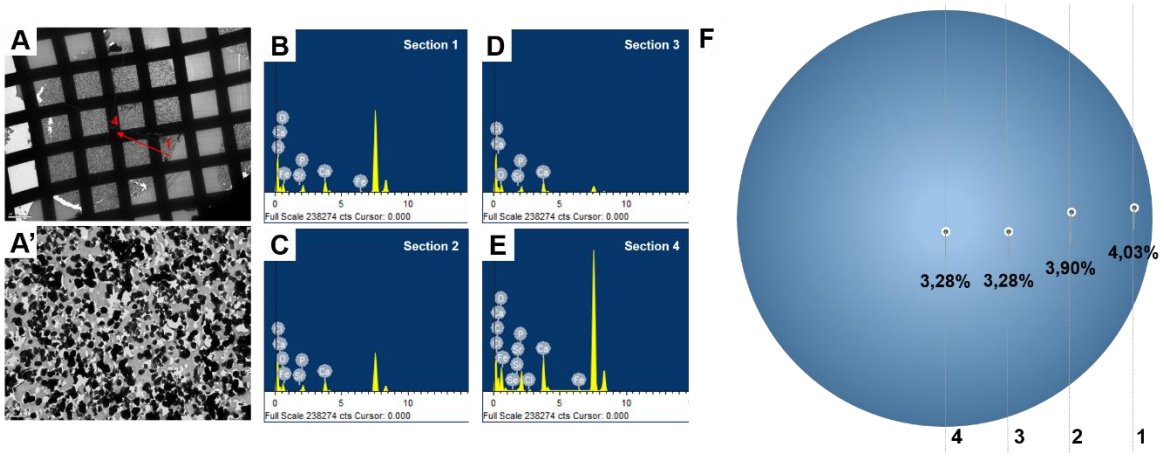


**Figure 7 – Strontium distribution within the HAp microspheres, by STEM-EDS analysis.** Ultrastructure images of Hap microspheres, with analyzed areas in red **(A)** and at high magnification **(A')**. **(B)** Sr weight (%) dispersion within the microspheres, from center to periphery, with the respective EDS spectra **(C–F)**.

The process of obtaining making particles of fetal membranes was optimized by experimenting an automatized method - mill (three pulses) – and a user-dependent method – cutting with scissors until all tissue fragments were transformed into small particles. Overall, particles obtained with scissors presented a smaller and more consistent size (median value of 330 μm; IQR = 273.7 μm) in comparison to particles produced with the mill (median value of 838 μm; IQR = 758.5 μm), as can be seen in Figure 8. When using the mill, although some particles presented a smaller size, some bigger fragments seemed to escape the blades, even when increasing the number of pulses.

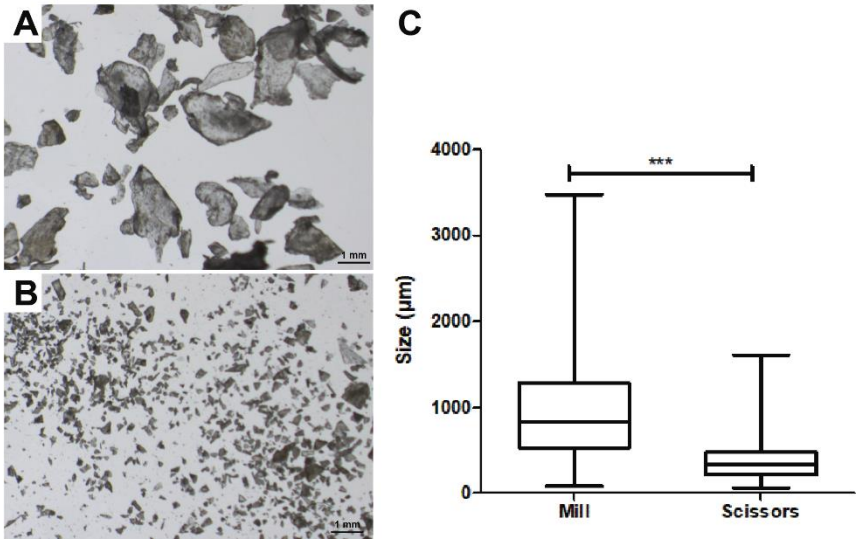


**Figure 8 – Fetal Membranes particles size quantification.** Particles were obtained using either a mill **(A)** or scissors **(B)** and particles size was measured and compared **(C)**. Particles obtained with scissors were significantly smaller (U=9557; p<0.0001; n=238).

Both GL and BL were tested in their simplest control formulations (Alginate and Sr-hybrid, respectively) – Figure 9A. DMA analysis was performed in freshly made materials (control) and after its culture with hGFs and hMSCs for 14 and 21 days, respectively, in order to mimic the *in vivo* environment and evaluate its effect on the mechanical resistance.

In respect to the GL, PRP was successfully dissolved into the alginate and FMs were found to be homogeneously distributed throughout the hydrogel. The incorporation of FMs lead to better mechanical properties in alginate, by increasing both storage and loss modulus (storage modulus: 4.4 and 5.2 MPa of FMs and FMs+PRP, against the 1.0 MPa of Alginate; loss modulus: 0.9 and 1.0 MPa of FMs and FMs+PRP, against the 0.1 MPa of Alginate), even though a significance was only observed in the loss modulus.

Regarding BL, all formulations showed a homogenous distribution of the microspheres within the alginate. In line with previous results, PRP was efficiently dissolved in the alginate and FMs particles were found to be incorporated within the spaces between the microspheres (Figure 9A-g and h). All BL formulations presented higher storage modulus with respect to the GL (Sr-hybrid: 30.2 MPa). A significant increase of the storage modulus of the BL was observed after cell culture (Sr-hybrid after cell culture: 86.9 MPa), with consequent increased stiffness, due to the change in the proportion of microspheres to alginate.

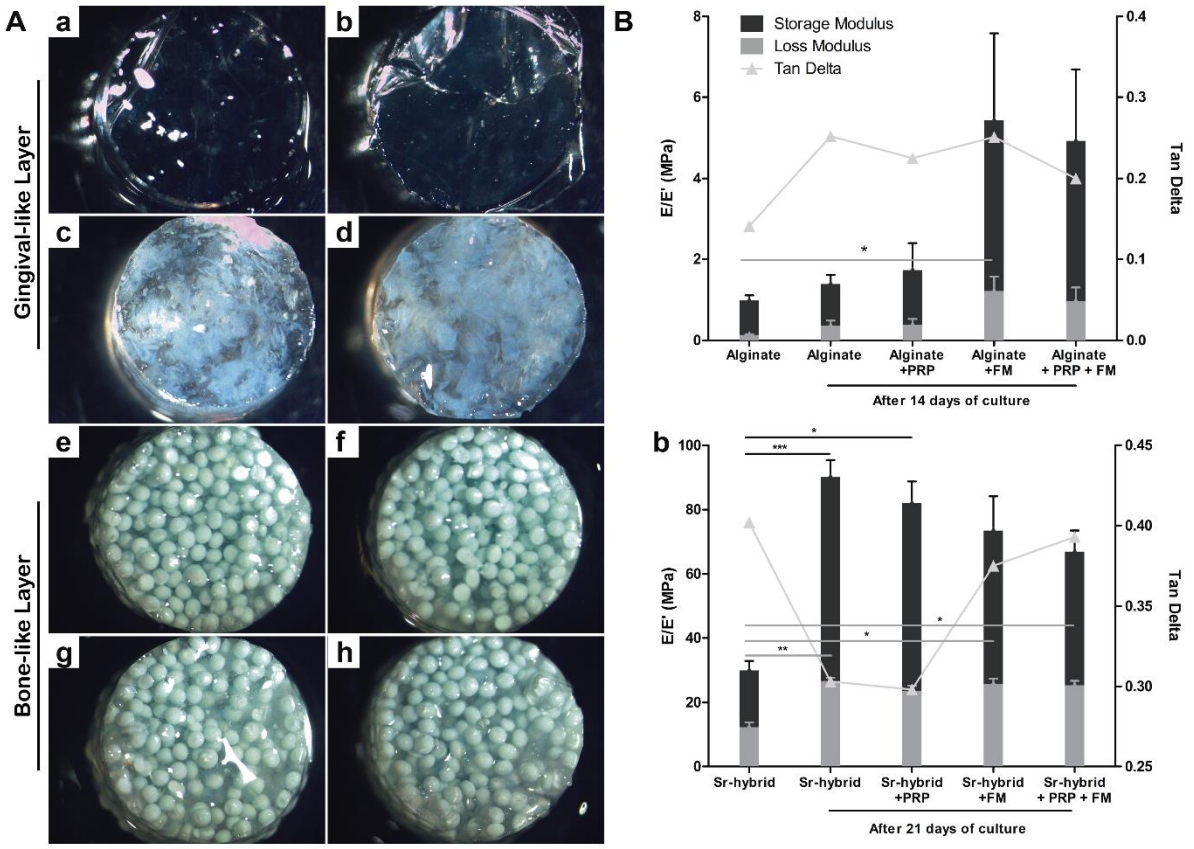


**Figure 9 – Mechanical comparison between different GL and BL formulations, by DMA. (A)** Macroscopic images of the different GL formulations (Alginate (a), Alginate with PRP (b), Alginate with FMs (c) and a combination of Alginate with PRP and FMs (d)) and BL formulations (Sr-hybrid (e), Sr-hybrid with PRP (f), Sr-hybrid with FMs (g), Sr-hybrid with both PRP and FMs (h)). **(B)** DMA analysis of GL formulations (a); and BL formulations (b), before and after cell culture (14 days for GL and 21 days for BL) (GL formulations: Storage Modulus: $X^2_{KW}$ (4) = 9.21; p= 0.0562; n=3; Loss Modulus: $X^2_{KW}$ (4) = 10.53; p= 0.0324; n=3; BL formulations: Storage Modulus: $X^2_{KW}$ (4) = 19.59; p= 0.0006; n=5; Loss Modulus: $X^2_{KW}$ (4) = 17.56; p= 0.0015; n=5).

Micro-CT imaging was performed to further explore the bilayer formulation, incorporating FMs in both layers (Figure 10A). MICRO-CT results further support the ones observed in Figure 9, regarding the successful incorporation of FMs into the Sr-hybrid.

Additionally, both GL and BL were tested either individually or in their bilayer construction (ratio of 1:3 GL to BL), in order to assess the bilayer material stability and mechanical behaviour (Figure 10B). During DMA analysis, no samples exhibited signals of breaking. A significant increase of both storage and loss modulus was observed in BL, comparing to GL and the bilayer formulation. Although non-significant, the bilayer formulation showed higher mechanical resistance that GL (from 1.0MPa to 3.3MPa) due to the microspheres incorporation in the BL.

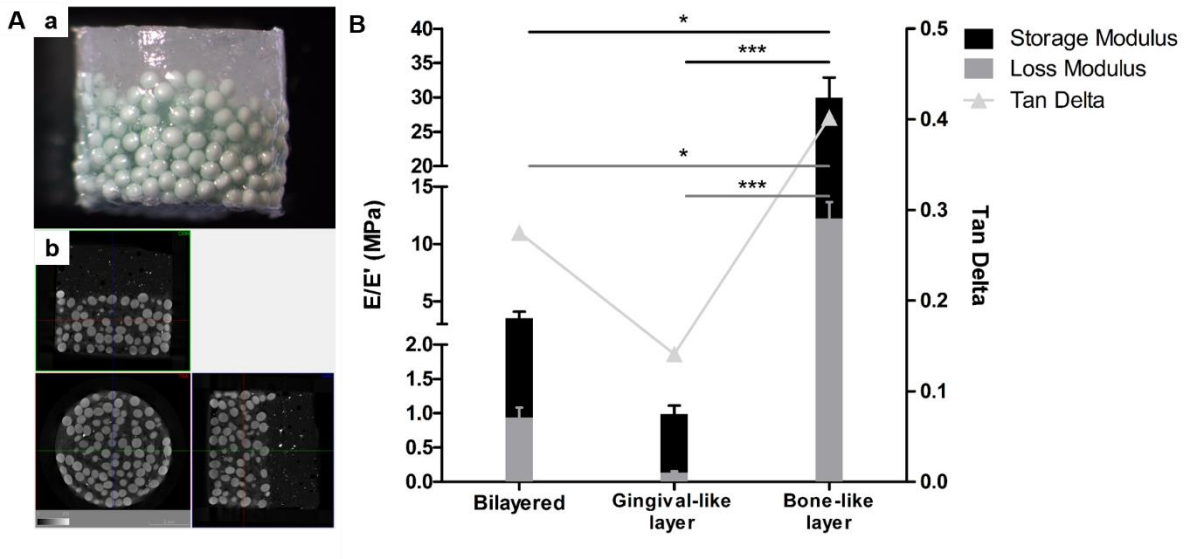


**Figure 10 – Characterization of the bilayer biomaterial, by Micro-CT (A) and DMA (B). (A) Macroscopic ima**ge of the bilayer biomaterial, composed of the gingival-like layer (upper layer - Alginate 3.5% with FMs) and the bone-like layer (bottom layer – Sr-hybrid with FMs) **(a)** and orthogonal reconstructed slices of micro-CT **(b)**. **(B)** DMA analysis of the bilayer biomaterial and its separated layers – GL and BL, all in absence of FMs. (Storage Modulus: $X^2_{KW}(2) = 14.74$; p= 0.0006; n=4; Loss Modulus: $X^2_{KW}(2) = 14.74$; p= 0.0006; n=4).

## 3.2. Fetal Membranes

### 3.2.1. FMs structure and decellularization efficacy

FMs underwent a decellularization process in order to remove cells from the tissue. HE and DAPI staining showed that cell nuclei appeared to be successfully removed from both AM and CM, while the overall architecture was preserved (Figure 11A). Picro-sirius Red staining, when viewed under polarized light, can distinguish between different types of collagen fibril exhibiting either green or red tones, commonly associated with collagen III and I, respectively. Although CM matrix seemed to be more open, no differences were observed in the collagen content, being the proportion of collagen I to collagen III similar to native state. When observing FMs using TEM analysis and although nuclei were removed, small debris of heterochromatin could still be observed. Meanwhile, both basal membrane and collagen matrix were preserved, after decellularization, even though the collagen matrix seemed looser.

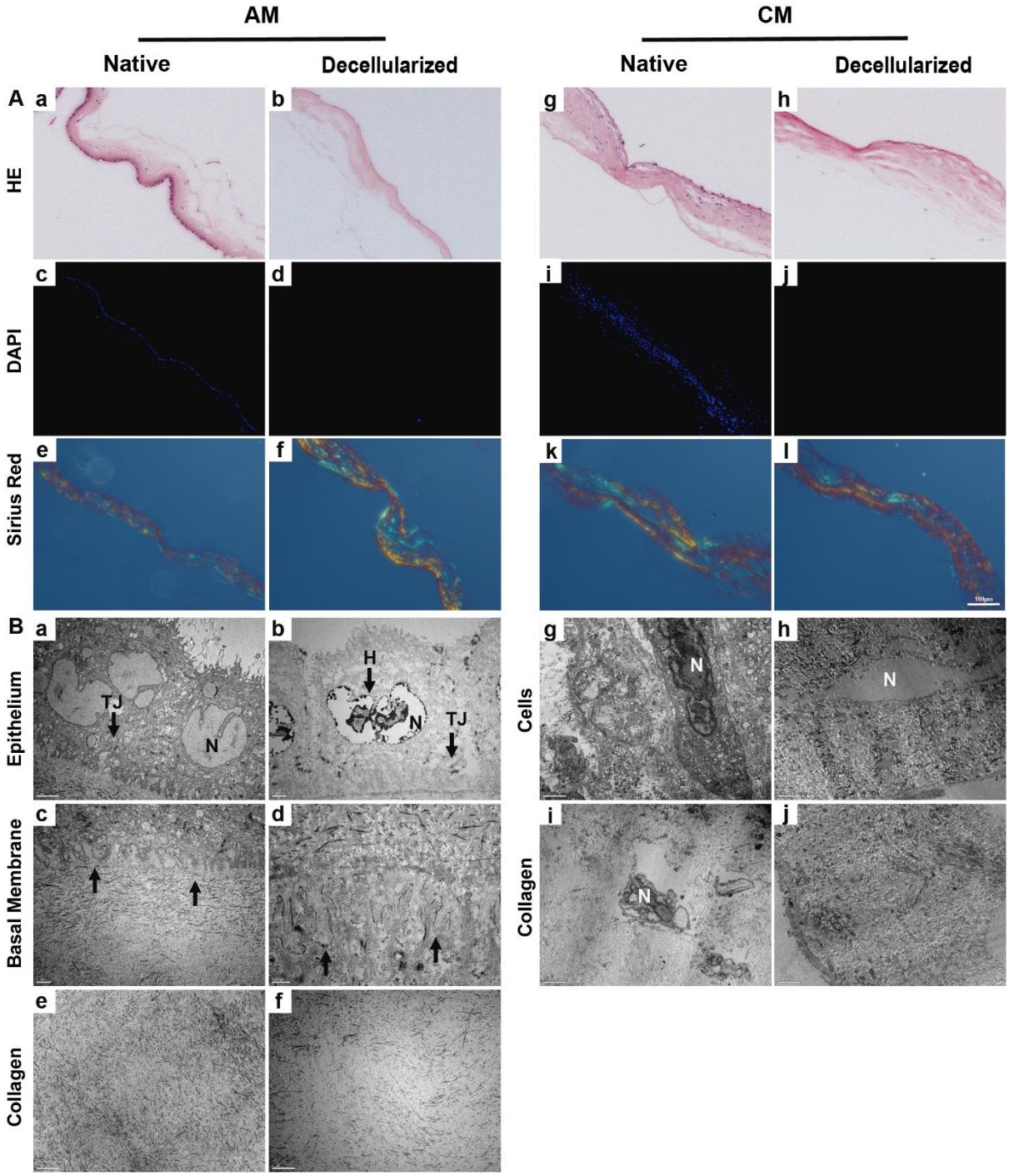


**Figure 11 – Evaluation of fetal membranes (FMs) extracellular matrix after decellularization, using histology (A) and transmission electron microscopy (B). (A)** Hematoxylin and Eosin (a,b, g, h), DAPI (c, d, I, j) and polarized images of PSR staining (e, f, k, l) of both AM (a–f) and CM (g–l), in their native and decellularized state. **(B)** TEM analysis of native and decellularized amniotic membrane (a–f) and chorionic membrane (g–j). N – nuclei; TJ – tight junctions; H – heterochromatin; basal membrane is identified with black arrows.

Furthermore, SEM analysis confirmed previous results (Figure 12A). AM presented an intact and uniform epithelium in their native state, which can be found partially disrupted, after decellularization. When observing the stromal side, collagen fibrils can be seen, with a looser matrix, after decellularization.

Likewise, CM showed the presence of some cell debris with the preservation of collagen fibrils in the stromal side, after the decellularization process.

AFM analysis provided information regarding FMs surface roughness (Figure 12B). As expected, CM was thicker, with a median height of 6.3 μm, comparing to 5.6 μm of the AM. After decellularization, a consistent decrease of both roughness and height was observed in both membranes, being statically significant for surface roughness, between CM and decellularized CM.

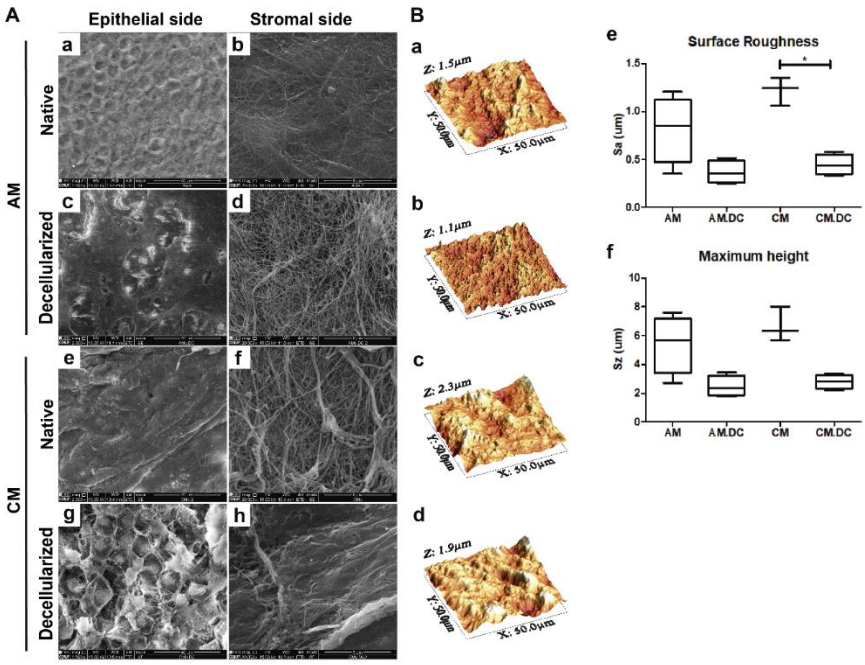


**Figure 12 – Evaluation of fetal membranes (FMs) extracellular matrix after decellularization, using both scanning electronic microscopy (A) and atomic force microscopy (B). (A)** SEM analysis of both amniotic (a–d) and chorionic membrane (e–g). In a and e, the intact epithelium of the native membranes can be found. After decellularization, nuclei were removed (c and g). Both membranes stroma maintained its fibrillar composition, where detailed fibers can be seen in d and h. **(B)** AFM analysis showed a reduction in thickness variability of both membranes. Surface roughness was found to be significantly decreased in chorionic membrane after decellularization ($X^2_{KW}(3) = 9.21$; $p = 0.0266$; $n=4$).

### 3.2.2. FMs effect on hDFs metabolic activity

The effect of relevant concentrations of FMs on human fibroblasts' behaviour was evaluated. Fibroblasts were cultured in the absence or presence of FMs, under different formulations (solubilized, extracts and particles) in the range of 0.5 to 20 mg/ml. Both in solubilized FMs and FM particles, native FMs were used as control for the evaluation of the decellularization effect. FM extracts were solubilized either in distilled water or DMEM. Cells were seeded on alginate alone (control) or containing FMs. Metabolic activity was measured along time (Figure 13).

Overall, there was an increase in the metabolic activity in all conditions, from day 3 to day 21. Additionally, overall native FMs showed a higher metabolic activity when compared to decellularized FMs, FMs solubilized and particles. Also, higher values were observed when using FMs extracts with DMEM as

substrate, which can be associated to the quicker Sr release, through the Ca (present in the media) trade. From all tested formulations, higher metabolic activity was found to be present when using FMs particles (20 mg/ml). Although native FMs presented higher values, its use carries higher risk of hostile immune response (75). From the decellularized FM particles, the concentration of 20 mg/ml reached an increase of 1.5-fold, compared to the control, and was, therefore, chosen.

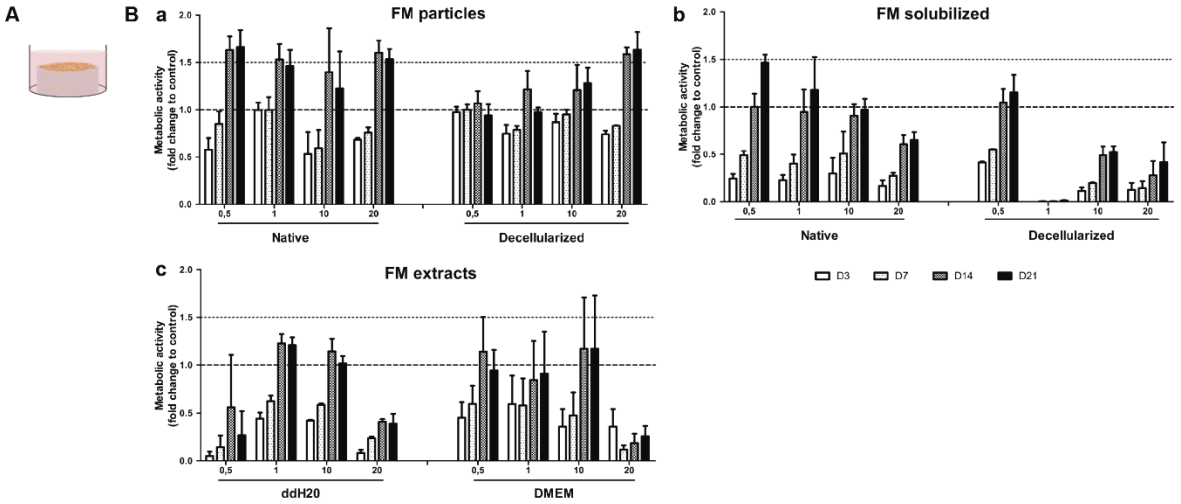


**Figure 13 – FMs concentration effect on fibroblast metabolic activity. (A)** Schematic representation of experimental design, with hDF seeded on top of the alginates discs. **(B)** Metabolic activity of fibroblasts from day 3 up to day 21, cultured on control (alginate 3,5%); alginate with FMs particles (a), alginate with solubilized FMs (b) and alginate with FMs extracts **(c)**, using concentrations of 0.5, 1, 10 and 20 mg/ml, both native and decellularized (with exception of FMs extracts which were tested using DMEM or distilled water as a substrate).

## 3.3. PRP effect on hDF viability and metabolic activity

The effect of different concentrations of PRP on human fibroblasts was evaluated. Fibroblasts were cultured in the absence or presence of PRP, in a concentration range from 5 to 100% (Figure 14). Cells were seeded on alginate in the presence of PRP and alginate alone was used as control. Metabolic activity was evaluated at both day 15 and 21 and viability was assessed at day 21 (Figure 14).

Live/Dead assay images show (Figure 14B) that a higher cell number was found at concentration of 10% and 100%. Although non-significant, a higher number of dead cells were identified at 5%. An increase in metabolic activity was observed in the presence of PRP at 10% and 100%, compared to the control, being the latter statistically significant at day 15. However, during the process of making the alginate discs, for the 100% concentration a higher reticulation time was needed (over 1 hour). Since the need for such time during a surgical procedure is highly impractical, this concentration was excluded and 10% of PPR was chosen.

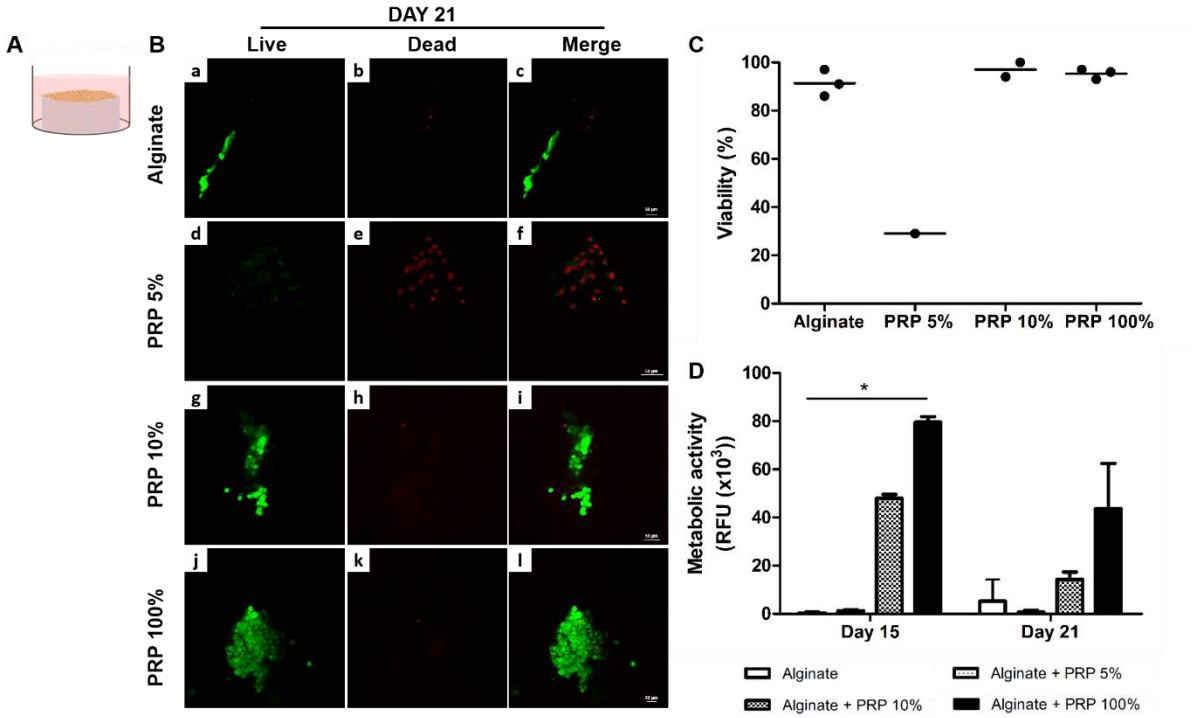


**Figure 14 – PRP concentration effect on fibroblast viability and metabolic activity. (A)** Schematic representation of experimental design, with hDF seeded on top of the alginates discs. **(B)** Viability of fibroblast, at 21 days, cultured on alginate (a-c); alginate +PRP 5% (d-f); alginate+PRP 10% (g-i); alginate+PRP 100% (j-l) ), imaged by CLSM (Z projection, live cells in green, dead cells in red, scale bar: 50µm.). **(C)** Quantification of viability (Nlive cells/Ntotal cells), using FIJI software. A Macro was produced in order to apply the same workflow to all images. **(D)** Metabolic activity, result of Resazurin assay (Day 15: $X^2_{KW}(3) = 9.0$; p= 0.0293; n=3 and Day 21: ($X^2_{KW}(3) = 7.8$; p= 0.0509 n=3).

## 3.4. Effect of GL in hGFs viability, proliferation and morphology

After establishing the effect of relevant concentrations of both PRP and FMs, the effect of the GL formulations on human fibroblasts was evaluated. Fibroblasts were cultured on alginate either with 10% of PRP, 20 mg/ml of FMs or with a combination of both. Alginate alone was used as control. After 14 days of culture, viability (Live/Dead assay) and morphology (Phalloidin staining) were assessed.

At day 14, no significant differences in viability were observed in all tested formulations (Figure 15). As shown in Figure 15C, fibroblasts seem to present a progressive increase in the number of cells from control to alginate with PRP, FMs and lastly, the combination of both PRP and FMs. Additionally, morphology did not seemed altered in all conditions, all cells presenting typical fibroblast-like phenotype (Figure 15C). However, while in the presence of either alginate or alginate with PRP, cells seemed to form small clusters of cells, when in contact with materials containing FMs cells formed dense panels of cells, surrounding the FMs particles, which was particularly more evident in the FMs with PRP formulation.

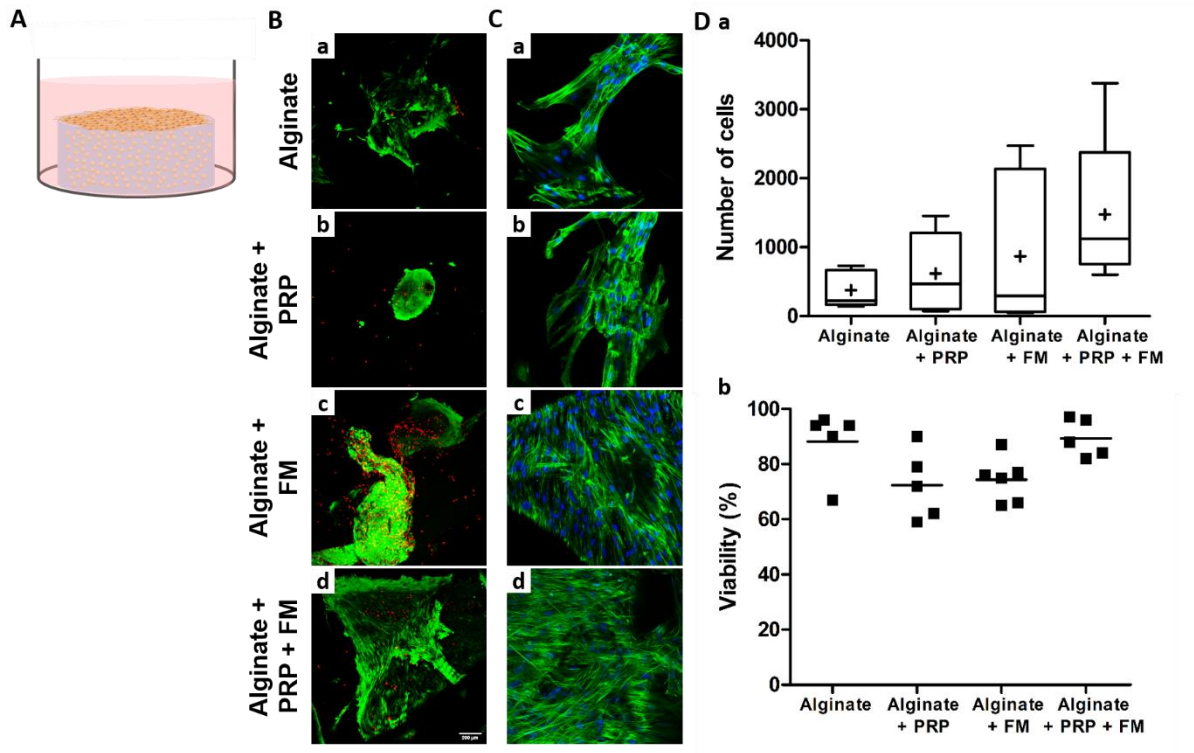


**Figure 15 – GL formulations effect on hGFs survival and morphology. (A)** Schematic representation of the experimental design, with hGFs seeded on top of the GL formulations. **(B)** Viability of hGFs cultured on Alginate (a), Alginate with PRP (b), Alginate with FMs (c) or Alginate with combination of both PRP and FMs (d), after 14 days, imaged by CLSM (Z projection; live cells in green; dead cells in red; scale bar: 200μm). **(C)** Phalloidin staining of hGFs cultured on Alginate (a), Alginate with PRP (b), Alginate with FMs (c) or Alginate with a combination of both PRP and FMs (d), after 14 days, imaged by CLSM (Z projection; phalloidin in green; nuclei in blue; scale bar: 50μm). **(D)** Quantification of live/dead images, for (a) number of cells and (b) viability ($N_{live\ cells}/N_{total\ cells}$).

In addition, after 14 days, proliferation was assessed through Ki67 staining. Metabolic activity was evaluated from day 3 up to day 14 (Figure 16). Consistent with previous results, a higher cell number was observed in alginate with FMs and alginate with PRP and FMs (Figure 16A). Interestingly, a significant decrease in the number of cells in proliferation was found in the alginate with PRP and FMs, compared to both alginate alone (control) and alginate with PRP. As depicted in Figure 16B, metabolic activity suffered an increase over time, in all formulations (with exception of control). The incorporation of FMs (both alone or in combination with PRP) lead to a slight increase in the metabolic activity, at all measured time-points, when compared to control, being this difference more significant at day 14.

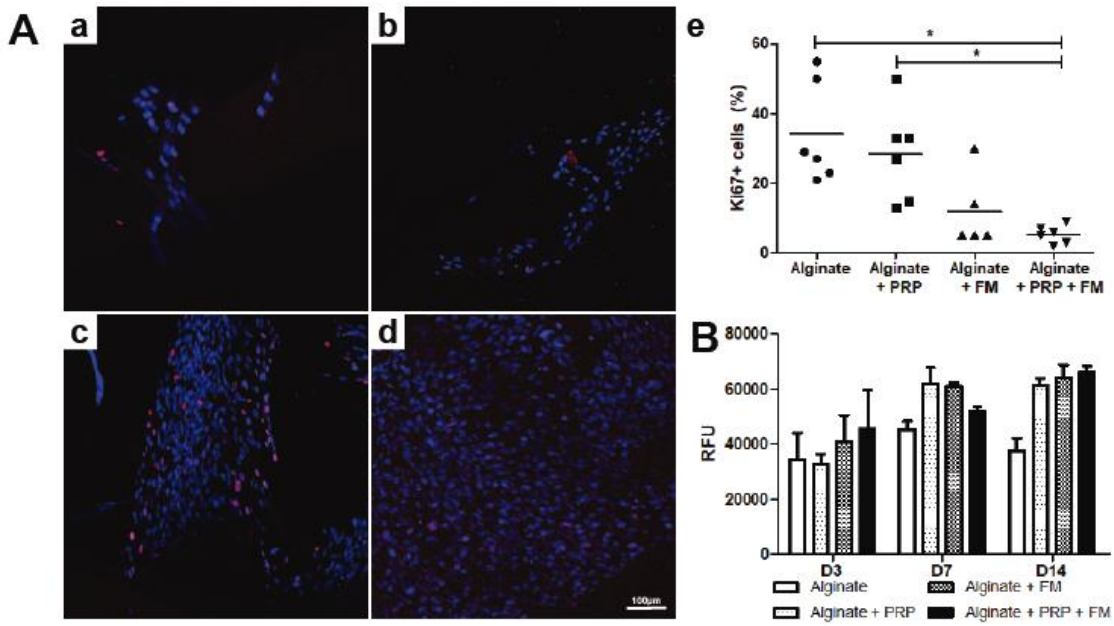


**Figure 16 – GL formulations effect on hGFs proliferation and metabolic activity. (A)** Ki67 staining of hGFs cultured on alginate alone (a), alginate with PRP (b), alginate with FMs (c) or alginate with PRP and FMs (d), after 14 days of culture, imaged by CLSM (Z projection; nuclei in blue and positive ki67 staining in pink; scale bar: 100µm). (e) Quantification of ki67+ cells percentage ($N_{Ki67+cells}$ / $N_{total\ cells}$) ($X^2_{KW}(3) = 13.52$; $p = 0.0036$; $n=5$). **(B)** Metabolic activity, result of Resazurin assay, at day 3, 7 and 14.

## 3.5. Effect of BL in hMSCs viability, morphology, proliferation and differentiation

Furthermore, a similar study was conducted, now addressing the effect of BL formulations on osteogenesis, using hMSCs. hMSCs were cultured on the Sr-hybrid (alginate with HAp-microspheres) either with 10% of PRP, 20 mg/ml of FMs or with both. The Sr-hybrid alone was used as control. Metabolic activity was evaluated from day 3 until day 21. After 21 days of culture, viability (Live/Dead assay), morphology (Phalloidin staining), proliferation (Ki67 staining) and differentiation capacity (ALP and Alizarin staining) were assessed.

In all BL formulations, viability was not compromised, after 21 days of culture (Figure 17), although a slight increase was observed in both formulations containing FMs. Moreover, no differences were observed regarding the morphology (Figure 17B). Similar to what was previously observed with hGFs, hMSCs seem to form a panel of cells when in the presence of FMs (both alone and with PRP). Additionally, a significant increase in cell number was observed with these formulations (Figure 17D). The combination of brightfield with fluorescence imaging facilitated the identification of cells co-localizing with the microspheres, thus, showing that cells were either located in the vicinities or surrounding the microspheres, which was particularly more significant in the formulations incorporating FMs.

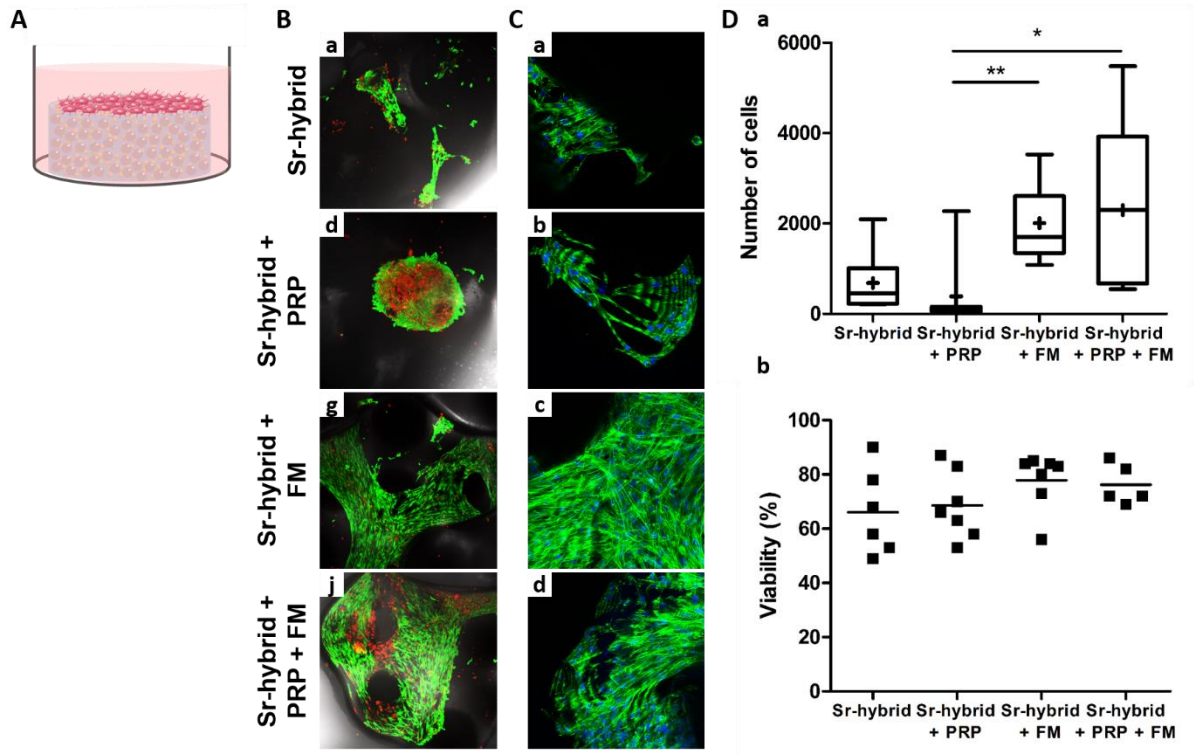


**Figure 17 – BL formulations effect on hMSCs survival and morphology. (A)** Schematic representation of the experimental design, with hMSCs seeded on top of the BL formulations. **(B)** Viability of hMSCs cultured on Sr-hybrid (a), Sr-hybrid with PRP (b), Sr-hybrid with FMs (c) or Sr-hybrid with a combination of both PRP and FMs (d), after 21 days, imaged by CLSM (Z projection; Live cells in green; dead cells in red; brightfield in grey scale showing the contour of the microspheres in black; scale bar: 200µm). **(C)** Phalloidin staining of hMSCs cultured on Sr-hybrid (a), Sr-hybrid with PRP (b), Sr-hybrid with FMs (c) or Sr-hybrid with combination of both PRP and FMs (d), after 21 days, imaged by CLSM (Z projection; phalloidin in green; nuclei in blue; scale bar: 50µm). **(D)** Quantification of live/dead images, for (a) number of cells and (b) viability ($N_{live\ cells}/N_{total\ cells}$). ($X^2_{KW}$ (3) = 13.73; p= 0.0033; n=5).

Furthermore, proliferation was assessed through Ki67 staining, after 21 days and metabolic activity was evaluated from day 3 up to day 21 (Figure 18). An increase in cell number was also found in formulations incorporating FMs. However, no significant differences were observed in the number of proliferating cells, among all tested formulations even though a tendency for an increase in the Sr-hybrid with PRP formulation was found.

In terms of metabolic activity, a peak seem to appear at day 7 and, afterwards, a slight decrease was observed (Figure 18B). Nevertheless, and although at an earlier time-point (day 7) higher values of metabolic activity were found in the formulation containing PRP, at day 21, the formulation incorporating both PRP and FMs presented the higher values among all tested formulations.

Differentiation was also investigated through ALP, an early osteogenic staining, and Alizarin, a staining for mineralized deposits (Figure 18C). At day 21, higher expression of ALP activity was found in the control and in the formulation containing FMs alone, while matrix mineralization was found to be present in Sr-

hybrid with FMs and Sr-hybrid containing both PRP and FMs, indicating the enhancement of osteogenic differentiation.

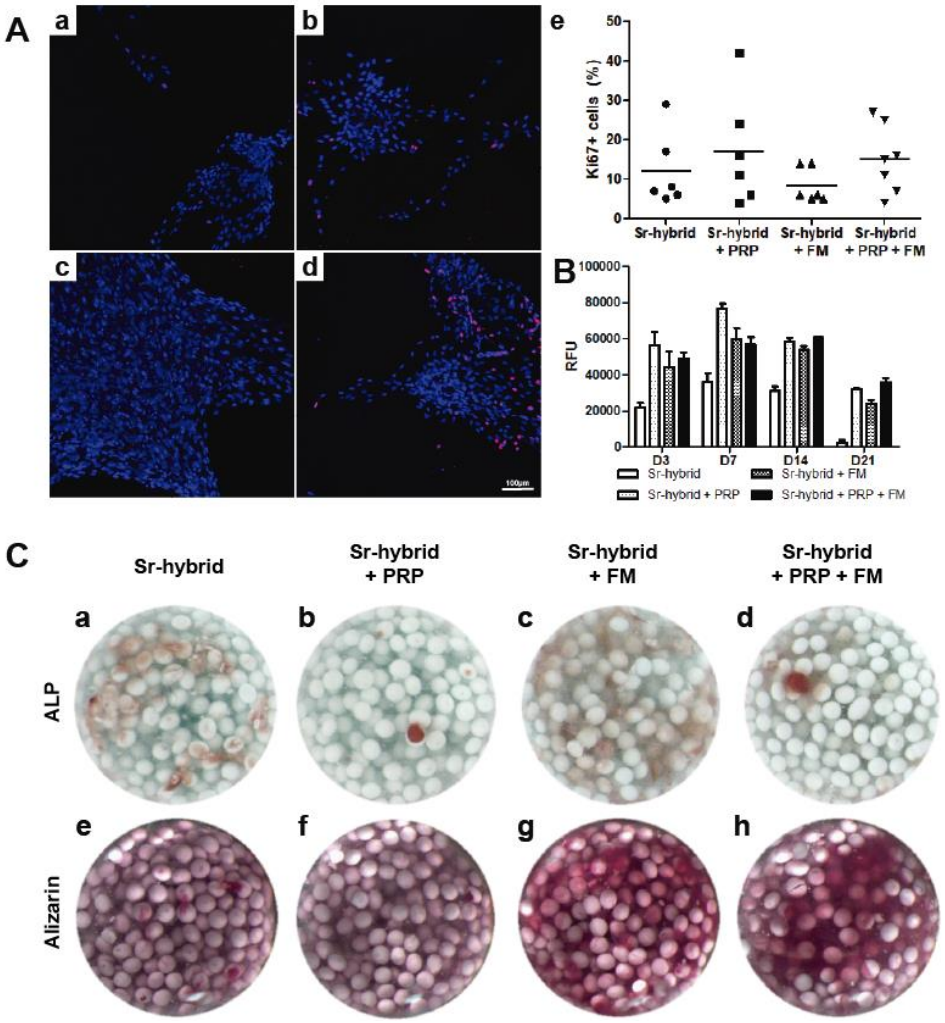


**Figure 18 – BL formulations effect on hMSCs proliferation, metabolic activity and differentiation. (A)** Ki67 staining of hMSCs cultured on Sr-hybrid alone (a), Sr-hybrid with PRP (b), Sr-hybrid with FMs (c) or Sr-hybrid with PRP and FMs (d), along 21 days of culture, imaged by CLSM (Z projection; nuclei in blue and positive ki67 staining in pink; scale bar: 100µm). (e) Quantification of ki67+ cells percentage ($N_{Ki67+cells}$ / $N_{total\ cells}$). **(B)** Metabolic activity, result of Resazurin assay, at day 3, day 7, 14 and 21. **(C)** ALP (a-d) and Alizarin (e-h) staining of Sr-hybrid (a and e), Sr-hybrid with PRP (b and f), Sr-hybrid with FMs (c and g) and Sr-hybrid with PRP and FMs (d and h).

## 3.6. Proteomic profile of hGFs response

Taking into account the results obtained from the previous experiments, formulations containing only PRP were not considered for the proteomic evaluation. Therefore, four samples were submitted for LC-MS/MS analysis: hGFs cell lysate acted as control (fibroblasts cultured in 2D without the biomaterial); hGFs cultured with alginate; hGFs cultured with alginate with FMs and, lastly, hGFs cultured with alginate with FMs and PRP. All experiments with biomaterials were performed in transwells, being the biomaterials placed in the top compartment and the cells seeded on the bottom. Fold-change was

obtained in relation to the protein expression level of the control. A fold-change of >2 and a p value of <0.05 was set to select the altered proteins.

Overall, a higher number of altered proteins (both up and downregulated) was observed for formulation containing FMs and the combination of FMs and PRP, which can be observed in the volcano plots shown in Figure 19.

After remotion of contaminants (albumin from BSA) and proteins which were not detected in all samples (which might be due to a technical error), a total of 392 altered proteins were considered. From those, 165 were found to be altered in alginate, 213 in alginate with FMs and 269 in alginate with FMs and PRP. A number of 47 proteins were only altered in alginate, while 64 were found in alginate with FMs and 95 in alginate with the combination of both FMs and PRP (Figure 19C).

Values of protein expression for the altered proteins were submitted to hierarchical clustering with Morpheus software, where a heat map and respective dendogram was obtained (Figure 19D).

In order to explore the biological processes affected by the different clusters found in the dendograms (K1-K6), we performed gene ontology enrichment analysis (through DAVID), using the proteins identified in the different clusters. This analysis allows for the determination of the GO terms that occurred more frequently than expected by chance. Within the first cluster (K1), which seem to be increased in formulations containing FMs (but specifically in the alginate with FMs and PRP), there was a significant enrichment of GO terms mainly related to ECM. Whereas in K2 (proteins decreased in alginate with FMs and increased in alginate with FMs and PRP), an enrichment of adenosine triphosphate (ATP) synthesis and of ATPase activity was found. Among the proteins found in K4 (which seems to be only increased in the alginate formulation), an enrichment of GO terms such as nucleosome and both positive and negative regulation of gene expression was found. Among the proteins (increased in the alginate with FMs formulation) within K6, an enrichment of "cytoskeleton" and "movement of cell" GO terms was found. No other significantly enriched GO terms were found for the remaining clusters. No other significantly enriched GO terms were found for the remaining clusters.

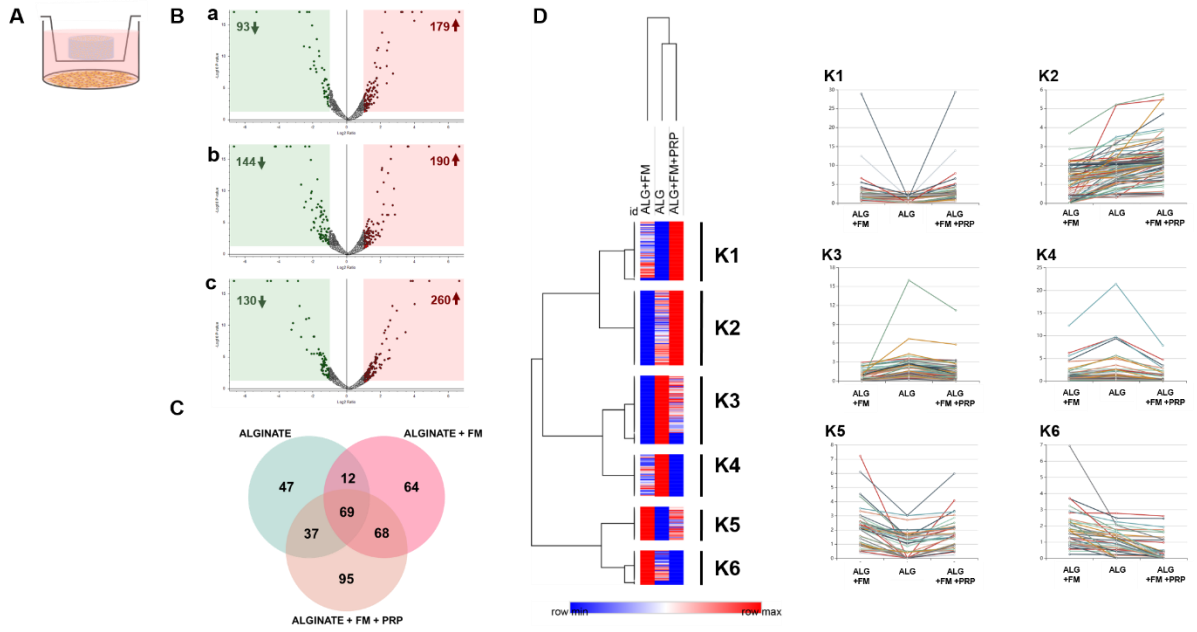


**Figure 19 – LC–MS/MS data analysis. (A)** Schematic representation of the experimental design, with hGFs seeded on 6-well plates and GL formulations placed on the transwell top compartment. **(B)** Volcano plots of protein expression in relation to control (hGFs cell lysate) for alginate (a), alginate with FMs (b) and alginate with FMs and PRP (c). A fold-change > 2 and a p value <0.05 was considered. Downregulated proteins can be found within the green box and upregulated proteins within the red box. **(C)** Venn diagram of altered cleaned proteins for the three formulations. **(D)** Heatmap with the respective dendograms representing the hierarchical clusters. Protein expression levels are represented by color gradient from blue (low) to red (high). Six main clusters were found (K1–K6), which were further represented on the right.

To explore the differences of fibroblast response to the different biomaterials into more detail, both up and down regulated proteins were subjected to the DAVID analysis (Figure 20). The most significant GO terms found to be upregulated in all formulation were "nucleosome" and "collagen catabolic process". Additionally, an enrichment of "protein transport" and "wound healing" terms was found only in the alginate formulation, whereas in alginate with a combination of FMs and PRP a larger number of GO terms was found to be enriched (proteolysis, ECM organization and Platelet alpha granule lumen, among others). The term "mitochondria inner membrane" was exclusive of alginate with FM. And this condition, together with alginate were the only ones associated with "cell-cell adhesion". Meanwhile, the "ECM" GO term was also found to be dowregulated in all formulations, accompanied by "cytoskeleton" and "GTP binding" in the alginate with FMs and PRP.

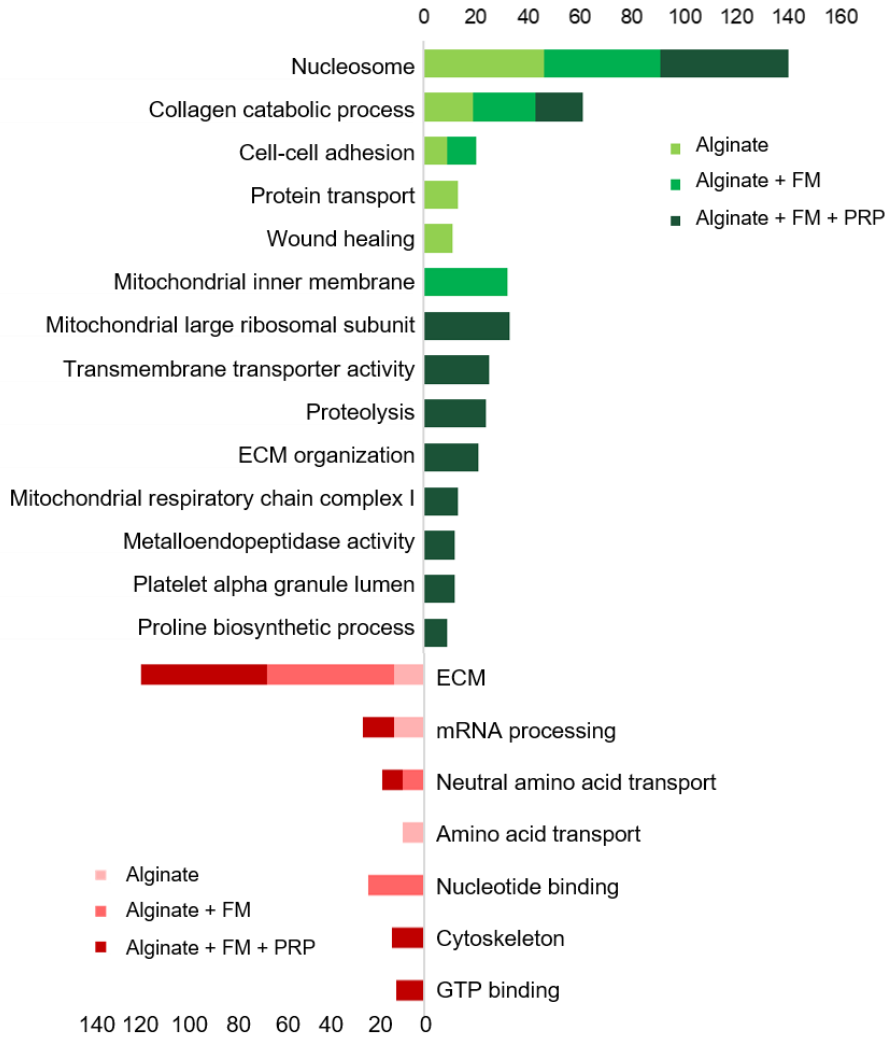


**Figure 20 – Enriched Gene Ontology clusters, following DAVID analysis, for hGFs response to the tested formulations.** Up and down regulated GO terms are identified in green and red, respectively.

Afterwards, reactome analysis was performed for each formulation, in order to assess the pathways in which the altered proteins were associated. When looking at the number of proteins involved in each pathway categories, an overall increase in the number of proteins was found for the alginate with FMs and PRP formulation (Figure 21B). Meanwhile, specifically for alginate with FMs, a decrease in the programmed cell death category can be seen. Moreover, for alginate with FMs and PRP, an increase in the number of proteins involved in ECM organization, metabolism, signal transduction and vesicle-mediated transport was found among other things. Both in gene expression and hemostasis categories, a similar number of proteins involved was observed for alginate with FMs and alginate with FMs and PRP. However, in the case of the immune system category, alginate formulation seems to have a higher number of proteins affecting these pathways, comparing to the two remaining formulations.

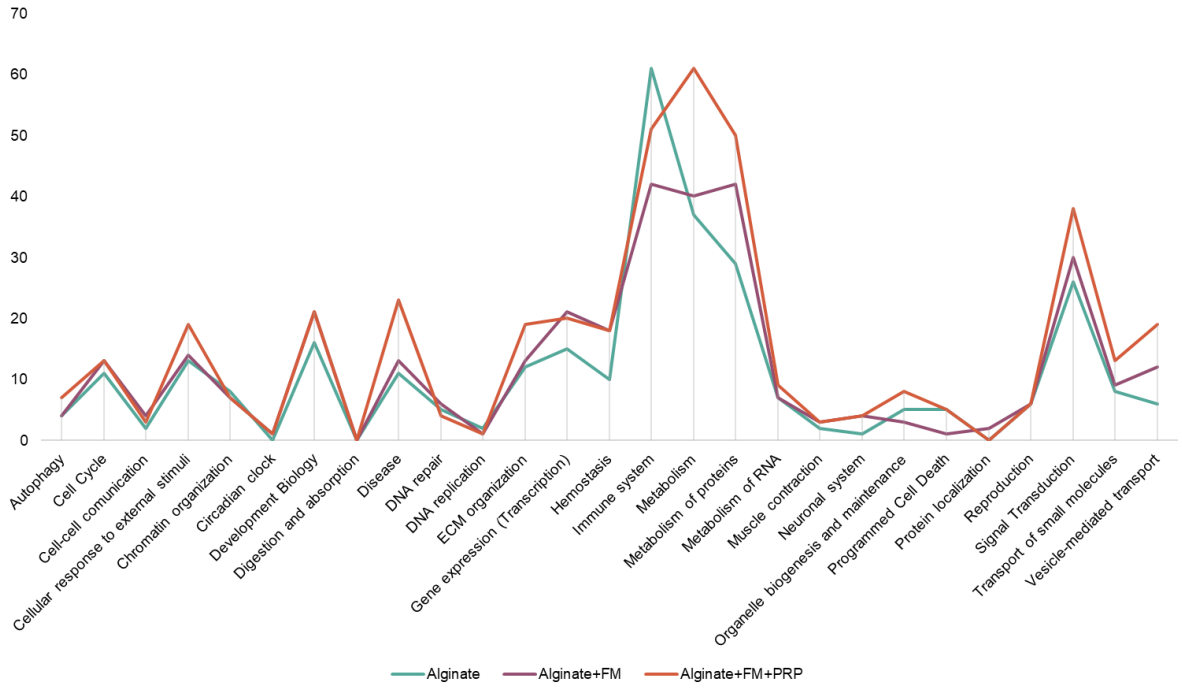


**Figure 21 – Reactome analysis organized by pathway categories.** Representation of the number of altered proteins involved in the pathways categories, for alginate, alginate with FMs and alginate with FMs and PRP.

Furthermore, a search for unique pathways altered in each formulation was conducted (Figure 22). For alginate formulation, and in accordance with previous results, immune pathways were mainly affected, namely: cytokine signaling, through regulation of both Interferon gamma and alpha and Interleukin-7 (IL-7); adaptive immune system pathways, through the Class I MHC mediated antigen processing & presentation. On the other hand, for alginate with FMs formulation, pathways involved in the hemostasis (platelet adhesion to exposed collagen), integrin signaling (MAPK signaling) and signaling by non-receptor tyrosine kinase (PTK6 regulation of RHO GTPases and MAP kinases), were found to be unique. Lastly, for alginate with FMs and PRP, pathways involved in the citric acid cycle and respiratory electron transport (namely in the ATP synthesis); in the receptor for tyrosine kinase (signaling by EGFR, MET, VEGFR2 mediated cell proliferation, ERBB4, NTRKs and IGF1R) and autophagy, were found to be altered only in this formulation.

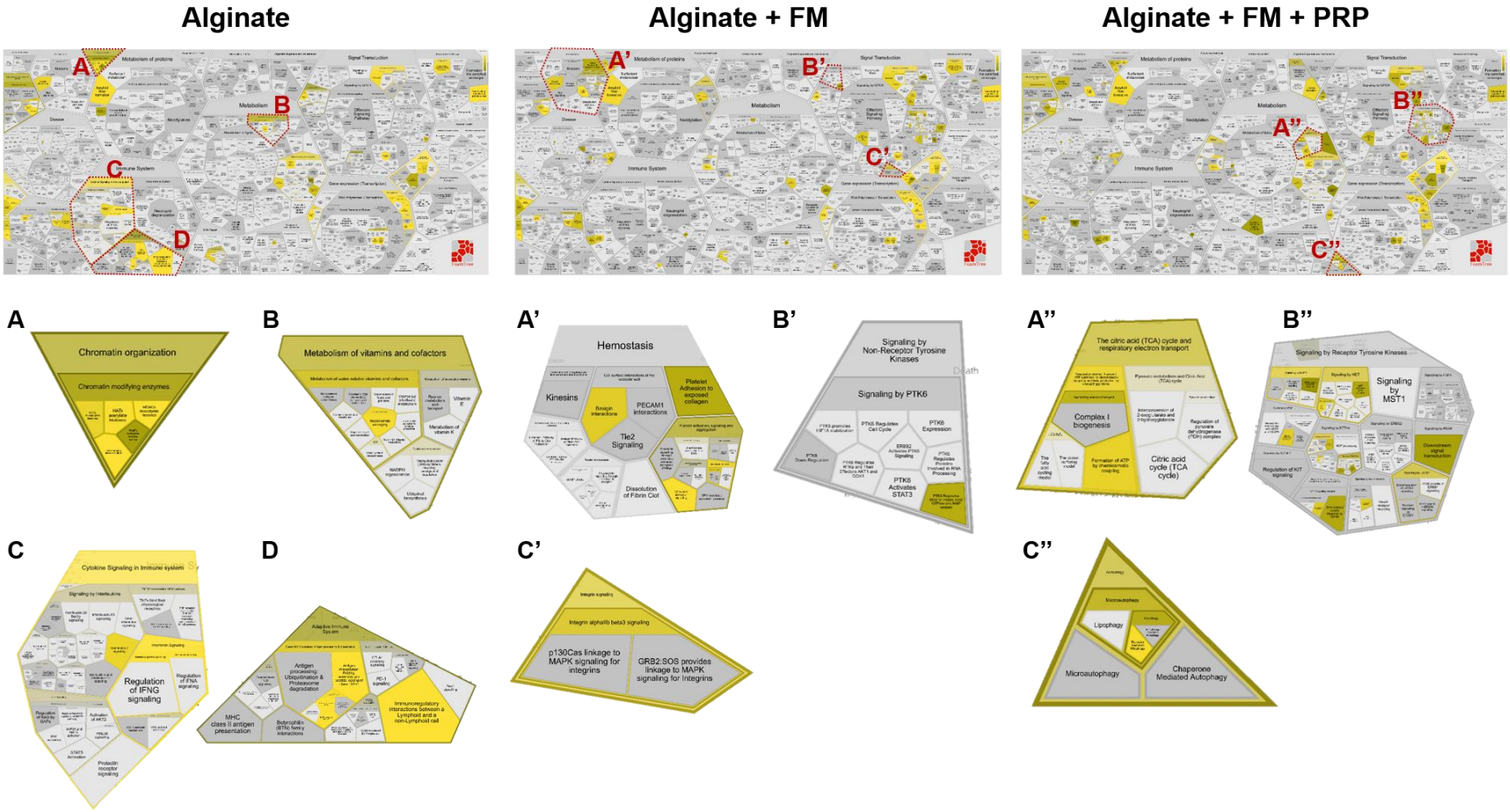


**Figure 22 – Unique pathways affected by each tested formulation, from reactome analysis.** A–D: Alginate unique affected pathways; A'–C': Alginate with FMs unique altered pathways; A''–C''; Alginate with FMs and PRP unique affected pathways. Dotted red lines in pathways overview representation represent the selected pathways below.

## 3.7. Proteomic profile of hMSCs response

The next step of this study was to analyze the proteomic profile of hMSCs response to the tested formulations. Similar to what was done for hGFs analysis, formulation of Sr-hybrid with PRP was excluded for this analysis on the basis of the previous results. Therefore, four samples were considered for LC-MS/MS analysis: hMSCs cell lysate (control); hMSCs cultured with Sr-hybrid; hMSCs cultured with Sr-hybrid with FMs and hMSCs cultured with Sr-hybrid with FMs and PRP. All experiments with biomaterials were performed in transwells, being the biomaterials placed in the top compartment and the cells seeded on the bottom. Once again, a fold-change of > 2 and $p<0.05$ was set to select altered proteins.

An increase in the number of protein found to be upregulated in Sr-hybrid with FMs and PRP was observed, although the same was not verified for downregulated proteins (Figure 23B).

Once more, as it is possible to observe in the Venn diagram, after the database cleaning (remotion of contaminants and possible technical errors), a total of 661 altered proteins were considered. From those, 285 were found to be altered in Sr-hybrid, 326 in Sr-hybrid with FMs and 365 in Sr-hybrid with FMs and PRP. A number of 122 proteins were found to be only altered in Sr-hybrid, while 119 were found in Sr-hybrid with FMs and 175 in Sr-hybrid with the combination of both FMs and PRP (Figure 23C).

Values of protein expression for the altered proteins were then submitted to hierarchical clustering with Morpheus software, where a heat map and respective dendogram was obtained (Figure 23D). Contrastingly, for hMSCs the response to both formulations incorporating FMs was found to exhibit a similar protein expression behavior, since these formulations were grouped together.

Akin to the workflow applied to hGFs response, clusters obtained from Morpheus were subjected to gene ontology enrichment analysis. The first cluster (K1), included proteins that were upregulated in formulations containing both FMs and PRP, but not in alginate, an enrichment of GO terms related to ECM organization, cell adhesion and blood coagulation was found. Among the proteins found in K2 (increased in Sr-hybrid with FMs and PRP, in contrast to FMs), an enrichment of GTP binding and well as platelet degranulation GO terms was found. On the other hand, K3 (proteins increased in Sr-hybrid with FMs) exhibited an enrichment of inflammatory GO terms, such as innate immune response. No other significantly enriched GO terms were found for the remaining clusters.

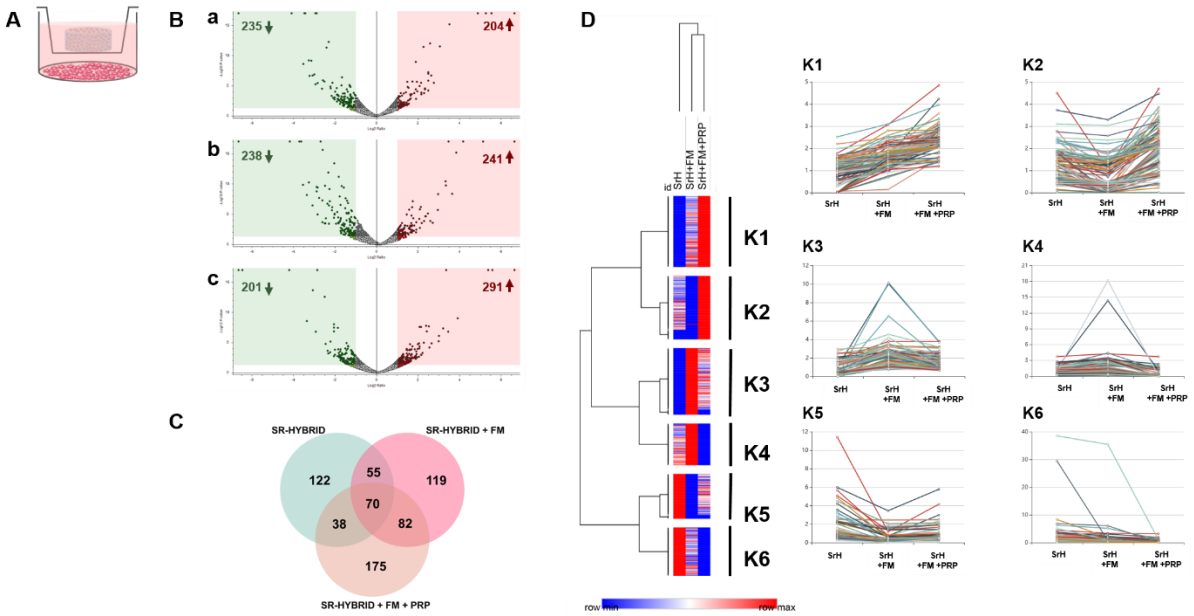


**Figure 23 – LC–MS/MS data analysis. (A)** Schematic representation of the experimental design, with hMSCs seeded on 6-well plates and BL formulations placed on the transwell top compartment. **(B)** Volcano plots of protein expression in relation to control (hMSCs cell lysate) for Sr-hybrid (a), Sr-hybrid with FMs (b) and Sr-hybrid with FMs and PRP (c). A fold-change > 2 and a p value <0.05 was considered. Downregulated proteins can be found within the green box and upregulated proteins within the red box. **(C)** Venn diagram of altered proteins for the three formulations. **(D)** Heatmap with the respective dendograms representing the hierarchical clusters. Protein expression levels are represented by color gradient from blue (low) to red (high). Six main clusters were found (K1–K6), which were further represented on the right.

Both up and downregulated proteins were submitted to DAVID analysis to better understand the hMSCs proteomic profile differences between formulations (Figure 24).

An enrichment in the upregulated proteins related to ECM was found to be present in all formulations, although more significantly in the Sr-hybrid with both FMs and PRP. In formulations containing FMs (Sr-hybrid with FMs and Sr-hybrid with FMs and PRP), both cell-adhesion and innate immune response GO terms were observed to be upregulated, among others. Not only the hybrid with FMs but also the simpler formulation were affecting a cluster of proteins associated with protein ubiquitination. Cytoskeleton and DNA binding GO terms were among those uniquely upregulated in the Sr-hybrid with FMs, while vesicle docking, vesicle-mediated transport, collagen trimer and mitochondrial electron transport were unique to the Sr-hybrid with both FMs and PRP. Regarding the down-regulated GO terms, all formulations present a cluster of cell-adhesion GO term downregulated with an equal number of proteins involved. While only Sr-hybrid with FMs showed a downregulation of terms such as ECM, GTPase activity, nucleotide binding and canonical Wnt signaling pathway. The hybrid with FM and PRP also had a unique downregulation of proteins associated with autoubiquitination and rRNA processing. Like SR-hybrid, when FMs were added without PRP, proteins involved with kinase activity were also underexpressed.

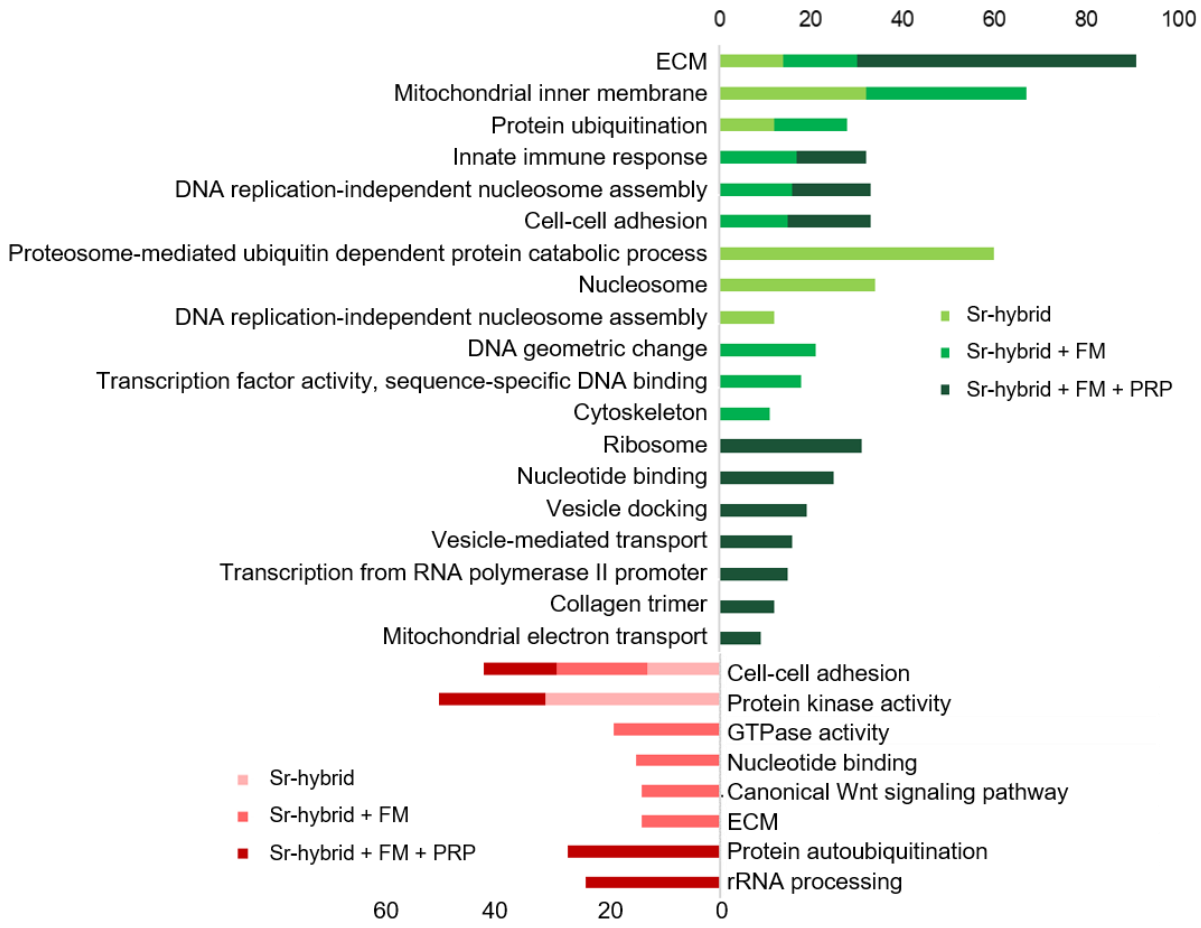


**Figure 24 – Enriched Gene Ontology clusters, following DAVID analysis, for hMSCs response to tested formulations.** Up and down regulated GO terms are identified in green and red, respectively.

When looking at the number of proteins involved in each pathway categories, the trend observed previously with the fibroblasts, with which the formulations containing FMs and PRP exhibited an increase in the number of proteins for all categories, was not observed (Figure 25). Sr-hybrid with FMs showed a higher number of proteins affecting gene expression, immune system, hemostasis, programmed cell death and signal transduction, among others. On the other hand, Sr-hybrid with FMs and PRP has shown an increase in the ECM organization and metabolism.

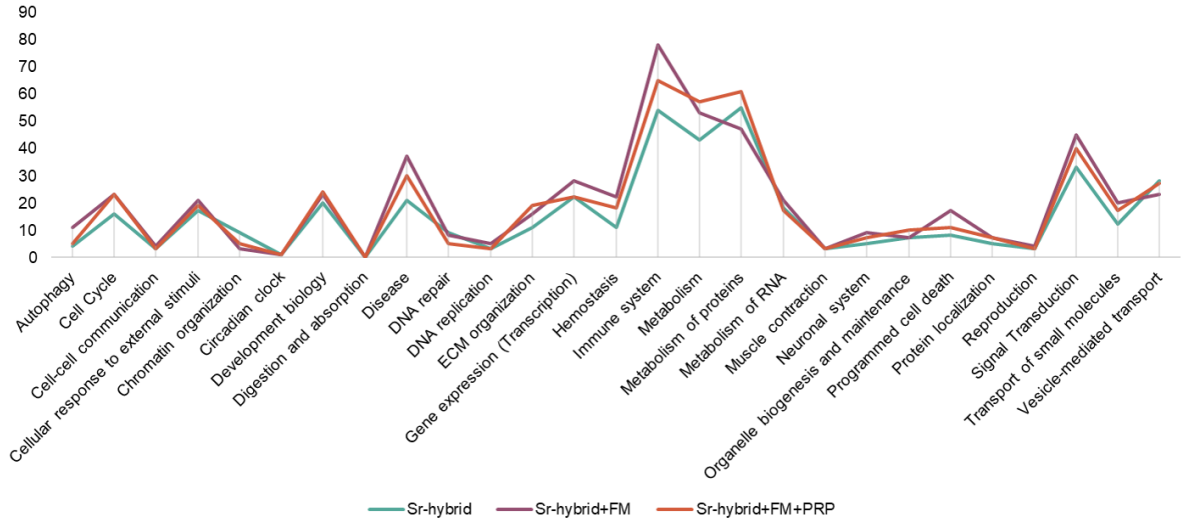


**Figure 25 – Reactome analysis organized by pathways categories.** Representation of the number of altered proteins involved in the pathways categories, for Sr-hybrid, Sr-hybrid with FM and Sr-hybrid with FM and PRP.

Then, a search for unique pathways altered in each formulation was conducted (Figure 26). For the Sr-hybrid formulation, the IGF pathway was found to be altered. On the other hand, for Sr-hybrid with FMs, the signaling transduction was found to be affected, particularly the regulation of NOTCH4, WNT signaling, RAF/MAP kinase cascade, Hedgehog signaling (namely the degradation of GL1, GL2 and the GL3 processing) and, EGFR transactivation. Moreover, Dectin-1 signaling was also uniquely affected as well as the regulation of RUNX3, ultimately leading to the regulation of WNT. Finally, for the Sr-hybrid with both FMs and PRP, the hemostasis category seemed the most uniquely affected, through the fibrin clot formation and the platelet adhesion to exposed collagen. Additionally, L1CAM was also found to be affected, namely the CHL1 interactions.

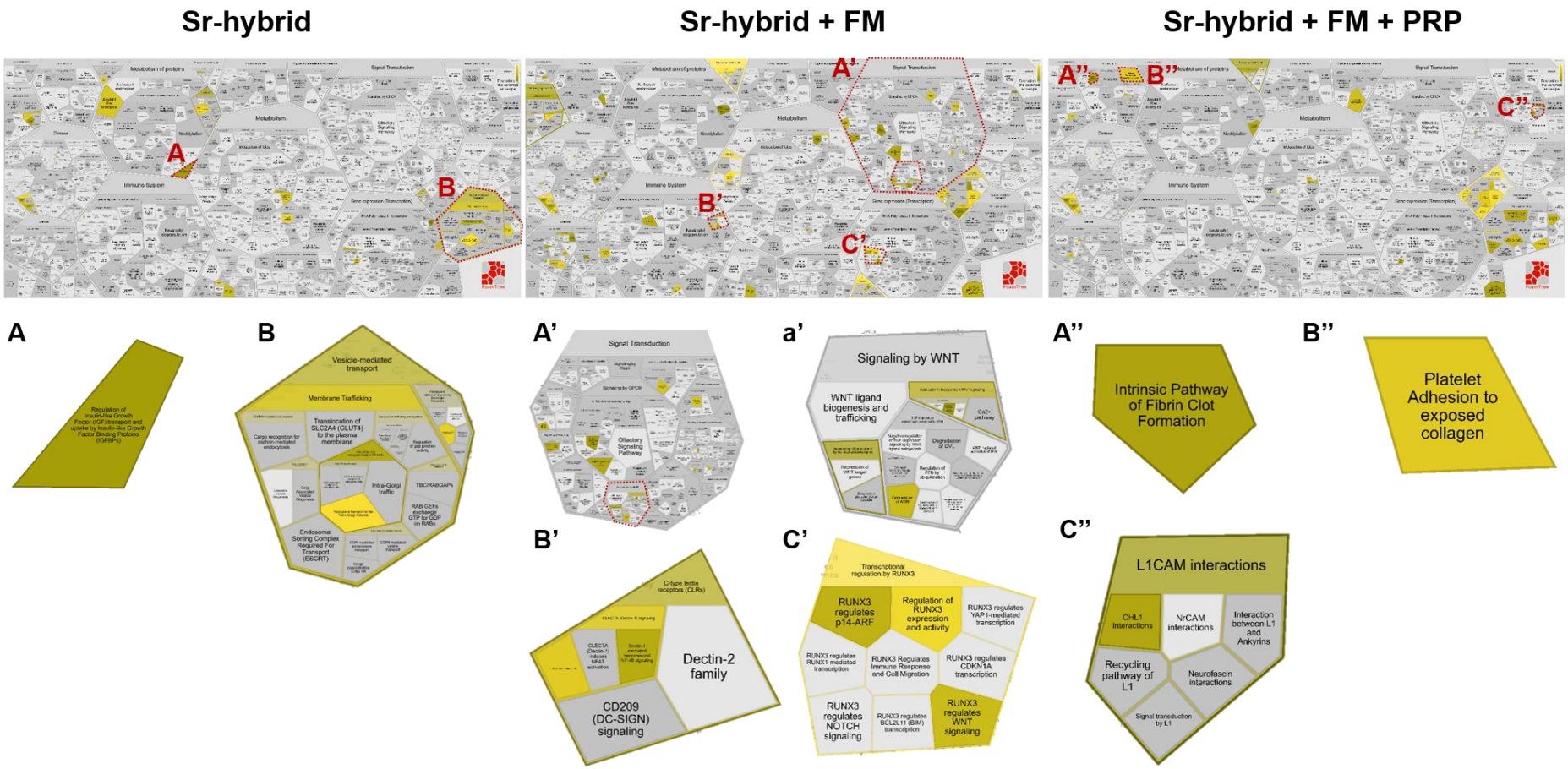


Figure 26 – **Unique pathways affected by each tested formulation, from reactome analysis.** A and B: Sr-hybrid unique affected pathways; A'-C': Sr-hybrid with FMs unique altered pathways, (a') close-up of Signaling by WNT, from the Signal Transduction (A') pathway category; A''-C''; Sr-hybrid with FMs and PRP unique affected pathways. Dotted red lines in pathways overview representation represent the selected pathways below.

## 4. Discussion

Despite recent and notorious advances in maxillofacial reconstructive medicine, there is still an increasing need for solutions to the current clinical problems, either in terms of functional or aesthetic issues. However, no ideal treatment has been found, mainly due to the unique features of each lesion.

In this work, we have designed a bilayer injectable biomaterial capable of promoting soft-tissue integration to one side (gingival-like layer), and of inducing bone formation to the other (bone-like layer). Through the development of a bilayer material, each layer can be designed with differential cues for the specific tissue site. This biomaterial was based on a previously injectable Sr-rich hybrid system developed and thoroughly studied by our group, (76-80). The Sr-hybrid is composed of HAp microspheres doped with Sr and an alginate vehicle, also crosslinked *in situ* with Sr. In this thesis, a gingival-like layer composed of alginate and a bone-like layer composed of the Sr-hybrid was developed. Each layer was further enhanced by incorporating PRP and/or FMs, aiming for the delivery of pro-regenerative cytokines and growth factors.

The developed system reticulates *in situ* and can be injected. Injectability is a big advantage of this material since it can easily fill irregularly shaped lesions and can be implanted through a minimally invasive procedure, thus reducing surgery time, decreasing infection risk and associated economical costs (94). Furthermore, the incorporation of hydroxyapatite microspheres in the bone-like layer confers the mechanical reinforcement, needed for bone defects. As was previously described in studies performed by our group, the microspheres diameter (500-560 μm) also provides an adequate porosity for new tissue ingrowth (76).

Sr incorporation has long been described in the literature as beneficial for bone regeneration. The elemental analysis of the microspheres has shown a uniform distribution of Sr within the particles with weight percentage of approximately 4%, consistent with previous results, described to have clinical relevance (79). Additionally, the size of the HAp crystals found in the TEM analysis (0.43-1.5μm) is in accordance to what was expected, since a micro-hydroxyapatite powder was used.

The process of fabricating particles from FMs was optimized. A median size of 330 μm was achieved, which is smaller than microspheres, conferring them the capacity of integrating the spaces between microspheres granting a homogenous distribution of both constituents.

The biomaterial mechanical properties was also addressed in the scope of this work. Initially, both layers were tested individually, in order to further understand the contribution of FMs and PRP to the mechanical resistance. While it was observed that FMs incorporation lead to a significant increase in the loss modulus of the GL, the same was not verified in the BL, which might be due to the microspheres contribution surpassing the one from FMs. In fact, the BL, even without any culture time, displayed an average of 30.2 MPa storage modulus against the 1.0 MPa from GL. This value further increased during time of culture to 86.9 MPa, due to the quicker degradation of alginate, thus leading to higher microspheres/alginate ratio.

A fully functional bilayer biomaterial was achieved, with a stable interface between both layers, that was maintained even when agitation and compressive forces were applied. Although an improvement of both storage and loss modulus were observed in the bilayere formulation, compared to the GL, it still was lower than desired since, as it was observed by Misch *et al*, cancellous bone of the jaw present an elastic modulus of 56.0 ± 29.6 MPa (95). Nevertheless, it should be taken into account that DMA studies were conducted without a confined setup. In bone defects the biomaterial will be surrounded by bone, thus altering the mechanical properties. Actually, when the Sr-hybrid was initially analyzed with DMA, a 16-fold increase was observed when using confined conditions, in relation to unconfined analysis. (76).

Although fetal membranes are a highly attractive natural source of bioactive factors, there is a need for the decellularization due to the risk of triggering an immune response. Previously in our group we optimized a decellularization protocol,,and verified its efficacy through histology and TEM analysis.

Although no standard criteria has been established for assessing the efficacy of tissue decellularization, several authors suggest the following: no visible nuclei per histological evaluation by HE and DAPI staining, the amount of DNA cannot exceed 50 ng per mg of material and a reduction of 90% of host DNA content is recommended (96, 97). Thus, during this work, the absence of nuclei was verified and, during the optimization process, a reduction of 96.96% and 93.68% in the DNA content for AM and CM, respectively, was observed (data not shown).

Moreover, it is well known that enzymatic decellularization protocols tend to result in high loss of matrix content, due to their aggressiveness (97). However, after decellularization, while FMs seem to exhibit a looser matrix, with less surface roughness, they also seem to preserve their collagen content. Additionally, the looser matrix may aid not only with the release of growth factors and cytokines preserved in the tissue but also with cell penetration.

Once the decellularization efficiency was properly assessed, the next step was to evaluate its influence on cell culture. Since studies described in the literature concerning FMs incorporation into hydrogels are very scarce and no consensus was found, fibroblasts were seeded on top of alginate disks containing FMs in three different formulations: particles, extracts and solubilized) in a range of concentrations between 0.5-20 mg/ml. Native FMs were used as control.

Native FMs seem to have a stronger effect on fibroblast metabolic activity, in comparison to decellularized FMs. It is expected a loss of growth factors/cytokines throughout the decellularization which can explain these results, although no studies were found adressing this issue. Within FM extracts, higher metabolic activity was found when DMEM was used as substrate for the extract fabrication. This can be due to the quicker Sr release. Since Ca is a component of the DMEM, the ionic exchange will lead to the release of Sr from the hydrogel to the media. From all tested formulations, FMs particles seemed to exhibit the best results. Considering that native tissue could not be used, due to the associated biological risk (75),

decellularized FMs particles, at 20 mg/ml concentration was chosen, since it exhibited the higher metabolic activity.

The strategy of using FMs in tissue regeneration has been increasingly reported. While in its native state, amniotic membrane has been used clinically for the treatment of a variety of lesions (such as skin and corneal wounds, periodontal surgery and soft tissue repair) resulting in a healing improvement (98); only more recently its incorporation into hydrogels has been described. In a study from Murphy *et al*, the use of a hydrogel of solubilized amniotic membrane and hyaluronic acid (1:1 ratio), proved to accelerate wound closure through re-epithelization, while promoting angiogenesis and cell proliferation, in a murine wound model (91).

PRP has been broadly used in tissue regeneration, particularly in the maxillofacial field, due to its capacity to potentiate wound healing (99). However, one of its main drawbacks is the associated patient variability. Here, we propose to incorporate lyophilized PRP. Studies report that the lyophilization process does not affect growth factors preservation and functionality, when comparing to fresh PRP (100). By lyophilizing PRP, we create an off the shelf product, incorporating a pool of different donors and thus, surpassing the current donor variability challenge found in the maxillofacial field.

Firstly, since the PRP range of concentrations described in the literature significantly varies, the most described concentrations were tested on fibroblasts - 5%, 10% and 100%. During live-dead assay performed in the 5% PRP concentration, no other cell clusters were found, hence the lack of replicas in the quantification of viability. In this experiment, alginate was used without its modification with RGD. Since RGD modification confer alginate the ability to provide cell anchorage and to improve cell survival and function (51), this might explain the low values found in the alginate group, for both metabolic acitivity and cell number.

Some controversy can be found in the literature regarding the effect of different PRP concentrations on different cell types. Some studies describe that concentrations between 2.5-20% of PRP seem to stimulate cell proliferation and migration (101, 102). Another study reports that at 5% concentration cell proliferation and migration was found to be enhanced in hMSCs derived from bone marrow (103). Moreover, a concentration of 10% has been shown to have a positive effect in both hGFs and OB-like cells adhesion and viability (104). In our studies, the incorporation of PRP for concentrations higher than 10%, has shown to be able to increase both metabolic activity, overall cell number and viability. Importantly, during the preparation of the hydrogel, PRP was easily dissolved in all concentrations but the reticulation time was severely affected at the 100% concentration and was, therefore, deemed not applicable in a surgical procedure.

Once both FMs and PRP concentration was optimized, the effect of each layer in both cell types was addressed. Although no differences were observed in the viability among the tested formulations, the incorporation of FMs, in both hGFs and hMSCs culture showed an increase in cell number. When

incorporating only PRP, small clusters of cells were observed. In turn, formulations with FMs seem to form aligned panels of cells, which can be associated with the decellularized FMs ECM serving as anchoring sites. This finding is in agreement with other studies that report FMs as possessing a suitable environment for both cell attachment and proliferation (105, 106).

In the gingival-like layer, hGFs cultured on alginate with FMs and or on alginate with both PRP and FMs displayed a significant decrease in proliferation. However, in the same formulations, a high cell confluence was encountered, which might indicate a decrease in the proliferation signals emitted by hGFs due to space constraints.

In the bone-like layer, where HAp microspheres were also incorporated, hMSC located preferentially in the vicinities or surrounding them. This was already described in a previous study by our group, where hMSCs were seeded on top of the Sr-hybrid and cultured under basal and osteogenic conditions (79). Since HAp microspheres are composed of an osteoconductive material (107, 108) and are doped with Sr, which is described as having osteoinductive properties (78, 109–112), this behavior is expected. In terms of hMSCs osteogenic differentiation, ALP staining, an early osteogenic marker, increased in both the control and in Sr-hybrid with FMs, while small clusters were found in the remaining formulations. On the other hand, an increase on the mineralization deposits was observed in both formulations containing FMs, whereas both control and Sr-hybrid with PRP formulation exhibited almost none. Thus, preliminary results indicate that FMs may be promoting the osteogenic differentiation, not only in the initial state of osteogenic differentiation, but also in the latter phase of matrix mineralization. Similar results have already been described in other studies, where the FMs osteogenic potential has been observed (113–115).

Omics technologies have emerged as powerful tools to uncover molecules and signaling pathways and have been critical to unravel the molecular mechanisms involved in diseases and in identifying targets for therapy (116). Proteomic-based studies have been increasingly rising and are widely used to discern the molecular mechanisms behind a cell response to a biomaterial (117–121).

Based on the results obtained from the *in vitro* study, the formulation incorporating only PRP was not considered for the proteomic analysis, since no significant differences were observed when compared to control formulations (alginate and Sr-hybrid), in terms of viability, metabolic activity, proliferation and in the case of the BL, differentiation.

Concerning the proteomic analysis of the alginate-based formulations co-cultured with hGFs, more proteins were found altered in the FM containing biomaterials (alginate+FMs and alginate+FMs+PRP), being highest in the PRP containing condition. Nevertheless, alginate clustered together with alginate+FMs+PRP, indicating a more similar behavior, in line with the trend observed in terms of cell viability in the different materials. A total of 95 proteins were found to be altered exclusively in the formulation containing both FMs and PRP, suggesting an additive/synergistic effect of both components when combined.

From the analysis of the heatmap's first cluster, we identified a significant enrichment of proteins involved in ECM, in formulations containing FM+PRP, comparing to the control formulation (alginate). Among these proteins, a downregulation of both COL I, COL VI, COL XII and COL XVI was found, accompanied by an upregulation of COL VIII, Fibulin-1, Serpin, Clusterin, MMP1 and MMP2. In addition, an upregulation of SPARC, VCAN, Laminin, Thrombospondin-1 was observed in the same condition. This pattern suggests an enrichment in ECM remodeling for this formulation, where its components are subject to cleavage, deposition or rearrangement, key processes in gingival regeneration (122). Importantly, while Metalloproteinases (MMP) are amongst the proteins found upregulated and are specialized in degrading ECM (123), Serpin is described has a collagen modulator, since it has the capacity to protect collagen against degradation (124). This suggests that Serpin may be inhibiting MMP activity, thus reducing collagen degradation. Interestingly, an increase of thrombospondin-1 (TSP) was also found in the formulation containing FMs and PRP. TSP is naturally expressed in response to injuries and regulates cell migration and proliferation. More recently, TSP has also been reported as an activator of TGF-β, which has a major role in wound healing promotion, through regulation of collagen deposition (125, 126).

Additionally, the second cluster reflects and upregulation of ATP synthesis in the formulations containing PRP. PRP is already described as having ATP in its composition and its release is commonly associated with platelet activation and granule secretion (127, 128). This may be particularly interesting since some studies report an improvement of tissue regeneration, with rapid ECM formation and improved angiogenesis, following ATP-vesicles delivery (129, 130). Moreover, studies have reported that during the cell death process, ATP synthesis is decreased and suggest that ATP quantification can be used as a valid marker for cell viability (131). High cell viability was already observed during the in vitro evaluation for this formulation, accompanied by a decrease in cell proliferation. The relation between proliferation and cell death have been described in the literature, where studies have shown that downregulation of apoptosis is commonly associated with a decrease in the proliferative rate (132).

Another cluster was shown as enrichment in proteins associated with the cytoskeleton and cell movement in the formulation containing Alginate and FMs (and then downregulated in alginate with FMs and PRP). The cytoskeleton in involved in several processes of wound repair, either regarding the assembly of a contractile actomyosin ring or the formation of cell protrusions at the leading edge of wounds, through the regulation of Rho family GTPases. Furthermore, the role of the cytoskeleton in cell migration has long been reported, since cells rely on the coordination of forward protrusion and rearward retraction forces, requiring the rearrangement of both actin and microtubule cytoskeleton (133).

From the GO term analysis of all the altered proteins in each biomaterial, we observed that, as expected, co-culture with all the different alginate-based biomaterials had a greater impact on ECM related processes, namely on collagen catabolism. Nucleosome was also found to be affected by all formulations (although not in the clusters, which might suggest a small difference among the fold change values).

Nucleosome determines the chromatin state, controlling gene expression or silencing (134). Through this mechanism, it is involved in several processes, namely in the cell response to the microenvironment, by conferring chromatin the flexibility needed to respond to the environmental, metabolic and developmental cues (135). In somatic cell reprogramming, it confers information to progeny cells during lineage commitment, thus having a defined role in bone, development, tissue regeneration, cell commitment and differentiation, as well as disease etiologies (136).

Moreover, alginate exhibited an enrichment in the wound healing GO term. This was expected since alginate has been used for a long time in the treatment of wounds, due to its capacity to absorb excess wound fluid, maintain a physiologically moist environment, and minimize bacterial infections at the wound site (137).

Cell-cell adhesion was also found to be upregulated in both alginate and alginate with FMs. This term refers to the macromolecular adhesive organelles that integrate cells into tissues and play a crucial part in organizing the formation of tissue and organs after injury (138). This term was not found for the alginate with FMs and PRP, in turn the term ECM organization and proteolysis were found uniquely upregulated, suggesting that this formulation may have a preponderant role in ECM remodeling, over the others.

Interestingly, an upregulation of the GO term "platelet alpha granule lumen" was found in the alginate with FMs and PRP formulation. Platelet alpha granules are described to incorporate a variety of both pro- and anti-angiogenic proteins, including VEGF, PDGF, FGF, EGF and IGF. These growth factors are described as promoting vessel wall permeability and contributing to the recruitment, growth and proliferation not only of endothelial cells but also of fibroblasts (139). Furthermore, studies have reported that PRP exerts its effects through the release of growth factors and other bioactive factors from its alpha granules (140).

While an upregulation of mitochondrial-related GO terms was already expected in the formulation containing PRP, since mitochondria is commonly associated with ATP regulation (141) and we had already observed an increase in ATP synthesis in this formulation, alginate with FMs also exhibited the "Mitochondrial inner membrane" term upregulated. Nonetheless, mitochondria also plays an important role in the regulation of cellular apoptosis and, as it will be further discussed, a decrease in the number of proteins involved in programmed cell death was observed.

In contrast, both cytoskeleton and GTP binding were found downregulated in the alginate with FMs and PRP, supporting the previously discussed heatmap clustering analysis. This terms are connected, since GTP is regulated through the Rho family, namely the Rho GTPases which, as was already mentioned, controls cytoskeleton organization and rearrangements (142). Although a relationship between RhoGTPase activity and ATP release has also been reported, being the latter released upon Rho activation (143), the same pattern was not observed here. This may be either due to a GTP downregulation through a non-canonical pathway or to a negative feedback loop. Since ATP is being released by PRP, the high

amount of ATP may be inhibiting the activation of RhoGTPases and, in consequence, the cytoskeleton rearrangements.

With respect to the signaling pathways analysis, the FMs and PRP formulation was consistently associated with an increase in the number of proteins involved in several different pathways. The increase in ECM-related pathways was in accordance with previous results. Additionally, several metabolic pathways (also increased in this formulation) are described as being key pathways in regulating both fibroblast behavior and ECM hemostasis (144). Moreover, an increase in the vesicle-mediated transport was also observed. Importantly, while this includes exocytosis, which is reported to not only be ATP dependent (145) but also represent the way that cells produce and secrete most of the proteoglycans and glycoproteins of the ECM (146), can also be related to the internalization of the soluble factors, released by the biomaterial. Additionally, ATP itself is also released to the extracellular space in a vesicle-mediated fashion.

An increase in the number of proteins involved in the hemostasis pathway category was also found for both alginate with FMs and alginate with FMs and PRP. Hemostasis is an important part of the first phase of acute wound healing and concerns both cell recruitment and formation of the blood clot where, among others, Fibronectin and Thrombospondin form a provisional matrix for the inflammatory cells migration (147). The incorporation of both PRP and FMs has shown the capacity to regulate VEGFR2, IGF1R, MET, ERBB4 signaling pathways, which is expected, given that these pathways are all major players in the wound healing cascade (148-150).

Furthermore, gene expression was also found to be increased by these formulations, which is expected since gene expression is responsible for the synthesis of a functional gene product and an increase in the proteins regulation is seen in these formulations. Meanwhile, a decrease in the programmed cell death was observed in the alginate with FMs formulation, as previously discussed. While no significant differences in viability were observed during the in vitro evaluation, there was a tendency for a decreased number of viable cells. In addition, a significant decrease in proliferation was observed for this condition. The relationship between apoptosis and proliferation has already been discussed above.

The alginate formulation seems to have an influence over immune pathways, as previously mentioned, namely through interferon gamma (IFN- $\gamma$ and $\alpha$) and IL-7. Both IFN- $\gamma$ and $\alpha$ have been reported as inhibitors of collagen synthesis by fibroblasts, leading to retardation of the wound healing process (151, 152). Furthermore, IL-7 is a known pro-inflammatory cytokine, which can enhance fibroblast production of IFN- $\gamma$, as well as inhibiting TGF-$\beta$ production (153). This effect seems to be counteracted by the FMs.

Regarding the hMSCs response to the bone-like layer, protein expression profile of both formulations containing FMs were grouped together, due to their similar expression behavior. This may suggest that hMSCs strongly respond to FMs growth factors, imposing its effect over the PRP.

Similar to what was observed with hGFs, an enrichment of ECM GO term was mainly observed in both Sr-hybrid with with FMs and PRP in the first cluster, mainly through the upregulation of COL VIII, COL XVI and ICAM1. Both collagens have been described has having a role in ECM regulation since COL XVI induces the recruitment of integrins into focal adhesion plaques, a principal step for integrin signaling (154). Additionally, they are frequently found in association with COL I and II, maintaining ECM integrity (155). Intracellular adhesion molecule (ICAM1) functions as cell-cell and cell-ECM adhesive interactions (156) and while some controversy can be found in relation to ICAM1 role on hMSCs differentiation, some studies report an inhibitory effect on osteogenesis (157), while others report a promotion of bone regeneration by promoting hMSCs migration and adhesion (158). Furthermore, ICAM1 has also been reported as being critical for MSC-mediated immunosuppression through regulation of T cell (159). When compared to the formulations incorporating FMs alone, this effect seems to be augmented when combining FMs with PRP, which presented an additional upregulation of COL I (OBs differentiation), Decorin (proteoglycan that binds to COL I, II, FN and TGF-$\beta$), Integrin 1, 2 and 3.

Another cluster unveiled an upregulation of both "GTP binding" and "Platelet degranulation" in the formulation containing both FMs and PRP. Platelet degranulation refers to process in which platelets are activated and release a variety of proteins, among them growth factors, ADP and ATP, as previously discussed. The relationship between ATP and GTP has already been adressed in this thesis, reporting that an increase in ATP is commonly associated with an increase in GTPase. Furthermore, GTPase is also involved in the regulation of platelet ativation and function (160). All together, this evidences helps to explain the upregulation found in the formulation containing PRP.

Regarding the cluster highlighting an overepresentation of inflammatory regulation terms found in the formulation containing FMs, an increase in the MSCs immunosuppresive potential seems to be observed. Among the identified proteins, an upregulation of IFN-$\gamma$, HMGB1 and Galectin 3 was found, which seem to indicate that FMs may be potentiating the immumodulatory properties of the Sr-hybrid (161-163).

In line with what was observed in the heatmap clustering analysis, the ECM GO term appeared enriched for all formulations, although more evident in the formulations containing both FMs and PRP. Contrastingly, ECM was also found in Sr-hybrid with FMs, with the proteins found mostly related to MSC differentiation, namely hMSCs migration (CD44), regulation of Wnt signaling (Heparan sulfate proteoglycans), matrix remodeling (RECK) or osteoblast differentiation (TGF-$\beta$)(164-167). These results are not in accordance with previous data obtained in the in vitro study where an increase in hMSCs osteogenic differentiation was observed.

Additionally, the incorporation of FMs did not seem to influence the innate immune response, as was previously discussed. However, it improved cell-cell adhesion both in the hybrid with FMs and with FMs with PRP. Although a downregulation for this term was found in all formulations, the incorporation of FMs appears to partly counteract this pattern. Cell-cell adhesion, as has already been said, is of great

importance in tissue regeneration and seems to be primarily regulated by integrins. Accordingly, an upregulation of ICAM1 and COL XVI (involved in the integrin regulation) was also observed for these formulations.

Similarly to what was observed with the fibroblasts, the formulation incorporating FMs presented an upregulation of cytosketon-related GO terms. Interestingly, this might be due to MSCs ostegenic differentiation, since alterations of MSCs cytoskeletal components have been reported during differentiation (168). Although not expected, Sr-hybrid with FMs appears to downregulate ECM, GTPase activity and the canonical Wnt pathway. Interestingly, RhoGTPases have emerged as key mediators of the Wnt signaling, promoting morphological and transcriptional changes affecting cell behavior (eg. cell migration) (169). This further suggests an impairment of cell migration in this formulation.

Moreover, and in line with what was previously described, ATP released by the PRP appears to influence both hMSCs vesicle-mediated transport and mitochondrial electron transport, which were already reported to be correlated to ATP.

Importantly, "collagen trimer" can also be found upregulated in the Sr-hybrid with FMs and PRP. This term refers to any triple hellical collagen that forms fibrils (eg COL I, II, III, V, XI). An upregulation of COL I was found uniquely in this formulation, which will be adressed further in this discussion.

Concerning the pathway analysis, the Sr-hybrid with FMs resulted in an increase in the number of proteins involved in the immune system, which is in accordance with previous results. Additionally, in line with the hGFs results, gene expression, hemostasis and signal transduction were also found overrepresented. MSCs are know to produce tissue factor (TF), a potent activator of coagulation (170), which appears to be increasing the fibrin clot formation and the platelet adhesion to exposed collagen. Contrastingly, programmed cell death was also found increased, although no significant differences in viability in vitro were observed. Nevertheless, both FM and FM with PRP seem to have a tendency to increment the number of viable cells.

Regarding the incorportation of both FMs and PRP, an overrepresentation of metabolism and ECM-associated pathways can be seen. The increase in ECM pathways was in accordance to previous results. Interestingly, while in their native environment, hMSCs present a quiescent state with low proliferation and high potentiality, when transferred to a nutrient-rich cell culture environment, an increase in cell proliferation is observed, accompanied by an increase in their metabolism (171). Since a greater level of growth factors is expected to be available when combining both FMs and PRP, this may induce hMSCs metabolic activity and proliferation. Moreover, even though no significant differences were observed in the number of proliferating cells, for this formulation, a slight increase was observed, comparing to control.

Finally, the Sr-hybrid with FMs seems to have a preponderant effect on signaling transduction, regulating several pathways as NOTCH4, MAPK, EGFR, DECTIN-1, RUNX3 and Hedgehog, which have been described as involved in bone lesions where bone formation was increased (172-175).

Looking into specific proteins of interest, an increase in overall ECM proteins was found in both conditions with FMs. Interestingly, an increase of Stromal Cell-derived factor 1 was observed in both formulations containing FMs. SDF is described as having a major role in hMSCs recruitment (176). Moreover, an increase in ALP was found to be present uniquely in the Sr-hybrid with FMs and PRP. This protein is described as being a major player in the hMSCs differentiation to OBs, as was already discussed in this thesis. These results, together with the COL I upregulation, suggest an increase in the osteogenic differentiation for this formulation.

During the direct contact experiments, an increase in both ALP and Alizarin was instead found in the Sr-hybrid with FMs. Nevertheless, the differences in both experimental setups should be taken into account. Due to technical restraints, a direct contact setup was not possible since, in order to retrieve the cells it would be necessary to dissolve the biomaterial, which would ultimately lead to the HAp degradation and a highly contaminated protein lysate. As so, the obtained data is the result of the paracrine action of the soluble factors released by the different biomaterials. As it was previously observed, FMs provided a strong anchoring site during repopulation, which might potentiate hMSC differentiation, in the direct contact experiments. Furthermore, proteomic analysis was made using only one technical replicate, due to time restraints. Thus, while some of the preliminary, results are highly promising, this should be taken into account.

## 5. Conclusion and Future Remarks

Overall, the results from this thesis suggest that the incorporation of bioactive factors in the bilayer biomaterial promoted both hGFs and hMSCs cell growth and hMSCs osteogenic differentiation. This seems to be particularly evident when associating FMs and PRP.

The obtained results indicate that the innovative developed bilayer biomaterial provides a very promising multifunctional approach for periodontal tissue regeneration. However, further studies should be conducted in order to explore the following questions:

- Although promising, proteomic analysis was performed based on one replica. A minimal of two additional independent analysis should be performed in order to confirm the results found in this thesis.
- After increasing sample number, the most interesting candidates from the proteomic study should be further validated by Western Blot analysis.
- Likewise, the results from the *in vitro* evaluation of both hGFs and hMSCs biological response to GL and BL should be repeated in order to increase the number of independent experiments.
- An increase in the ALP expression was found in the formulation containing FMs, at day 21. Nonetheless, the peak of ALP expression is at day 14. In future experiments, this should be assessed.
- A decrease in the metabolic activity was found when comparing native vs decellularized FMs. This suggests a loss of growth factors/cytokines content during the decellularization process. In order to further understand this results, a thorough study concerning the effect of decellularizarion in the FMs protein content, should be carried out.
- The tight relationship between OBs and OCs is well documented. Moreover, the Sr-hybrid has proven to possess anti-osteoclastogenic properties. A study investigating the biomaterial effect on osteoclasts should be performed.
- Previous results from our group report an antimicrobial effect of the Sr-hybrid. Moreover, this characteristic has also been described for both FMs and PRP. Thus, the biomaterial should be tested against *Porphyromonas gingivalis*, *Lactobacillus casei*, and *Actinomyces viscosus*, the most common microorganisms involved in oral infections.

## References


1. Cho MI, Garant PR. Development and general structure of the periodontium. Periodontol 2000. 2000;24:9–27.
2. Chen FM, Jin Y. Periodontal tissue engineering and regeneration: current approaches and expanding opportunities. Tissue Eng Part B Rev. 2010;16(2):219–55.
3. Hienz SA, Ivanovski S. Chapter II: Periodontal Microbiology and Immunobiology. In: Klineberg I, Eckert S, editors. Functional Occlusion in Restorative Dentistry and Prosthodontics. UK: Elsevier Health Sciences UK; 2015. p. 23–32.
4. Ghantous Y, Yaffi V, Abu-Elnaaj I. [Oral cavity cancer: epidemiology and early diagnosis]. Refuat Hapeh Vehashinayim (1993). 2015;32(3):55–63, 71.
5. Nanci A, Bosshardt DD. Structure of periodontal tissues in health and disease. Periodontol 2000. 2006;40:11–28.
6. Klineberg I, Eckert S. Functional Occlusion in Restorative Dentistry and Prosthodontics. UK: Elsevier Health Sciences UK; 2015. p. 23–32.
7. Kornman KS, Page RC, Tonetti MS. The host response to the microbial challenge in periodontitis: assembling the players. Periodontol 2000. 1997;14:33–53.
8. Bartold PM, Walsh LJ, Narayanan AS. Molecular and cell biology of the gingiva. Periodontol 2000. 2000;24:28–55.
9. Birkedal-Hansen H. Role of matrix metalloproteinases in human periodontal diseases. J Periodontol. 1993;64(5 Suppl):474–84.
10. Matalová E, Lungová V, Sharpe P. Development of Tooth and Associated Structures. In: Vishwakarma A, Sharpe P, Shi S, Ramalingam M, editors. Stem Cell Biology and Tissue Engineering in Dental Sciences2015. p. 335–46.
11. Chu TMG, Liu SSY, Babler WJ. Craniofacial Biology, Orthodontics, and Implants. In: Burr DB, Allen MR, editors. Basic and Applied Bone Biology: Elsevier Inc.; 2013. p. 225–42.
12. The healthy mouth. In: Walmsley AD, Walsh TF, Pretty IA, editors. Restorative Dentistry2007.
13. Chu TMG, Sciences BaA, tgchu@iu.edu, Liu SSY, University-Purdue I, Babler WJ, et al. Craniofacial Biology, Orthodontics, and Implants. In: Burr DB, Allen MR, editors. Basic and Applied Bone Biology: Elsevier Inc.; 2013. p. 225–42.
14. Florencio-Silva R, Sasso GS, Sasso-Cerri E, Simões MJ, Cerri PS. Biology of Bone Tissue: Structure, Function, and Factors That Influence Bone Cells. Biomed Res Int. 2015;2015.
15. Rutkovskiy A, Stenslokken KO, Vaage IJ. Osteoblast Differentiation at a Glance. Med Sci Monit Basic Res. 2016;22:95–106.
16. Anderson HC. Matrix vesicles and calcification. Curr Rheumatol Rep. 2003;5(3):222–6.
17. Bar-Shavit Z. The osteoclast: a multinucleated, hematopoietic-origin, bone-resorbing osteoimmune cell. J Cell Biochem. 2007;102(5):1130–9.
18. Sodek J, McKee MD. Molecular and cellular biology of alveolar bone. Periodontol 2000. 2000;24:99–126.
19. Yavropoulou MP, Yovos JG. Osteoclastogenesis--current knowledge and future perspectives. J Musculoskelet Neuronal Interact. 2008;8(3):204–16.
20. Longhini R, Aparecida de Oliveira P, Sasso-Cerri E, Cerri PS. Cimetidine reduces alveolar bone loss in induced periodontitis in rat molars. J Periodontol. 2014;85(8):1115–25.
21. Boyce BF, Xing L. Functions of RANKL/RANK/OPG in bone modeling and remodeling. Arch Biochem Biophys. 2008;473(2):139–46.
22. Gulabivala K, Ng Y-L. Tooth organogenesis, morphology and physiology. In: Gulabivala K, Ng Y-L, editors. Endodontics2014. p. 2–32.
23. Jazayeri HE, Tahriri M, Razavi M, Khoshroo K, Fahimipour F, Dashtimoghadam E, et al. A current overview of materials and strategies for potential use in maxillofacial tissue regeneration. Materials Science and Engineering: C. 2017;70:913–29.
24. Hovhannisyan S. R. MKA, Zopunyan V. R. Maxillofacial Defects 2009. Available from: https://ysmubooks.am/uploads/5_y_1_s.pdf.

25. Gupta A, Verma A, Islam J, Agarwal S. Maxillofacial Defects And Their Classification: A Review. International Journal of Advanced Research. 2016.
26. Wang HL, Greenwell H, Fiorellini J, Giannobile W, Offenbacher S, Salkin L, et al. Periodontal regeneration. J Periodontol. 2005;76(9):1601–22.
27. Alpiste Illueca FM, Buitrago Vera P, de Grado Cabanilles P, Fuenmayor Fernandez V, Gil Loscos FJ. Periodontal regeneration in clinical practice. Med Oral Patol Oral Cir Bucal. 2006;11(4):E382–92.
28. Bhavsar A, Parween S, Karthikehyan B, Prabhuji M. Critical Issues in Periodontal Regeneration – A Review. Journal of Oral Health and Dental Science. 2018;2(2).
29. Rosling B, Nyman S, Lindhe J, Jern B. The healing potential of the periodontal tissues following different techniques of periodontal surgery in plaque-free dentitions. A 2-year clinical study. J Clin Periodontol. 1976;3(4):233–50.
30. Zohar R, Tenenbaum HC. How predictable are periodontal regenerative procedures? J Can Dent Assoc. 2005;71(9):675–80.
31. Sheikh Z, Hamdan N, Ikeda Y, Grynpas M, Ganss B, Glogauer M. Natural graft tissues and synthetic biomaterials for periodontal and alveolar bone reconstructive applications: a review. Biomater Res. 212017.
32. Damien CJ, Parsons JR. Bone graft and bone graft substitutes: a review of current technology and applications. J Appl Biomater. 1991;2(3):187–208.
33. Sukumar S, Drizhal I. Bone grafts in periodontal therapy. Acta Medica (Hradec Kralove). 2008;51(4):203–7.
34. Wang W, Yeung KWK. Bone grafts and biomaterials substitutes for bone defect repair: A review. Bioact Mater. 2017;2(4):224–47.
35. Urist MR, Sato K, Brownell AG, Malinin TI, Lietze A, Huo YK, et al. Human bone morphogenetic protein (hBMP). Proc Soc Exp Biol Med. 1983;173(2):194–9.
36. Garrett S. Periodontal regeneration around natural teeth. Ann Periodontol. 1996;1(1):621–66.
37. Niu CC, Tsai TT, Fu TS, Lai PL, Chen LH, Chen WJ. A comparison of posterolateral lumbar fusion comparing autograft, autogenous laminectomy bone with bone marrow aspirate, and calcium sulphate with bone marrow aspirate: a prospective randomized study. Spine (Phila Pa 1976). 2009;34(25):2715–9.
38. Lewis KN, Thomas MV, Puleo DA. Mechanical and degradation behavior of polymer-calcium sulfate composites. J Mater Sci Mater Med. 2006;17(6):531–7.
39. Tan H, Yang S, Dai P, Li W, Yue B. Preparation and physical characterization of calcium sulfate cement/silica-based mesoporous material composites for controlled release of BMP-2. Int J Nanomedicine. 2015;10:4341–50.
40. Ding Y, Tang S, Yu B, Yan Y, Li H, Wei J, et al. In vitro degradability, bioactivity and primary cell responses to bone cements containing mesoporous magnesium–calcium silicate and calcium sulfate for bone regeneration. J R Soc Interface. 2015;12(111):20150779.
41. Eggli PS, Muller W, Schenk RK. Porous hydroxyapatite and tricalcium phosphate cylinders with two different pore size ranges implanted in the cancellous bone of rabbits. A comparative histomorphometric and histologic study of bony ingrowth and implant substitution. Clin Orthop Relat Res. 1988(232):127–38.
42. Nuttelman CR, Henry SM, Anseth KS. Synthesis and characterization of photocrosslinkable, degradable poly(vinyl alcohol)-based tissue engineering scaffolds. Biomaterials. 2002;23(17):3617–26.
43. Xu X, Gu Z, Chen X, Shi C, Liu C, Liu M, et al. An injectable and thermosensitive hydrogel: Promoting periodontal regeneration by controlled-release of aspirin and erythropoietin. Acta Biomater. 2019;86:235–46.
44. Merino S, Martin C, Kostarelos K, Prato M, Vazquez E. Nanocomposite Hydrogels: 3D Polymer–Nanoparticle Synergies for On-Demand Drug Delivery. ACS Nano. 2015;9(5):4686–97.
45. Laurenti M, Abdallah M-N. Natural and synthetic hydrogels for periodontal tissue regeneration. International Dental Journal of Student Research. 2015;3(2):49–51.
46. Valderrama P, Jung RE, Thoma DS, Jones AA, Cochran DL. Evaluation of parathyroid hormone bound to a synthetic matrix for guided bone regeneration around dental implants: a histomorphometric study in dogs. J Periodontol. 2010;81(5):737–47.

47. Carlini A, Adamiak L, Gianneschi NC. Biosynthetic Polymers as Functional Materials. Macromolecules. 2016;49(12):4379–94.
48. Chirani N, Yahia L, Gritsch L, Motta F, Chirani S, F, S. History and Applications of Hydrogels. J Biomedical Sci. 2015;4(2).
49. Tanzi MC FS, Candiani G. Biomaterials and Applications. Foundations of Biomaterials Engineering2019. p. 199–287.
50. Burdick JA, Stevens MM. Biomedical hydrogels. In: Biomaterials WPSi, editor. Biomaterials, Artificial Organs and Tissue Engineering2005. p. 107–15.
51. Bidarra SJ, Barrias CC, Fonseca KB, Barbosa MA, Soares RA, Granja PL. Injectable in situ crosslinkable RGD-modified alginate matrix for endothelial cells delivery. Biomaterials. 2011;32(31):7897–904.
52. Seol YJ, Park JY, Jeong W, Kim TH, Kim SY, Cho DW. Development of hybrid scaffolds using ceramic and hydrogel for articular cartilage tissue regeneration. J Biomed Mater Res A. 2015;103(4):1404–13.
53. Lima G, Campos L, Junqueira A, Devine D, Nugent M. A novel pH-sensitive ceramic-hydrogel for biomedical applications. Polymers for Advanced Technologies. 2015.
54. Oliveira SM, Barrias CC, Almeida IF, Costa PC, Ferreira MR, Bahia MF, et al. Injectability of a bone filler system based on hydroxyapatite microspheres and a vehicle with in situ gel-forming ability. J Biomed Mater Res B Appl Biomater. 2008;87(1):49–58.
55. Matsuno T, Hashimoto Y, Adachi S, Omata K, Yoshitaka Y, Ozeki Y, et al. Preparation of injectable 3D-formed beta-tricalcium phosphate bead/alginate composite for bone tissue engineering. Dent Mater J. 2008;27(6):827–34.
56. Saidak Z, Marie PJ. Strontium signaling: molecular mechanisms and therapeutic implications in osteoporosis. Pharmacol Ther. 2012;136(2):216–26.
57. Reginster JY. Cardiac concerns associated with strontium ranelate. Expert Opin Drug Saf. 2014;13(9):1209–13.
58. Meininger S, Moseke C, Spatz K, Marz E, Blum C, Ewald A, et al. Effect of strontium substitution on the material properties and osteogenic potential of 3D powder printed magnesium phosphate scaffolds. Mater Sci Eng C Mater Biol Appl. 2019;98:1145–58.
59. Ehret C, Aid-Launais R, Sagardoy T, Siadous R, Bareille R, Rey S, et al. Strontium-doped hydroxyapatite polysaccharide materials effect on ectopic bone formation. PLoS One. 2017;12(9).
60. Bose S, Fielding G, Tarafder S, Bandyopadhyay A. Understanding of dopant-induced osteogenesis and angiogenesis in calcium phosphate ceramics. Trends Biotechnol. 2013;31(10):594–605.
61. Carlson NE, Roach RB, Jr. Platelet-rich plasma: clinical applications in dentistry. J Am Dent Assoc. 2002;133(10):1383–6.
62. Pachito DV, de Oliveira Cruz Latorraca C, Riera R. Efficacy of Platelet-Rich Plasma for non-transfusion use: Overview of Systematic Reviews. Int J Clin Pract. 2019:e13402.
63. Fennis JP, Stoelinga PJ, Jansen JA. Mandibular reconstruction: a histological and histomorphometric study on the use of autogenous scaffolds, particulate cortico-cancellous bone grafts and platelet rich plasma in goats. Int J Oral Maxillofac Surg. 2004;33(1):48–55.
64. Verma R, Negi G, Kandwal A, Chandra H, Gaur DS, Harsh M. Effect of autologous PRP on wound healing in dental regenerative surgeries and its correlation with PDGF levels. Asian J Transfus Sci. 2019;13(1):47–53.
65. Pham TAV, Tran TTP, Luong NTM. Antimicrobial Effect of Platelet-Rich Plasma against Porphyromonas gingivalis. Int J Dent. 2019;2019.
66. Bielecki TM, Gazdzik TS, Arendt J, Szczepanski T, Krol W, Wielkoszynski T. Antibacterial effect of autologous platelet gel enriched with growth factors and other active substances: an in vitro study. J Bone Joint Surg Br. 2007;89(3):417–20.
67. Anitua E, Alonso R, Girbau C, Aguirre JJ, Muruzabal F, Orive G. Antibacterial effect of plasma rich in growth factors (PRGF(R)-Endoret(R)) against Staphylococcus aureus and Staphylococcus epidermidis strains. Clin Exp Dermatol. 2012;37(6):652–7.

68. Wilshaw SP, Kearney JN, Fisher J, Ingham E. Production of an acellular amniotic membrane matrix for use in tissue engineering. Tissue Eng. 2006;12(8):2117–29.
69. Bryant-Greenwood GD. The extracellular matrix of the human fetal membranes: structure and function. Placenta. 1998;19(1):1–11.
70. Kjaergaard N, Hein M, Hyttel L, Helmig RB, Schonheyder HC, Uldbjerg N, et al. Antibacterial properties of human amnion and chorion in vitro. Eur J Obstet Gynecol Reprod Biol. 2001;94(2):224–9.
71. Ashraf H, Font K, Powell C, Schurr M. Antimicrobial Activity of an Amnion-Chorion Membrane to Oral Microbes. Int J Dent. 2019;2019.
72. Diaz-Prado S, Rendal-Vazquez ME, Muinos-Lopez E, Hermida-Gomez T, Rodriguez-Cabarcos M, Fuentes-Boquete I, et al. Potential use of the human amniotic membrane as a scaffold in human articular cartilage repair. Cell Tissue Bank. 2010;11(2):183–95.
73. McQuilling JP, Kammer M, Kimmerling KA, Mowry KC. Characterisation of dehydrated amnion chorion membranes and evaluation of fibroblast and keratinocyte responses in vitro. Int Wound J. 2019;16(3):827–40.
74. McQuilling JP, Vines JB, Kimmerling KA, Mowry KC. Proteomic Comparison of Amnion and Chorion and Evaluation of the Effects of Processing on Placental Membranes. Wounds. 2017;29(6):E38–e42.
75. Wilshaw SP, Kearney J, Fisher J, Ingham E. Biocompatibility and potential of acellular human amniotic membrane to support the attachment and proliferation of allogeneic cells. Tissue Eng Part A. 2008;14(4):463–72.
76. Neves N, Campos BB, Almeida IF, Costa PC, Cabral AT, Barbosa MA, et al. Strontium-rich injectable hybrid system for bone regeneration. Mater Sci Eng C Mater Biol Appl. 2016;59:818–27.
77. Ribeiro-Machado C, Lourenço A, Neves N, Alexandre N, Lamghari M, Barbosa M, et al. Evaluation of an injectable hybrid system for strontium local delivery in a sheep vertebra model. [in preparation]
78. Lourenço AH, Neves N, Ribeiro-Machado C, Sousa SR, Lamghari M, Barrias CC, et al. Injectable hybrid system for strontium local delivery promotes bone regeneration in a rat critical-sized defect model. Scientific Reports. 2017;7(1):5098.
79. Lourenço AH, Torres AL, Vasconcelos DaP, Ribeiro-Machado C, Barbosa JN, Barbosa MA, et al. Osteogenic, anti-osteoclastogenic and immunomodulatory properties of a strontium-releasing hybrid scaffold for bone repair. Materials Science and Engineering:C. 2019;99:1289–303.
80. Baptista LM, Lourenço AH, Barbosa MA, Gonçalves IC, Ribeiro CC. Antimicrobial properties of Sr-rich microspheres for bone regeneration. [in preparation]
81. Ribeiro CC, Barrias CC, Barbosa MA. Calcium phosphate-alginate microspheres as enzyme delivery matrices. Biomaterials. 2004;25(18):4363–73.
82. Maia FR, Lourenco AH, Granja PL, Goncalves RM, Barrias CC. Effect of cell density on mesenchymal stem cells aggregation in RGD-alginate 3D matrices under osteoinductive conditions. Macromol Biosci. 2014;14(6):759–71.
83. Fonseca KB, Bidarra SJ, Oliveira MJ, Granja PL, Barrias CC. Molecularly designed alginate hydrogels susceptible to local proteolysis as three-dimensional cellular microenvironments. Acta Biomater. 2011;7(4):1674–82.
84. Sell SA, Wolfe PS, Ericksen JJ, Simpson DG, Bowlin GL. Incorporating platelet-rich plasma into electrospun scaffolds for tissue engineering applications. Tissue Eng Part A. 2011;17(21–22):2723–37.
85. Wang X, Zhang Y, Choukroun J, Ghanaati S, Miron RJ. Effects of an injectable platelet-rich fibrin on osteoblast behavior and bone tissue formation in comparison to platelet-rich plasma. Platelets. 2018;29(1):48–55.
86. Lu T, Hixon KR, Ona WJ, Carletta MN, Garg K, Sell SA. An in vitro analysis of injectable methacrylated alginate cryogels incorporated with PRP targeting minimally invasive treatment of bone nonunion. Biomedical Physics & Engineering Express. 2018;4(5).
87. Kieb M, Sander F, Prinz C, Adam S, Mau-Moller A, Bader R, et al. Platelet-Rich Plasma Powder: A New Preparation Method for the Standardization of Growth Factor Concentrations. Am J Sports Med. 2017;45(4):954–60.

88. Shiga Y, Orita S, Kubota G, Kamoda H, Yamashita M, Matsuura Y, et al. Freeze-Dried Platelet-Rich Plasma Accelerates Bone Union with Adequate Rigidity in Posterolateral Lumbar Fusion Surgery Model in Rats. Sci Rep. 2016;6.
89. Alves A, Ribeiro-Machado C, Oliveira M, Barbosa M, Ribeiro C. Acellular and solubilized fetal membranes: a natural source of bioactive factors for regeneration. 29th Annual Meeting of the European Society for Biomaterials; Maastricht, Netherlands2018.
90. Baradaran-Rafii A, Asl NS, Ebrahimi M, Jabbehdari S, Bamdad S, Roshandel D, et al. The role of amniotic membrane extract eye drop (AMEED) in in vivo cultivation of limbal stem cells. Ocul Surf. 2018;16(1):146-53.
91. Murphy SV, Skardal A, Song L, Sutton K, Haug R, Mack DL, et al. Solubilized Amnion Membrane Hyaluronic Acid Hydrogel Accelerates Full-Thickness Wound Healing. Stem Cells Transl Med. 2017;6(11):2020-32.
92. Hughes CS, Moggridge S, Muller T, Sorensen PH, Morin GB, Krijgsveld J. Single-pot, solid-phase-enhanced sample preparation for proteomics experiments. Nat Protoc. 2019;14(1):68-85.
93. Fabregat A, Jupe S, Matthews L, Sidiropoulos K, Gillespie M, Garapati P, et al. The Reactome Pathway Knowledgebase. Nucleic Acids Res. 2018;46(D1):D649-d55.
94. Poultsides LA, Liaropoulos LL, Malizos KN. The socioeconomic impact of musculoskeletal infections. J Bone Joint Surg Am. 2010;92(11):e13.
95. Misch CE, Qu Z, Bidez MW. Mechanical properties of trabecular bone in the human mandible: implications for dental implant treatment planning and surgical placement. J Oral Maxillofac Surg. 1999;57(6):700-6; discussion 6-8.
96. Londono R, Badylak SF. Biologic scaffolds for regenerative medicine: mechanisms of in vivo remodeling. Ann Biomed Eng. 2015;43(3):577-92.
97. Gilpin A, Yang Y. Decellularization Strategies for Regenerative Medicine: From Processing Techniques to Applications. Biomed Res Int. 2017;2017.
98. Lei J, Priddy L, Lim J, Koob T. Dehydrated Human Amnion/Chorion Membrane (dHACM) Allografts as a Therapy for Orthopedic Tissue Repair. Techniques in Orthopaedics. 2019;32(3):149-57.
99. Albanese A, Licata ME, Polizzi B, Campisi G. Platelet-rich plasma (PRP) in dental and oral surgery: from the wound healing to bone regeneration. Immun Ageing. 2013;10:23.
100. da Silva LQ, Montalvao SAL, Justo-Junior ADS, Cunha Junior JLR, Huber SC, Oliveira CC, et al. Platelet-rich plasma lyophilization enables growth factor preservation and functionality when compared with fresh platelet-rich plasma. Regen Med. 2018;13(7):775-84.
101. Zheng C, Zhu Q, Liu X, Huang X, He C, Jiang L, et al. Effect of platelet-rich plasma (PRP) concentration on proliferation, neurotrophic function and migration of Schwann cells in vitro. J Tissue Eng Regen Med. 2016;10(5):428-36.
102. Steller D, Herbst N, Pries R, Juhl D, Hakim SG. Positive impact of Platelet-rich plasma and Platelet-rich fibrin on viability, migration and proliferation of osteoblasts and fibroblasts treated with zoledronic acid. Sci Rep. 2019;9.
103. Nguyen ATM, Tran HLB, Pham TAV. In Vitro Evaluation of Proliferation and Migration Behaviour of Human Bone Marrow-Derived Mesenchymal Stem Cells in Presence of Platelet-Rich Plasma. Int J Dent. 2019;2019:9639820.
104. Vahabi S, Yadegary Z, Karamshahi M. Evaluating the adhesion of human gingival fibroblasts and MG-63 osteoblast-like cells to activated PRP-coated membranes. Cell Tissue Bank. 2019;20(3):339-49.
105. Krishnamurithy G, Shilpa PN, Ahmad RE, Sulaiman S, Ng CL, Kamarul T. Human amniotic membrane as a chondrocyte carrier vehicle/substrate: in vitro study. J Biomed Mater Res A. 2011;99(3):500-6.
106. Boo L, Sofiah S, Selvaratnam L, Tai C, Pingguan-Murphy B, Kamarul T. A Preliminary Study of Human Amniotic Membrane as a Potential Chondrocyte Carrier. Malaysian Orthopaedic Journal. 2009;3(2).
107. Woodard JR, Hilldore AJ, Lan SK, Park CJ, Morgan AW, Eurell JA, et al. The mechanical properties and osteoconductivity of hydroxyapatite bone scaffolds with multi-scale porosity. Biomaterials. 2007;28(1):45-54.

108. Tai IC, Fu YC, Wang CK, Chang JK, Ho ML. Local delivery of controlled-release simvastatin/PLGA/HAp microspheres enhances bone repair. Int J Nanomedicine. 2013;8:3895-905.
109. Mao Z LY, Yang Y, Fang Z, CHen X, Wang Y, Kang J, Qu X, Yuan W, Dai K, Yue B. Osteoinductivity and Antibacterial Properties of Strontium Ranelate-Loaded Poly(Lactic-co-Glycolic Acid) Microspheres With Assembled Silver and Hydroxyapatite Nanoparticles. Frontiers in Pharmacology. 2018;9(368).
110. Offermanns V, Andersen OZ, Sillassen M, Almtoft KP, Andersen IH, Kloss F, et al. A comparative in vivo study of strontium-functionalized and SLActive implant surfaces in early bone healing. Int J Nanomedicine. 2018;13:2189-97.
111. Bretaña R. M. G-LJR, Sena L.A., editor An overview on biological effects of trace-element in substituted calcium phosphates. VII Latin American Congress on Biomedical Engineering CLAIB 2016; 2017; Bucaramanga, Santander, Colombia: IFMBE Proceedings.
112. Neves N, Linhares D, Costa G, Ribeiro CC, Barbosa MA. In vivo and clinical application of strontium-enriched biomaterials for bone regeneration: A systematic review. Bone Joint Res. 2017;6(6):366-75.
113. Koushaei S, Samandari MH, Razavi SM, Khoshzaban A, Adibi S, Varedi P. Histological Comparison of New Bone Formation Using Amnion Membrane Graft Versus Resorbable Collagen Membrane: An Animal Study. J Oral Implantol. 2018;44(5):335-40.
114. Tang K, Wu J, Xiong Z, Ji Y, Sun T, Guo X. Human acellular amniotic membrane: A potential osteoinductive biomaterial for bone regeneration. J Biomater Appl. 2018;32(6):754-64.
115. Go YY, Kim SE, Cho GJ, Chae SW, Song JJ. Differential effects of amnion and chorion membrane extracts on osteoblast-like cells due to the different growth factor composition of the extracts. PLoS One. 2017;12(8):e0182716.
116. Calciolari E, Donos N. The use of omics profiling to improve outcomes of bone regeneration and osseointegration. How far are we from personalized medicine in dentistry? J Proteomics. 2018;188:85-96.
117. Lozano RM, Perez-Maceda BT, Carboneras M, Onofre-Bustamante E, Garcia-Alonso MC, Escudero ML. Response of MC3T3-E1 osteoblasts, L929 fibroblasts, and J774 macrophages to fluoride surface-modified AZ31 magnesium alloy. J Biomed Mater Res A. 2013;101(10):2753-62.
118. Xu JL, Khor KA, Sui JJ, Zhang JH, Chen WN. Protein expression profiles in osteoblasts in response to differentially shaped hydroxyapatite nanoparticles. Biomaterials. 2009;30(29):5385-91.
119. Xu J, Khor KA, Sui J, Zhang J, Tan TL, Chen WN. Comparative proteomics profile of osteoblasts cultured on dissimilar hydroxyapatite biomaterials: an iTRAQ-coupled 2-D LC-MS/MS analysis. Proteomics. 2008;8(20):4249-58.
120. Kim CS, Lee KJ, Kim JE, Park YG, Ryu JJ, Kim HR. Proteomic analysis of the biological response of MG63 osteoblast-like cells to titanium implants. Odontology. 2014;102(2):241-8.
121. Zhao M, Li H, Liu X, Wei J, Ji J, Yang S, et al. Response of Human Osteoblast to n-HA/PEEK—Quantitative Proteomic Study of Bio-effects of Nano-Hydroxyapatite Composite. Scientific Reports. 2016;6.
122. Smith PC, Martínez C, Martínez J, McCulloch CA. Role of Fibroblast Populations in Periodontal Wound Healing and Tissue Remodeling. Front Physiol. 2019;10.
123. Lu P, Takai K, Weaver VM, Werb Z. Extracellular Matrix Degradation and Remodeling in Development and Disease. Cold Spring Harb Perspect Biol. 2011;3(12).
124. Cipriani C, Pascarella S, Errante F, Menicacci B, Magnelli L, Mocali A, et al. Serpin A1 and the modulation of type I collagen turnover: Effect of the C-terminal peptide 409-418 (SA1-III) in human dermal fibroblasts. Cell Biol Int. 2018;42(10):1340-8.
125. Sakai K, Sumi Y, Muramatsu H, Hata K, Muramatsu T, Ueda M. Thrombospondin-1 promotes fibroblast-mediated collagen gel contraction caused by activation of latent transforming growth factor beta-1. J Dermatol Sci. 2003;31(2):99-109.
126. Lichtman MK, Otero-Vinas M, Falanga V. Transforming growth factor beta (TGF-beta) isoforms in wound healing and fibrosis. Wound Repair Regen. 2016;24(2):215-22.
127. Everts PA, Knape JT, Weibrich G, Schönberger JP, Hoffmann J, Overdevest EP, et al. Platelet-Rich Plasma and Platelet Gel: A Review. J Extra Corpor Technol. 2006;38(2):174-87.

128. Miller CH, Rice AS, Garrett K, Stein SF. Gender, Race, and Diet Affect Platelet Function Tests in Normal Subjects Contributing to a High Rate of Abnormal Results. Br J Haematol. 2014;165(6):842–53.
129. Sarojini H, Billeter AT, Eichenberger S, Druen D, Barnett R, Gardner SA, et al. Rapid tissue regeneration induced by intracellular ATP delivery—A preliminary mechanistic study. PLoS One. 2017;12(4).
130. Chiang B, Essick E, Ehringer W, Murphree S, Hauck MA, Li M, et al. Enhancing skin wound healing by direct intracellular ATP delivery. Am J Surg. 2007;193(2):213–8.
131. Méry B, Guy JB, Vallard A, Espenel S, Ardail D, Rodriguez-Lafrasse C, et al. In Vitro Cell Death Determination for Drug Discovery: A Landscape Review of Real Issues. J Cell Death. 2017;10.
132. Pucci B, Kasten M, Giordano A. Cell Cycle and Apoptosis. Neoplasia. 2000;2(4):291–9.
133. Abreu-Blanco MT, Watts JJ, Verboon JM, Parkhurst SM. Cytoskeleton Responses in Wound Repair. Cell Mol Life Sci. 2012;69(15):2469–83.
134. Tao Y, Zheng W, Jiang Y, Ding G, Hou X, Tang Y, et al. Nucleosome organizations in induced pluripotent stem cells reprogrammed from somatic cells belonging to three different germ layers. BMC Biol. 2014;12.
135. Becker PB, Workman JL. Nucleosome remodeling and epigenetics. Cold Spring Harb Perspect Biol. 2013;5(9).
136. Gordon JAR, Stein JL, Westendorf JJ, van Wijnen AJ. Chromatin modifiers and histone modifications in bone formation, regeneration, and therapeutic intervention for bone-related disease. Bone. 2015;81:739–45.
137. Aderibigbe BA, Buyana B. Alginate in Wound Dressings. Pharmaceutics. 2018;10(2).
138. Alberts B, Johnson A, Lewis J, Raff M, Roberts K, Walter P. Cell-Cell Adhesion. 2002.
139. R F. Platelet Secretion. In: A.D. M, editor. Platelets: Academic Press; 2013. p. 343–66.
140. Middleton KK, Barro V, Muller B, Terada S, Fu FH. Evaluation of the Effects of Platelet-Rich Plasma (PRP) Therapy Involved in the Healing of Sports-Related Soft Tissue Injuries. Iowa Orthop J. 2012;32:150–63.
141. Paliwal S, Chaudhuri R, Agrawal A, Mohanty S. Regenerative abilities of mesenchymal stem cells through mitochondrial transfer. J Biomed Sci. 2018;25(1):31.
142. Nayak RC, Chang KH, Vaitinadin NS, Cancelas JA. Rho GTPases control specific cytoskeleton-dependent functions of hematopoietic stem cells. Immunol Rev. 2013;256(1).
143. Blum AE, Joseph SM, Przybylski RJ, Dubyak GR. Rho-family GTPases modulate Ca2+-dependent ATP release from astrocytes. Am J Physiol Cell Physiol. 2008;295(1):C231–41.
144. Zhao X, Psarianos P, Ghoraie LS, Yip K, Goldstein D, Gilbert R, et al. Metabolic regulation of dermal fibroblasts contributes to skin extracellular matrix homeostasis and fibrosis. Nature Metabolism. 2019;1(1):147–57.
145. Rodríguez A, Webster P, Ortego J, Andrews NW. Lysosomes Behave as Ca2+-regulated Exocytic Vesicles in Fibroblasts and Epithelial Cells. J Cell Biol. 1997;137(1):93–104.
146. Alberts B, Johnson A, Lewis J, Raff M, Roberts K, Walter P. Transport from the Trans Golgi Network to the Cell Exterior: Exocytosis. 2002.
147. Reinke JM, Sorg H. Wound repair and regeneration. Eur Surg Res. 2012;49(1):35–43.
148. Bao P, Kodra A, Tomic-Canic M, Golinko MS, Ehrlich HP, Brem H. The Role of Vascular Endothelial Growth Factor in Wound Healing. J Surg Res. 2009;153(2):347–58.
149. Demidova-Rice TN, Hamblin MR, Herman IM. Acute and Impaired Wound Healing: Pathophysiology and Current Methods for Drug Delivery, Part 2: Role of Growth Factors in Normal and Pathological Wound Healing: Therapeutic Potential and Methods of Delivery. Adv Skin Wound Care. 2012;25(8):349–70.
150. Emmerson E, Campbell L, Davies FC, Ross NL, Ashcroft GS, Krust A, et al. Insulin-like growth factor-1 promotes wound healing in estrogen-deprived mice: new insights into cutaneous IGF-1R/ERalpha cross talk. J Invest Dermatol. 2012;132(12):2838–48.
151. Ishida Y, Kondo T, Takayasu T, Iwakura Y, Mukaida N. The essential involvement of cross-talk between IFN-gamma and TGF-beta in the skin wound-healing process. J Immunol. 2004;172(3):1848–55.

152. Stout AJ, Gresser I, Thompson WD. Inhibition of wound healing in mice by local interferon alpha/beta injection. Int J Exp Pathol. 1993;74(1):79–85.
153. Huang M, Sharma S, Zhu LX, Keane MP, Luo J, Zhang L, et al. IL-7 inhibits fibroblast TGF-β production and signaling in pulmonary fibrosis. J Clin Invest. 2002;109(7):931–7.
154. Grässel S RS. COL16A1 (collagen, type XVI, alpha 1). Atlas of Genetics and Cytogenetics in Oncology and Haematology. 2010;14(7).
155. NCBI. COL16A1 collagen type XVI alpha 1 chain Homo sapiens (human): Pubs; 2019 [Available from: https://www.ncbi.nlm.nih.gov/pubmed/.
156. Guo J, Zhang H, Xia J, Hou J, Wang Y, Yang T, et al. Interleukin-1beta induces intercellular adhesion molecule-1 expression, thus enhancing the adhesion between mesenchymal stem cells and endothelial progenitor cells via the p38 MAPK signaling pathway. Int J Mol Med. 2018;41(4):1976–82.
157. Xu FF, Zhu H, Li XM, Yang F, Chen JD, Tang B, et al. Intercellular Adhesion Molecule-1 Inhibits Osteogenic Differentiation of Mesenchymal Stem Cells and Impairs Bio-Scaffold-Mediated Bone Regeneration In Vivo. Tissue Eng Part A. 2014;20(19-20):2768–82.
158. Chang W, Kim R, Park SI, Jung YJ, Ham O, Lee J, et al. Enhanced Healing of Rat Calvarial Bone Defects with Hypoxic Conditioned Medium from Mesenchymal Stem Cells through Increased Endogenous Stem Cell Migration via Regulation of ICAM-1 Targeted-microRNA-221. Mol Cells. 2015;38(7):643–50.
159. Ren G, Zhao X, Zhang L, Zhang J, L'Huillier A, Ling W, et al. Inflammatory cytokine-induced intercellular adhesion molecule-1 and vascular cell adhesion molecule-1 in mesenchymal stem cells are critical for immunosuppression. J Immunol. 2010;184(5):2321–8.
160. Aslan JE, McCarty OJT. Rho GTPases in Platelet Function. J Thromb Haemost. 2013;11(1):35–46.
161. Sioud M, Mobergslien A, Boudabous A, Floisand Y. Evidence for the involvement of galectin-3 in mesenchymal stem cell suppression of allogeneic T-cell proliferation. Scand J Immunol. 2010;71(4):267–74.
162. Polchert D, Sobinsky J, Douglas G, Kidd M, Moadsiri A, Reina E, et al. IFN-γ activation of mesenchymal stem cells for treatment and prevention of graft versus host disease. Eur J Immunol. 2008;38(6):1745–55.
163. Vogel S, Börger V, Peters C, Förster M, Liebfried P, Metzger K, et al. Necrotic cell-derived high mobility group box 1 attracts antigen-presenting cells but inhibits hepatocyte growth factor-mediated tropism of mesenchymal stem cells for apoptotic cell death. Cell Death Differ. 2015;22(7):1219–30.
164. Zhu H, Mitsuhashi N, Klein A, Barsky LW, Weinberg K, Barr ML, et al. The role of the hyaluronan receptor CD44 in mesenchymal stem cell migration in the extracellular matrix. Stem Cells. 2006;24(4):928–35.
165. Mansouri R, Jouan Y, Hay E, Blin-Wakkach C, Frain M, Ostertag A, et al. Osteoblastic heparan sulfate glycosaminoglycans control bone remodeling by regulating Wnt signaling and the crosstalk between bone surface and marrow cells. Cell Death Dis. 2017;8(6):e2902.
166. Paiva KBS, Granjeiro JM. Matrix Metalloproteinases in Bone Resorption, Remodeling, and Repair. Prog Mol Biol Transl Sci. 2017;148:203–303.
167. Chen G, Deng C, Li YP. TGF-β and BMP Signaling in Osteoblast Differentiation and Bone Formation. Int J Biol Sci. 2012;8(2):272–88.
168. Yourek G, Hussain MA, Mao JJ. Cytoskeletal Changes of Mesenchymal Stem Cells During Differentiation. ASAIO J. 2007;53(2):219–28.
169. Schlessinger K, Hall A, Tolwinski N. Wnt signaling pathways meet Rho GTPases. Genes Dev. 2009;23(3):265–77.
170. Christy BA, Herzig MC, Montgomery RK, Delavan C, Bynum JA, Reddoch KM, et al. Procoagulant activity of human mesenchymal stem cells. J Trauma Acute Care Surg. 2017;83(1 Suppl 1):S164–s9.
171. Yuan X, Logan TM, Ma T. Metabolism in Human Mesenchymal Stromal Cells: A Missing Link Between hMSC Biomanufacturing and Therapy? Front Immunol. 2019;10.
172. Goel PN, Moharrer Y, Hebb JH, Egol AJ, Kaur G, Hankenson KD, et al. Suppression of Notch Signaling in Osteoclasts Improves Bone Regeneration and Healing. J Orthop Res. 2019;37(10):2089–103.

173. Zhang X, Tamasi J, Lu X, Zhu J, Chen H, Tian X, et al. Epidermal growth factor receptor plays an anabolic role in bone metabolism in vivo. J Bone Miner Res. 2011;26(5):1022–34.
174. Wigner NA, Soung do Y, Einhorn TA, Drissi H, Gerstenfeld LC. Functional role of Runx3 in the regulation of aggrecan expression during cartilage development. J Cell Physiol. 2013;228(11):2232–42.
175. Miller MQ, McColl LF, Arul MR, Nip J, Madhu V, Beck G, et al. Assessment of Hedgehog Signaling Pathway Activation for Craniofacial Bone Regeneration in a Critical-Sized Rat Mandibular Defect. JAMA Facial Plast Surg. 2019;21(2):110–7.
176. Pereira CL, Goncalves RM, Peroglio M, Pattappa G, D'Este M, Eglin D, et al. The effect of hyaluronan-based delivery of stromal cell-derived factor-1 on the recruitment of MSCs in degenerating intervertebral discs. Biomaterials. 2014;35(28):8144–53.